BioTechniques®

eBook: Cancer Immunology

The latest updates, brought to you by BioTechniques

Sponsored by Sartorius

Content includes:

Introduction

Cancer immunology is a vital link in the chain of cancer research. By furthering understanding of the interplay between immune systems and cancerous cells, researchers can begin to identify aspects of the immune system susceptible to the influence of tumors, while highlighting any weaknesses in tumor immune evasion.

With these aspects exposed, it is possible to harness this information to design therapies that can exploit weaknesses in tumor immune evasion or compensate for the failings of the immune system. These immunotherapies come in many forms and can require complex technology and methodology to design and produce.

In this eBook on cancer immunology, we will explore some of the foundational research into cancer immunology, the models required for exploration and the techniques involved in both foundational research and the development of immunotherapies. Opening with a Technology News article, this piece gives an insight into five key types of immune therapy being deployed in cancer research. Exploring each approach, its prevalence and stage of development, the article then goes on to address questions of efficacy in immunotherapeutic approaches to cancer.

“...we will explore some of the foundational research into cancer immunology, the models required for exploration and the techniques involved in both foundational research and the development of immunotherapies.”

Next a White Paper on the hallmarks of cancer outlines the latest insights into each of these fundamental features of oncology, exploring how these new insights are contributing to cancer research and highlighting the key technologies that are supporting this research. This leads into two Report articles. The first describes a 2D transwell and a 3D spheroid assay designed to quantitatively determine the invasive behavior of glioblastoma. The second explores the isolation of spheroid-forming cells and the enrichment of cancer stem-like cells, revealing insights into the evasion of apoptosis. These reports provide key examples of techniques supporting the study of hallmarks of cancer – invasion and evasion of apoptosis.

Focusing in on the technologies involved, a Sartorius White Paper explores the “Ten applications of live-cell analysis in immunology” highlighting the utility and versatility of the technique before a Review and Expert Opinion dive into the biology of T cells and the use of developing techniques, such as CRISPR, to develop CAR-T therapies.

A White Paper on the development of live-cell killing assays that use live-cell imaging and analysis then provides the key updates in these approaches that are leading to fascinating insights into immuno-oncology.

Finally, an Application Note provides a practical example of the use of live cell imaging and analysis to better study the cell cycle, improving the chances of identifying novel targets for immunotherapies.

Tristan Free
Digital Editor, Future Science Group,
Unitec House, 2 Albert Place, London, UK.
t.free@future-science.com

BioTechniques **is a peer-reviewed journal dedicated to the publication of original laboratory methods, related technical tools, and methods-oriented review articles that are of broad interest to scientists engaged in basic applied life science research. Complete Instructions for Authors are available at: https://mc04.manuscriptcentral.com/fs-btn,** ***BioTechniques'*** **website for online manuscript submission. All manuscripts should be submitted at this site.**

Opinion

How is cancer immunology being utilized in the fight against cancer?

Written by Katie Gordon

Katie Gordon
Former Assistant Editor at BioTechniques, London, UK

"Developments in the field over the past 30 years has allowed immunotherapy to establish itself as a vital pillar of cancer treatment."

Read more online
http://bit.ly/BTNOpinion_OSirenko

Cancer immunology refers to the immune system's role in the progression and development of cancer. As with all disease, our bodies have certain immune defenses intended to protect us from tumor development. However, tumor cells have developed ways to evade immune surveillance, and can even create immunosuppressive tumor microenvironments to develop without interference from the immune system.

For the last few decades, cancer immunology research has focused on taking what we know about our immune response to cancer and cancer's defense against this to develop new treatments for cancer patients, known as immunotherapy.

CANCER IMMUNOLOGY: WHAT IS IMMUNOTHERAPY?

In general, cancer immunotherapy involves using natural or synthetic substances to restore or enhance the patient's immune system, allowing the body to 'naturally' fight off cancer. Many patients view this as preferable over traditional chemotherapeutic methods, as it's utilizing the body's own resources rather than using toxic chemicals to destroy the tumors.

The first US FDA approved cancer treatment utilizing cancer immunology was the bacillus Calmette–Guérin (BCG) vaccine, which was approved for bladder cancer treatment back in 1990. Since then, there have been huge developments in the field of cancer immunotherapy and, as of December 2019, the FDA has approved immunotherapy treatments for nearly 20 different cancer types.

Immunotherapies have already seen huge successes in several cancer types, such as in metastatic melanoma where combination immunotherapy drugs are the only successful treatment option. Researchers working in the field believe that immunotherapy has the potential to provide effective treatment for every type of cancer.

IMMUNOTHERAPY TYPES

Immunotherapies currently in use for the treatment of cancer can be broken down into five main types: adoptive cell therapy, targeted antibodies, cancer vaccines, immunomodulators and oncolytic virus therapy.

ADOPTIVE CELL THERAPY

Adoptive cell therapy involves taking advantage of the body's natural defenses by using immune cells (either isolated from the body or genetically engineered in the laboratory) to destroy cancerous cells.

The form of this treatment that has experienced the highest level of clinical success is CAR-T Cell therapy. This involves isolating or generating T cells and equipping them with a synthetic chimeric antigen receptor (CAR). These antibodies are then transfused back into the body where they bind with the proteins on the cancer cells surface and destroy them.

Some other applications of adoptive cell therapies, which all follow the same general principle as CAR-T, are; tumor-infiltrating lymphocyte therapy, where naturally occurring T cells that have already entered the patient's tumor are isolated, activated and expanded in the lab before being reinfused back into the patient; and engineered t cell receptor therapy, where a patients T cells are harvested and armed with new t cell receptors that target specific cancer antigens.

There are only two types of adoptive cell therapy currently approved by the FDA, and both are a form of CAR-T therapy designed to treat leukemiaand lymphoma. There are currently many other adoptive cell therapies under evaluation in clinical trials in the US, such as mesothelin-directed CAR T therapy to treat a range of cancers including malignant mesothelioma and breast cancer. Researchers are also working on utilizing new cell editing techniques, such as CRISPR, to heighten the effectiveness of current and potential therapies.

TARGETED ANTIBODIES

Another type of immunotherapy is engineering antibodies that are able to target cancer antigens. This is considered a form of passive

immunotherapy, as it involves targeting tumor cells directly rather than the immune cells.

Traditionally, monoclonal antibody treatment involved treating patients with antibodies that would bind to cancer cells and prevent them from growing, whilst also sending signals to other immune cells to stimulate the destruction of the tumor cells. The first targeted antibody cancer treatment was approved by the FDA in 1997 for Non-Hodgkin's lymphoma, though its approved uses have since been expanded, and since then 18 more therapies of this kind have been approved, including necitumumab, a monocolonal antibody used in conjunction with chemotherapy drugs to treat previously untreatable metastatic squamous non small cell lung cancer.

In recent years, researchers have refined this therapy type to produce antibody drug conjugates. This involves treating patients with antibodies loaded with anti-cancer drugs, which are released into the body upon binding with the cancer cell and act to directly kill the cancer cell. This has been successful so far, with 9 antibody-drug conjugates currently earning FDA approval.

CANCER VACCINES

Cancer vaccines generally utilize the same principles as vaccines of viral or bacterial infections, with the main difference being that, unlike bacteria and viruses, cancer cells are not 'foreign' and can quite closely resemble healthy cells. Therefore, in order to develop vaccines to prevent or fight cancer, more sophisticated techniques must be used.

There have been a reasonably high number of successes in developing preventative vaccines for cancers where development is stimulated by viral infection. For example, it has been discovered that HPV infection can result in the development of cervical or head and neck cancer and, in theory, developing a vaccine against HPV should help protect individuals both from the viral infection and the consequential cancer development.

There are currently four preventative cancer vaccines approved by the FDA, including three to prevent HPV infection and one to protect against hepatitis B infection, which researchers have shown to be responsible for the development of certain liver cancers.

Less success has been found in developing therapeutic cancer vaccines to target specific tumor antigens. This is due to each individual's tumor being unique with slightly different antigens on each tumor cell. However, there have been some successes, and two therapeutic cancer vaccines are approved by the FDA: BCG which stimulates immune system to fight early-stage bladder cancer and Sipuleucel-T, which targets proteins on prostate cancer cells.

IMMUNOMODULATORS

Immunomodulators are molecules that regulate the activity of the immune system. Immunotherapies involving immunomodulators utilize the molecules to enhance the body's natural immune defenses to destroy cancer cells. This field of immunotherapy is the area that has seen the highest level of success over recent years.

Immunomodulators can be divided into four broad types: cytokines, messenger molecules that regulate immune cell maturation, growth and responsiveness; agonists, molecules that activate pathways and promote adaptive immune responses; adjuvants, molecules that activate innate immune pathways and enhance general immune responses; and checkpoint Inhibitors, which block immune checkpoints to enhance immune responses against cancer cells.

There are currently 14 different immunomodulators approved by the FDA for the treatment of a range of different cancer. Immune checkpoint inhibitors have experienced the highest success rates, with seven of these approved therapies representing immune checkpoint inhibitors alone. The first was approved only in 2015, demonstrating how fast the field is developing. Furthermore, several single immune checkpoint inhibitors, including pembrolizumab and nivolumab, have demonstrated success in treating a wide range of different cancer types, increasing the overall value of the drugs.

ONCOLYTIC VIRUS THERAPY

For oncolytic virus therapy, cancer cells are infected with certain viruses, known as oncolytic viruses, which then attack and destroy the tumor. Cancer cells themselves have impaired antiviral defenses, leaving them vulnerable to infection. Furthermore, once the virus infects the tumor cell, the cell explodes and releases the cancer antigens, which can then go on to stimulate further immune responses to destroy the remaining tumor cells.

Whilst there is currently only one form of the therapy with FDA approval, a modified herpes simplex virus to treat certain melanoma patients, it is believed that this treatment has the potential to be very effective. Current clinical trials in the US are evaluating the use of a range of other viruses including measles, picornavirus and adenovirus to treat a range of different cancers in this way.

HOW EFFECTIVE IS IMMUNOTHERAPY?

Whilst several trials have demonstrated very high effectiveness in the treatment of different cancer types, the level of effectiveness for different immunotherapies are extremely variable. Factors affecting the effectiveness include the type and length of treatment; biological characteristics of the patient and the cancer, and lifestyle factors such as diet and exercise.

To improve the effectiveness of immunotherapy, further study into cancer immunology is required, there have been increased efforts to develop predictive biomarkers, which would allow researchers to determine the most effective therapy before administration. Recently, there have considerable advances in developing immunotherapy predictors, including research that demonstrates potential applications for artificial intelligence, as well as the discovery of the role the gut microbiota could play in predicting immunotherapy response.

Developments in the field over the past 30 years has allowed immunotherapy to establish itself as a vital pillar of cancer treatment. Amongst many oncologists, there is even a feeling that immunotherapy may render chemotherapy obsolete in the future, though others believe that a combination of the two therapies will become the new 'gold standard' treatment.

Regardless of what the future holds in terms of the position of immunotherapy in cancer treatment, we can be sure that there is still a lot of research needed until the true potential of cancer immunology is determined.

DISCLAIMER

The opinions expressed in this Opinion are those of the author and do not necessarily reflect the views of Future Science Ltd.

SARTORIUS

White Paper

August, 2020

Keywords or phrases:
Live-cell analysis; cancer hallmarks; cell biology; imaging and analysis; instrumentation; 2D cells; 3D cells; spheroids; cell dynamics; translational models; therapeutics;

Revolutionary Insight Into Cancer Hallmarks With Real-Time Live-Cell Analysis

Abstract

The seven hallmarks of cancer have now been firmly established after rounds of minor updates and revisions[1-3], and we can move to the next chapter of this critically important research area. Our understanding has already improved immensely following the various breakthroughs over the past decade, and this has offered vital insight into new pharmacological targets and treatment strategies. We have also seen huge strides made in the field of in vitro translational models and live-cell assays in the last ten years, using both traditional 2D and advanced 3D cell culture systems.

We now have much more information regarding these hallmarks than was previously available, and are able to delve further into exactly how they interact and influence each other. Much of this progress has been driven by technological advances, enabling previously unachievable studies to be performed and, now, we are able to use these methods to collectively look at multiple hallmarks in the context of each other, rather than in isolation.

We have previously discussed how the advent of purpose-built live-cell analysis instruments – such as the Incucyte® Cell Analysis Systems (Sartorius) – has revolutionized the field for this research, offering the ability to observe and quantify cancer cell biology over time, in a completely non-perturbing way. This whitepaper follows on directly from that review, and discusses the research that is now underway thanks to our improved understanding of the hallmarks, as well as how the latest technological advances are supporting this research.

The seven hallmarks of cancer

1. Selective proliferative advantage
2. Altered stress response
3. Vascularization
4. Invasion and metastasis
5. Metabolic rewiring
6. Immune modulation
7. An abetting microenvironment

Find out more: www.sartorius.com/Incucyte

1. Selective proliferative advantage

Continual unregulated proliferation is a fundamental abnormality to the development of cancers. As such, almost every study of cancer cell biology includes measures of cell growth and proliferation in one form or another. Live-cell analysis, in both 2D and 3D formats (see Figure 1), has become the 'gold standard' method for these measurements. This is due to the unique combination of morphological insights, full time-course data and non-perturbing workflows that the approach provides. There are now over 725 research publications referring to the use of this technology, including a recent study looking at mammalian cell growth dynamics during mitosis, which provides valuable new information about the action of antimitotic cancer chemotherapies[4].

Cancer stem cells (CSCs) are responsible for tumor development and relapse, and result from one or more significant changes to cell signaling pathways that affect growth ligands, their corresponding receptors or cytosolic signaling molecules. Novel fluorescent reporters targeting stem cell transcription factors can be combined with live cell analysis to assess the spatial distribution of CSCs in cell models that retain tumor microenvironmental and structural cues, and this same approach can also be used to monitor CSC plasticity and response to therapeutics in real time[5]. Another critical property of CSCs is self-renewal, and the signaling pathways involved in this process have been extensively characterized using the Incucyte® Live-Cell Analysis System[6].

One of the current hot topics in this area is chemoresistance, as this is a major hurdle in the treatment and ongoing management of many cancer patients. Several cancers – particularly glioblastoma and epithelial ovarian cancer – currently have a poor prognosis due the rapid recurrence of aggressive, chemoresistant tumors. A number of interesting studies using live-cell analysis have been published looking at how this resistance may be conferred by a subpopulation of CSCs which comprise only a small proportion of the primary tumor, as well as the potential of combination therapies to overcome this chemoresistance[7,8].

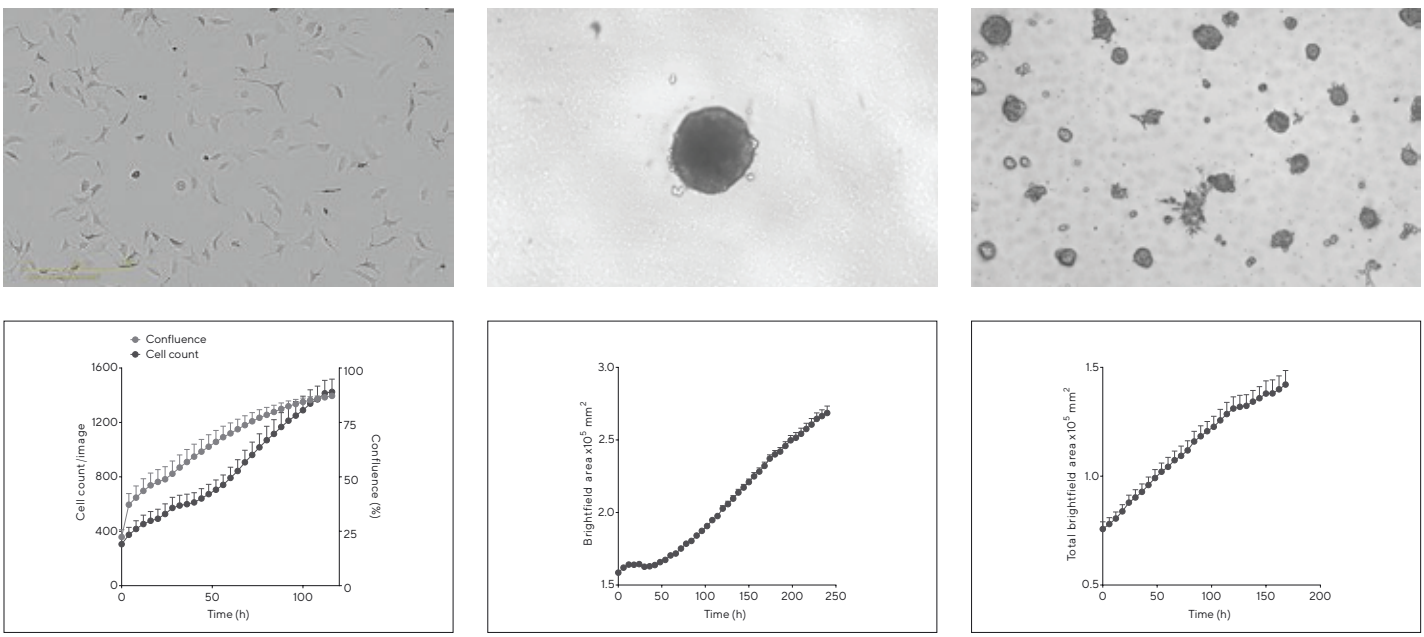

Figure 1: Growth of SKOV3 ovarian epithelial cancer cells as 2D cultures, 3D single spheroids and multi-spheroids.
[LEFT] To observe 2D growth, SKOV3 cells were seeded onto a clear, flat bottom, tissue culture-treated 96-well microplates at 1K cells/well, and phase contrast images were acquired every 4h using the Incucyte® Cell-By-Cell Analysis Software Module. [Top left] Image of cells 1 day post-seeding; [Bottom left] Time course showing the increase in confluence and cell count.
[CENTER] To generate 3D single spheroids, SKOV3 cells were seeded into ultra-low attachment (ULA) microplates at 5K cells/well and centrifuged for 10 minutes at 100g. Spheroid formation and growth was monitored by acquisition of phase contrast and brightfield images using the Incucyte® Spheroid Analysis Software Module every 6h. [Top center] Image of a single spheroid 5 days post-seeding; [Bottom center] Time course showing increase in the largest brightfield object area.
[RIGHT] Multi-spheroid formation and growth was monitored by acquisition of phase contrast and brightfield images using the Incucyte Spheroid Analysis Software Module every 6h. [Top right] Image of multi-spheroids on day 7 post-seeding; [Bottom right] Time course showing increase in total brightfield object area.

2. Altered stress response

Cancer cells face a wide range of stresses – including excessive signaling, DNA damage, hypoxia, nutrient starvation and anticancer therapies – and have developed or adapted a number of stress responses to ensure their survival and propagation. Live-cell imaging is ideally suited to investigating these altered stress responses, as well as looking at how

these changes can be exploited in cancer therapies[9,10]. All tumors feature persistent mutations which are not eliminated by the cells' various DNA repair mechanisms and, logically, many cancers have characteristic defects in DNA repair pathways. But some malignancies – such as leukemia, breast and pancreatic cancers – over-express DNA repair proteins. Several recent studies have used real-time analysis to look at the potential of over-expression patterns as therapeutic targets[11]. This approach also naturally lends itself to drug validation studies, providing an effective and convenient method to look at, for example, synthetic lethality mechanisms[12].

The Incucyte® Live-Cell Analysis System is widely recognized as a versatile tool for real-time multiplexed measurements of proliferation, cell health and apoptosis[13,14], and can be combined with numerous validated assay reagents (e.g. caspase 3/7 substrates, annexin V labels or cytotoxicity probes) to establish how cancer cells avoid the effects of apoptotic stimuli[15] (Figure 2). Similarly, it can be used to investigate the complex interplay between oncogenes and tumor suppressors which lead to senescence[16, 17].

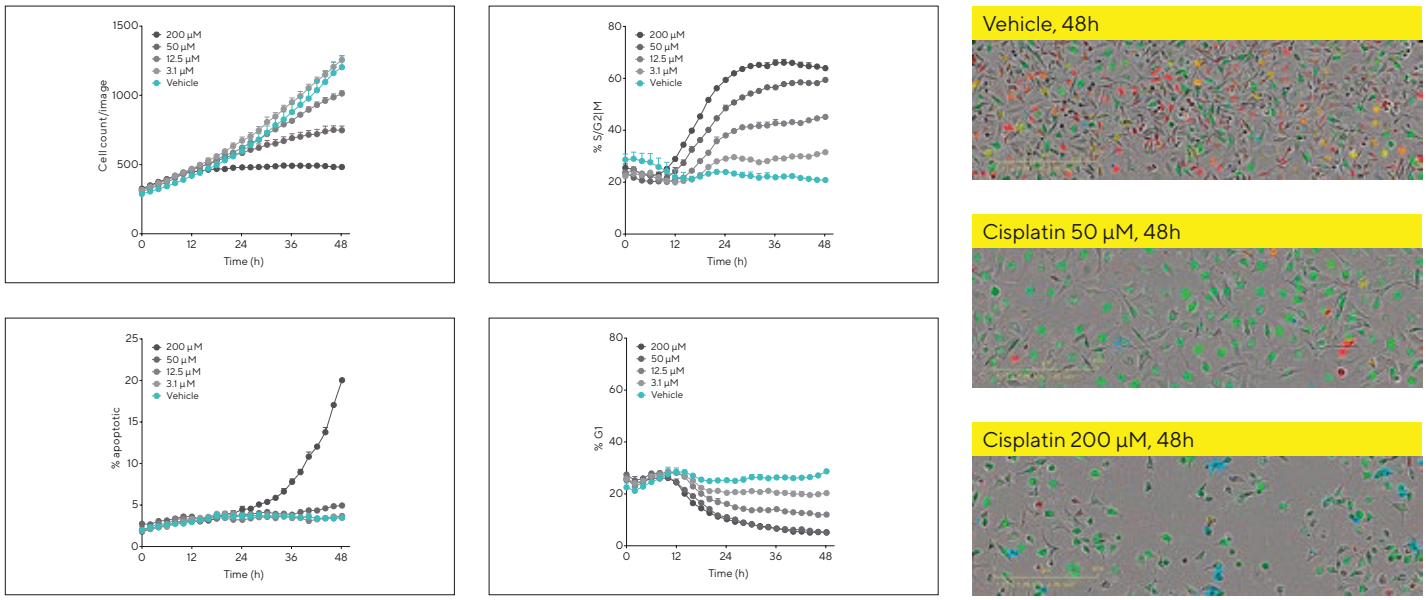

Figure 2: Cisplatin-induced DNA damage causes cell cycle arrest and apoptosis in MDA-MB-231 cells.
MDA-MB-231 triple-negative breast cancer cells expressing Incucyte® Cell Cycle Lentivirus were seeded into a 96-well plate at 3K cells/well in the presence of Incucyte® Annexin V NIR Dye (1:200). Cells were incubated for 18h to allow adherence and then treated with cisplatin (3-200 µM). Phase contrast and fluorescence images were acquired using the Incucyte® Cell-By-Cell Analysis Software Module every 2h for 48h. Images of cells were segmented and classified to assess the percentage of apoptotic (annexin V-positive) cells, as well as cells in each stage of the cell cycle (cells expressing only green fluorescence correspond to S/G2/M, while those expressing orange fluorescence only correspond to G1). [Top left] Time course of cell count indicating that proliferation starts to reduce after 12h in the presence of cisplatin concentrations of ≥12.5 µM; [Bottom left] Apoptosis is only observed after 24h in the presence of 200 µM cisplatin. Analysis of the cell cycle indicates a concentration dependent increase in the percent cells in S/G2/M after 12h [Top center], with a corresponding decrease in percent cells in G1 [Bottom center]. This data indicates that cisplatin concentrations up to 50 µM induce cell cycle arrest and inhibit proliferation, while the higher concentration of 200 µM induces arrest from 12-24h followed by apoptosis after 24h. Therefore, at low concentrations, cisplatin treatment leads to early arrest as the cells attempt to activate DNA repair mechanisms, whereas the damage to DNA is too great at higher concentrations, and apoptosis is induced.

3. Vascularization

Despite their self-renewal capabilities and differing stress responses, tumors are not immune to the effects of hypoxia, and so require a blood supply to grow beyond a few millimeters in size. Angiogenesis – the sprouting of new vasculature from existing vessels – is therefore key to tumor growth and development.

Live-cell analysis is ideally suited to following the proliferation, clustering and differentiation of endothelial cells that occur during vascularization – as well as the critical functions of fibroblast and pericyte stromal cells1[8, 19]. Using advanced cell models, it is possible to dissect these processes, yielding critical morphological information and insights into the sequence of events[20]. A range of chemical and physical stimuli have been characterized using this approach, including classical growth factors (e.g. VEGF, FGF[21]), established anti-angiogenic therapies (e.g. bevacizumab) and novel angiogenic regulators – such as HSP70-1A[22], piezo1[23] and melflufen[24]. Scratch wound studies on human vascular endothelial cells (HUVECs) are also commonly used to probe the signaling pathways involved in cell migration (Figure 3).
Approaching this same topic from the opposite direction, a number of studies have used Incucyte® Live-Cell Imaging

and Analysis to study the effects of hypoxia in both tumors and healthy cells. One particularly interesting analysis looked at the uptake and efficacy of colloidal gold nanoparticles – which are increasingly being used as drug delivery vehicles and radiation dose enhancers – and identified that hypoxia significantly reduced the toxicity of the nanoparticles compared to normoxic conditions in HeLa and MCF-7 cells[23]. Another looked at the accumulation of intracellular H_2S in clear cell renal cell carcinoma (ccRCC), combining live-cell imaging, ATP assays and flow cytometry studies to suggest that inhibition of H_2S production could be an attractive new therapeutic target for ccRCC[26].

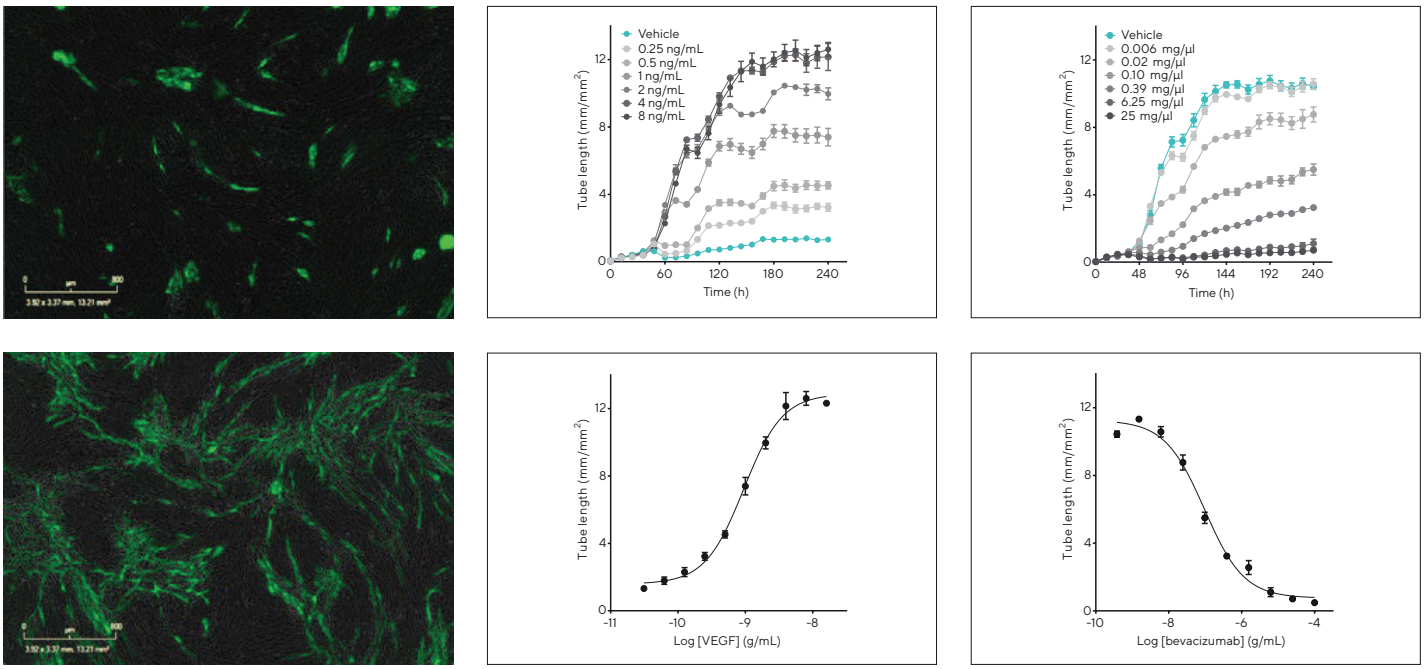

Figure 3: Bevacizumab inhibits VEGF-driven vascularization in a HUVEC/fibroblast angiogenesis model.
HUVECs pre-labelled with green fluorescent protein (GFP) were thawed and co-cultured with human dermal fibroblasts on a 96-well assay plate for 2 days. Either VEGF alone or VEGF (4 ng/mL) in the presence of bevacizumab (a clinical anti-VEGF antibody) were then added. Vascular tube formation was monitored kinetically using live cell analysis, with images acquired and analyzed for tube length and number of branch points every 12h for 10 days. Media and test agents were replaced every 2-3 days. Representative images for media control [Top left] and VEGF- treated wells [Bottom Left] taken at 192h. VEGF induced tube formation in a time- [Top center] and concentration-dependent [Bottom center] manner, yielding an EC_{50} value of 0.9 ng/mL. Bevacizumab, elicited time- [Top right] and concentration-dependent [Bottom right] inhibition of VEGF-driven tube formation, with an IC_{50} value of 1.0 ng/mL.

4. Invasion and metastasis

The ability to invade surrounding tissues and seed secondary sites is a defining feature of malignancy. Split into distinct phases – invasion of the extracellular matrix, escape into the vasculature, survival in circulation, seeding of secondary sites and adaptation of the new microenvironment – invasion and metastasis is a broad and complex subject area, and is further complicated by the intrinsic heterogeneity of tumors[27]. There are a number of Incucyte assays that can be used to dissect the sequential steps and genetic origins of metastasis, including 'scratch wound' migration and invasion assays[28,29] (Figure 4), chemotaxis experiments[30], and growth and colonization studies[31,32]. Combining these live-cell assays with 3D cell culture models has also provided valuable information which might otherwise be overlooked[33] (Figure 5).

Elucidating the various signaling pathways involved in each step of invasion and metastasis is essential to understanding these processes[34]. For example, a panel of Incucyte® Cell Migration and Invasion Assays – combining over-expression, shRNA knockdown and pharmacological inhibition studies – has been used to characterize a novel signaling pathway regulating cell migration and metastasis in liver, lung, colon, and breast cancer cell lines[35,36]. This technology can also be used to investigate how the invasion and metastasis process is affected by chemotherapy drugs[37,] and to screen for potential therapeutics to reduce the risk of secondary tumor formation or relapse[38] (Figure 5). Colonization of the secondary tumor site can also be followed using real-time imaging of co-culture invasion assays to identify the various mechanisms by which invading cancer cells remodel the extracellular matrix to enable rapid proliferation[39].

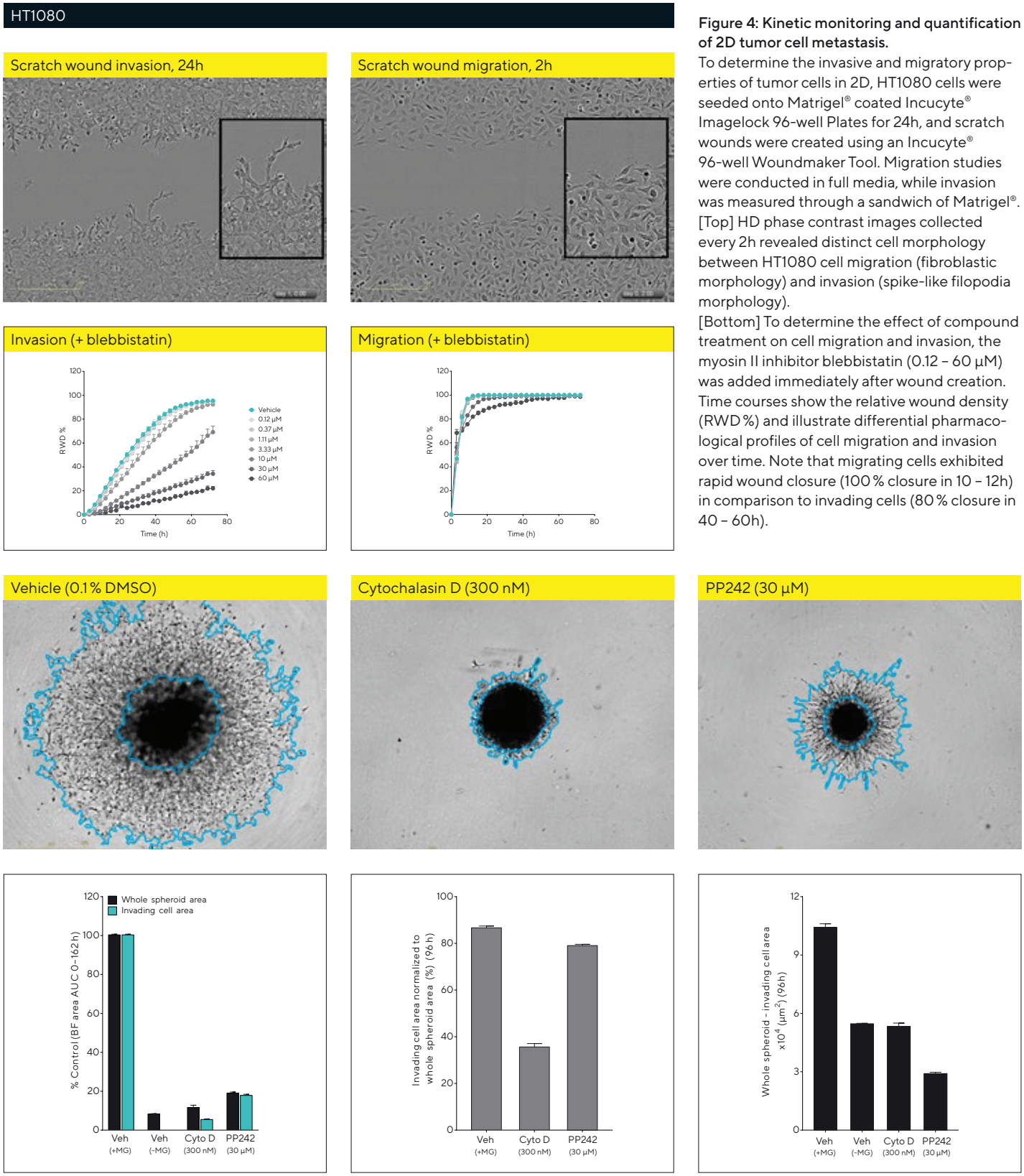

Figure 4: Kinetic monitoring and quantification of 2D tumor cell metastasis.
To determine the invasive and migratory properties of tumor cells in 2D, HT1080 cells were seeded onto Matrigel® coated Incucyte® Imagelock 96-well Plates for 24h, and scratch wounds were created using an Incucyte® 96-well Woundmaker Tool. Migration studies were conducted in full media, while invasion was measured through a sandwich of Matrigel®. [Top] HD phase contrast images collected every 2h revealed distinct cell morphology between HT1080 cell migration (fibroblastic morphology) and invasion (spike-like filopodia morphology).
[Bottom] To determine the effect of compound treatment on cell migration and invasion, the myosin II inhibitor blebbistatin (0.12 – 60 µM) was added immediately after wound creation. Time courses show the relative wound density (RWD %) and illustrate differential pharmacological profiles of cell migration and invasion over time. Note that migrating cells exhibited rapid wound closure (100 % closure in 10 – 12h) in comparison to invading cells (80 % closure in 40 – 60h).

Figure 5: Effect of cell signaling inhibitors on spheroid invasion.
To elucidate treatment effects of cell signaling inhibitors on spheroid invasion, U87-MG cells were seeded in a round bottom ULA 96-well plate (2,500 cells/well) and allowed to form 3D spheroids prior to treatment with cytochalasin D (300 nM) or PP242 (30 µM). Spheroids were subsequently embedded in Matrigel® (4.5 mg/mL) to induce invasion and incubated in an Incucyte® Live-Cell Analysis System for 162 h, with data collection at 6h intervals. [Top] brightfield images (4× magnification) taken 4 days post-treatment show the effects of cytochalasin D/PP242 on spheroid invasion. [Bottom left] Bar chart representing the area under the curve analysis of the whole spheroid (Black) and invading cell area (Teal) at 0 – 162h post-treatment. Cytochalasin D and PP242 reduced overall spheroid size by 90 % and 80 % respectively. [Bottom center] Data normalization (96 h post-treatment) revealed that only cytochalasin D effectively inhibited the invasive phenotype. [Bottom right] Subtraction of the invading cell area from the whole spheroid area provided a measure for spheroid proliferation, and showed the anti-proliferative rather than anti-invasive properties of PP242.

5. Metabolic rewiring

There are various ways that the metabolism of cancer cells can be 'rewired' to provide selective advantages, such as increased uptake of glucose, amino acids or nitrogen, opportunistic nutrient acquisition, use of glycolysis and TCA cycle intermediates, or altered gene regulation. Characterizing these aberrant metabolic activities can provide greater insight into tumor progression, as well as potentially offering new therapeutic targets.

Investigating how this reprogramming of the metabolic pathways occurs is a priority for researchers looking to target these activities, and long-term, live-cell studies are proving vital. The rewiring of both metastatic breast cancer and malignant melanoma have both been looked at using this approach[40], with a further study also looking at how alterations to metabolic activity affect characteristics such as invasion[41] and chemoresistance[42].

Abnormal nutrient uptake and usage is another area currently garnering a lot of interest, due to the obvious potential to 'starve' tumors. Figure 6 shows how the glutaminase blocker CB-839 can be used to effectively 'starve' the triple-negative breast cancer cell line MDA-MB-231 of ATP, leading to a sustained, concentration-dependent decrease inhibition of ATP levels. In another recent example, raltime apoptosis assays were used to demonstrate that endothelial cells infected with Kaposi's sarcoma-associated herpesvirus become glutamine 'addicted' – similar to many cancer cells – and that glutamine starvation leads to apoptosis[43]. Live-cell imaging has also been used to monitor and quantify the effects of NAD depletion – a proposed therapeutic strategy – on proliferation, motility and cell death[44].

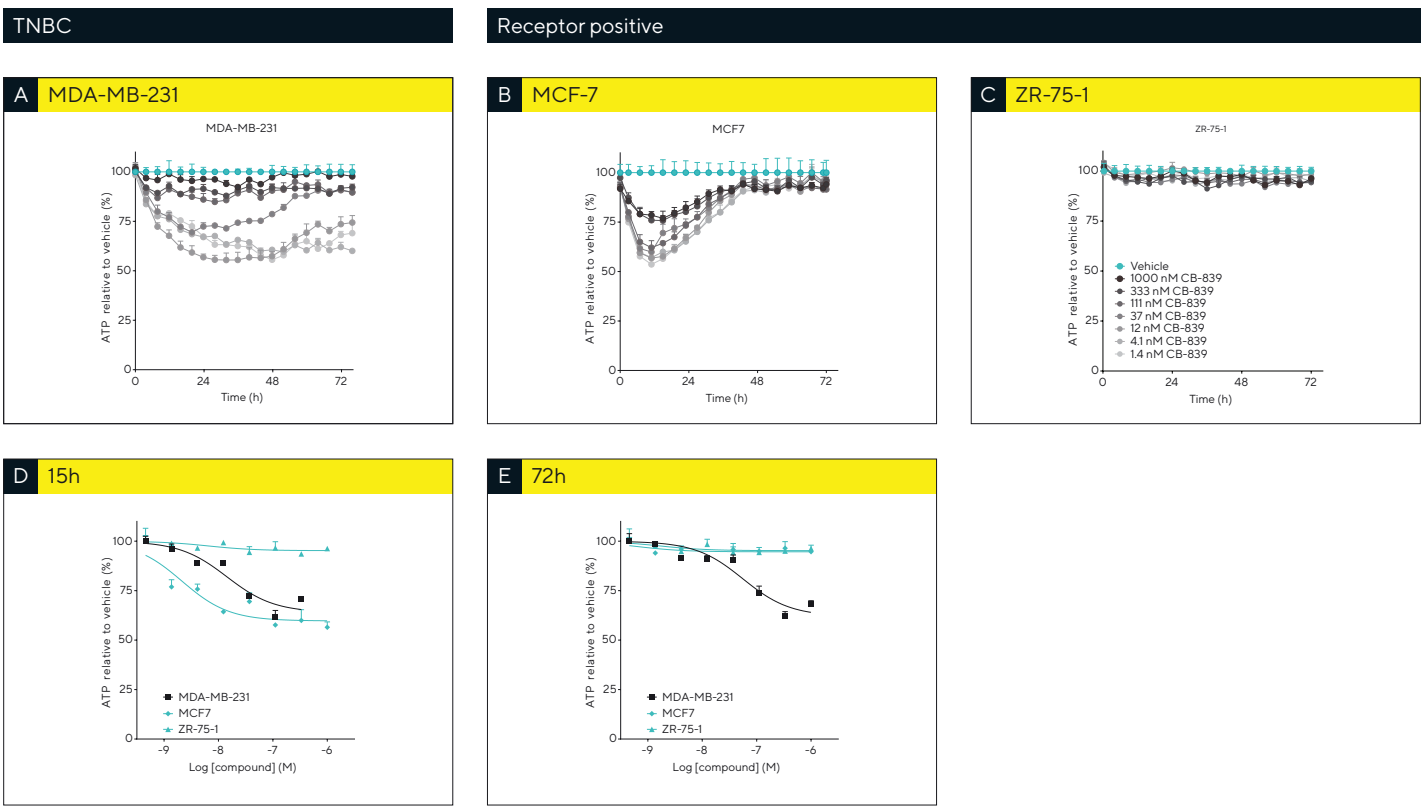

Figure 6: Inhibition of glutaminase selectively attenuates ATP levels in triple-negative breast cancer (TNBC).
The TNBC cell line MDA-MB-231 and receptor-positive breast cancer cell lines MCF-7 and ZR-75-1 (all stably expressing Incucyte® CytoATP Lentivirus or Incucyte® CytoATP Non-Binding Control Lentivirus) were seeded at 8K cells/well, and cellular changes in ATP were quantified using the Incucyte® ATP Analysis Software Module.
The glutaminase blocker CB-839 causes a sustained, concentration-dependent decrease inhibition of ATP levels in MDA-MB-231 cells [Top left], whereas only a transient reduction was observed in MCF-7 cells [Top center]. In contrast, little or no effect was observed in ZR-75-1 cells [Top right]. Concentration response curves taken at 15h [Bottom left] and 72h [Bottom right] support the observation that CB-839 causes sustained decrease of ATP levels in MDA-MB-231 cells.

6. Immune modulation

The immune system's constant surveillance for developing cancer cells clearly plays a role in tumor suppression and eradication, but this also places selective pressures on these cell populations. This can lead to so-called 'cancer immunoediting', providing a selective advantage to variants which can 'escape' the innate and adaptive immune responses. This has become an increasingly hot topic over the last five years, particularly the interactions between cancer cells and natural killer or cytotoxic T cells.

However, it has become clear that this is an over-simplification of the tumor-host immunological interactions, and many cancer cells may evade immune destruction by actively disabling immune system components. The Incucyte® Live-Cell Analysis is proving a valuable tool for investigating the behaviors of immune cells – such as innate immune response[45], T cell activation, clustering and chemotaxis – both independently and in co-culture with tumor cells using 2D and 3D immune cell killing and phagocytosis studies[46] (Figure 7, 8). The system's unique design, where the optical path moves around the static cell plate, allows non-perturbing imaging studies on a wide range of cell types, including non-adherent cells (e.g. white blood cells).

A number of new reagents – including nuclear-targeted fluorescent probes (e.g. Incucyte® Nuclight Reagents) for labeling tumor cells and pH-sensitive dyes for tracking internalization – are now being widely used in combination with the Incucyte® Live-Cell Analysis System to create time-lapse movies. This strategy has been particularly helpful in elucidating the physical interaction between immune and cancer cells, as well as the resulting morphological changes. This technology is also now a proven frontline technology for developing new immunotherapies, such as CAR-T[47], checkpoint inhibitors[48], T cell activators[49], monocytes and macrophages stimulators[50], cancer vaccines[51] and oncolytic viruses[52].

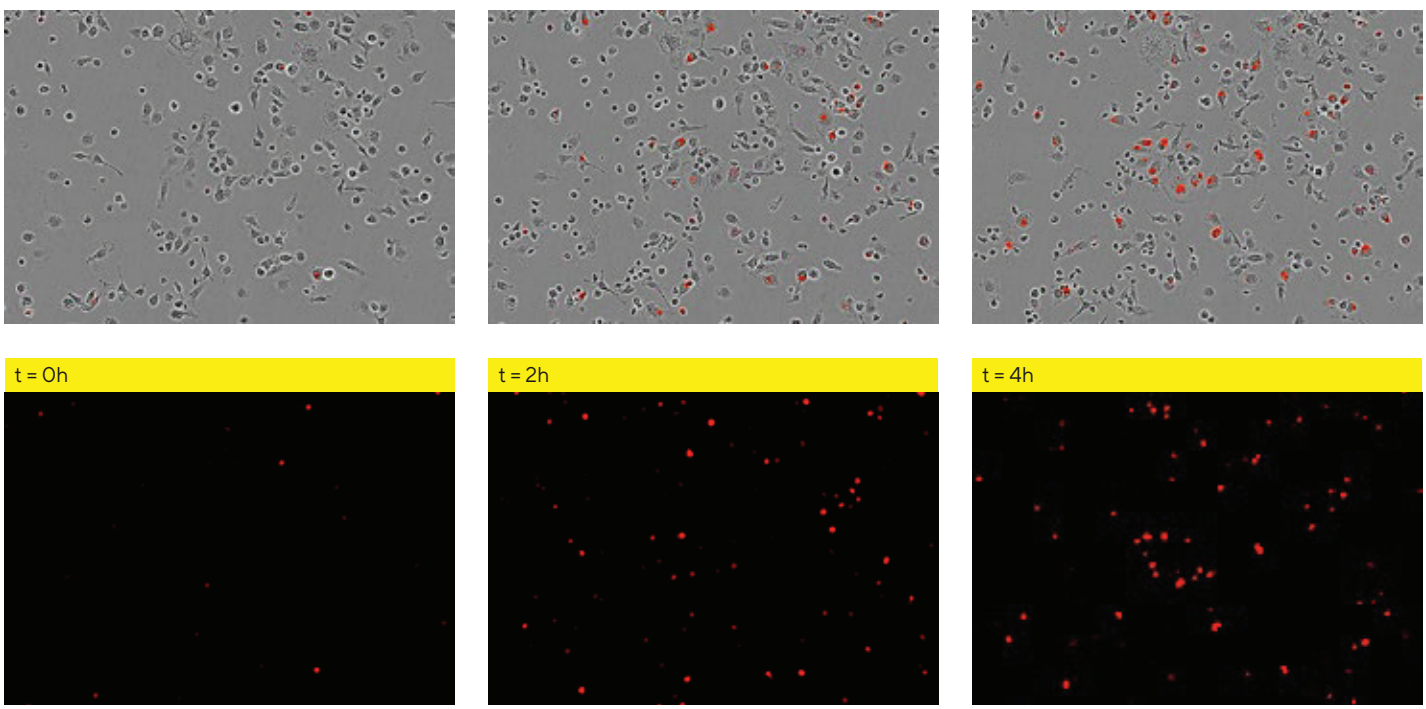

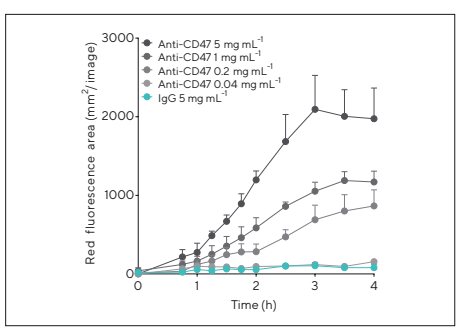

Figure 7: Blockade of CD47 'don't eat me' signal by monoclonal antibodies induces phagocytosis of target tumor cells.
Primary mouse bone marrow derived macrophages (BMDM) were seeded into a 96-well plate at 10K cells/well. CCRF-CEM acute lymphocytic leukemia cells were labelled with the Incucyte® pHrodo® Red Cell Labelling Kit, and incubated with anti-CD47 (clone B6H12, 0-5 µg/mL) or isotype control IgG1 (0-5 µg/mL) for 30 minutes prior to addition to BMDM assay plates (15K cells/well). Phase contrast [Top] and fluorescence-blended [Bottom] images show increased fluorescence within the cytoplasm of BMDM in the presence of CCRF-CEM (anti-CD47, 5 µg/mL) over time. [Right] The time course demonstrates that the presence of anti-CD47 led to an increase in fluorescence intensity as the pH-sensitive label is moved into an acidic phagolysosome, indicating that live CCRF-CEM cells have been engulfed. This increase in fluorescence was not observed in the presence of the non-binding control antibody (teal line).

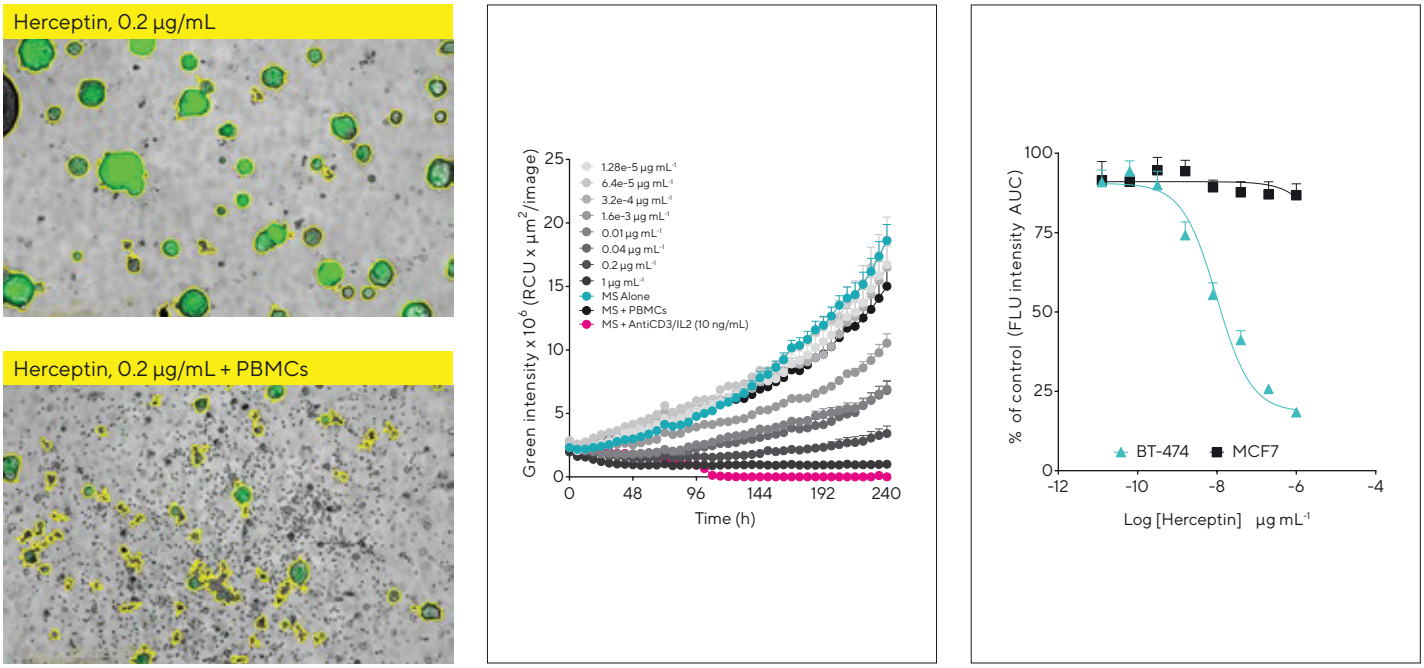

Figure 8: Herceptin-induced, antibody-dependent cell-mediated cytotoxicity (ADCC) of breast cancer multi-spheroids.
BT474 cells expressing Incucyte® Cytolight Green Lentivirus (2K cells/well) were seeded onto a layer of basement membrane extract (Matrigel®, >4.5 mg/mL) and multi-spheroids were formed for 3 days. Peripheral blood mononuclear cells (PBMCs) were isolated from fresh blood and added to the multi-spheroids in the presence of either anti-Her2 (trastuzumab, 0-1 µg/mL) or activation cytokines (anti-CD3 and IL-2, both 10 ng/mL). Phase contrast, brightfield and fluorescence images were acquired every 6 h for 10 days. Blended brightfield and green fluorescence images of trastuzumab-treated spheroids in the absence [Top left] and presence [Bottom left] of effector PBMCs show that spheroids are smaller with lower fluorescence intensity in the presence of effector cells, as the green-expressing target cells lose viability. [Right] Time course shows a trastuzumab concentration-dependent decrease in green fluorescence, indicating a reduction in the number of viable target cells.

7. An abetting microenvironment

Tumors do not grow in isolation, and there is continuous communication between cancerous and stromal cells throughout all stages of carcinogenesis. There is still much confusion – and several conflicting theories – around how this microenvironment influences tumor growth but, over the past decade, tumors have increasingly been seen as complex organs. When viewed from this perspective, the biology of a tumor can only be understood by studying the individual specialized cell types within and around it.

Live-cell imaging has been used to analyze the function of a wide range of biomatrices and important tumor-associated cells – including stroma[53, 54], fibroblasts[55], endothelia[56, 57] and pericytes[58]. This technology is also allowing researchers to observe spatial and temporal cellular interactions of co-culture tumor models in real time (Figure 9), providing unprecedented insights into dynamic changes in the tumor microenvironment, as well as highlighting previously overlooked therapeutic targets. For example, Incucyte® co-culture invasion assays have helped to elucidate the role of cancer-associated fibroblasts in cancer cell invasion driven by extracellular matrix remodeling[59]. In another co-culture study, the system was used to demonstrate the transfer of microRNAs between cells in in vitro models of osteosarcoma and ovarian cancer[60].

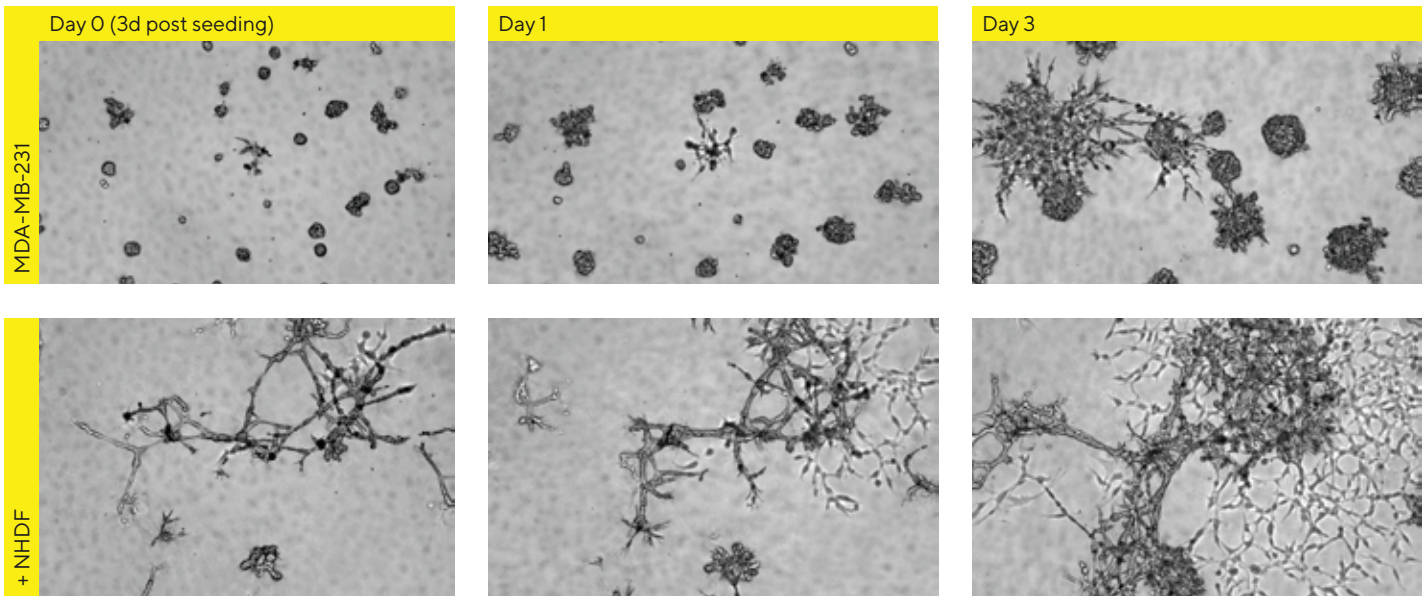

Figure 9: Temporal effects of fibroblasts on tumor multi-spheroid morphology.
MDA-MB-231 cells were seeded in flat bottom 96-well plates on a bed of Matrigel® (>4.5 mg/mL) in mono-culture (1,000 cells/well), or co-cultured with normal human dermal fibroblasts (NHDFs, 1:1 ratio, 1,000 cells/well) and multi-spheroids allowed to form for 3 days. Depth of focus brightfield (BF) images were captured every 6 h for up to 10 days, using the Incucyte® Spheroid Analysis Software Module. BF images compare mono- and co-culture conditions over 3 days (6 days post-cell seeding). Note the temporal impact of NHDFs on spheroid morphology. In the presence of NHDFs, MDA-MB-231 multi-spheroids instantly exhibited a more stellate invasive phenotype. These stellate protrusions were only observed 3 days post-formation in the mono-culture model. Bar chart shows the Total brightfield Object Area of MDA-MB-231 in mono- or co-culture, illustrating the impact of NHDFs on multi-spheroid size over time.

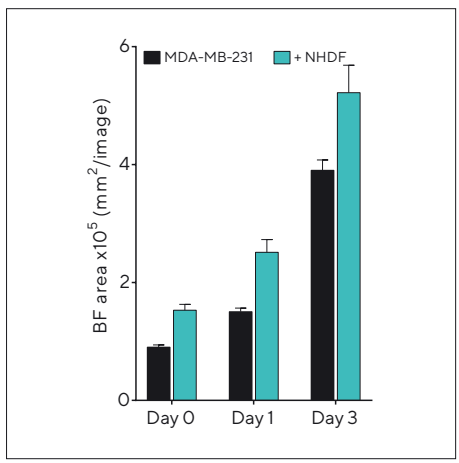

Summary

We have made significant progress in our understanding of the seven hallmarks of cancer in recent years, and are now starting to look to the potential of what we can do with this information in future research. While each hallmark is well defined individually, we now need to explore new models that will allow us to piece these features back together and analyze them as a whole, in order to gain more context around their biological relationship.

One of the key factors dictating the rate of progress has been the availability of suitable investigative tools; from biochemical assay reagents and sequencing chemistries to patient-derived primary tissue samples, 3D cell culturing methods and novel imaging systems. Thanks to rapid advances in technology, we have now demonstrated a whole host of models that can be used to research these various aspects of cancer, paving the way for the next step of the journey.

As this whitepaper documents, live-cell imaging and analysis using the Incucyte® Live-Cell Analysis System continues to play a central role in the elucidation of cancer biology, as well as providing more effective and relevant ways of evaluating potential therapeutics. Based on the evidence so far, this real-time imaging capability will remain increasingly important to building upon our understanding of the complex behavior of tumors, and how the hallmarks of cancer interact and influence each other.

References

Introduction

1. Hanahan D & Weinberg, RA. The hallmarks of cancer. Cell, 2000, 100(1), 57-70.
2. Hanahan D & Weinberg, RA. The hallmarks of cancer: The Next Generation. Cell, 2011, 144(1), 646-674.
3. Fouad, YA & Aanei, C. Revisiting the hallmarks of cancer. American Journal of Cancer Research. 2017, 7(5), 1016-1036.

Selective proliferative advantage

4. Miettinen et al. Mammalian cell growth dynamics in mitosis. eLife, 2019, 8, e44700.
5. Tang, B et al. A Flexible Reporter System for Direct Observation and Isolation of Cancer Stem Cells. Stem Cell Reports, 2015, 4, 155-169.
6. Nair, R et al. c-Myc and Her2 cooperate to drive a stem-like phenotype with poor prognosis in breast cancer. Oncogene, 2014, 33(30), 3992-4002.
7. Blum, W et al. Stem Cell Factor-Based Identification and Functional Properties of InVitro-Selected Subpopulations of Malignant Mesothelioma Cells. Stem Cell Reports, 2017, 8(4), 1005-1017.
8. Craveiro, V et al. Phenotypic modifications in ovarian cancer stem cells following Paclitaxel treatment. Cancer Medicine, 2013, 2(6), 751–762.

Altered stress response

9. Balvers, RK et al. ABT-888 enhances cytotoxic effects of temozolomide independent of MGMT status in serum free cultured glioma cells. Journal of Translational Medicine, 2015, 13, 74.
10. Gautam, P et al. Identification of selective cytotoxic and synthetic lethal drug responses in triple negative breast cancer cells. Molecular Cancer, 2016, 15, 34.
11. Kalimutho, M et al. Enhanced dependency of KRAS mutant colorectal cancer cells on RAD51-dependent homologous recombination repair identified from genetic interactions in Saccharomyces cerevisiae. Molecular Oncology, 2017, 11(5), 470-490.
12. Single, A et al. A Comparison of Real-Time and Endpoint Cell Viability Assays for Improved Synthetic Lethal Drug Validation. Journal of Biomolecular Screening, 2016, 20(10), 1286-1293.
13. Gelles, JD & Chipuk, JE. Robust high-throughput kinetic analysis of apoptosis with real-time high-content live-cell imaging. Cell Death & Disease, 2016, 7, e2493.
14. Aftab, ON et al. Label free high throughput screening for apoptosis inducing chemicals using time-lapse microscopy signal processing. Apoptosis, 2014, 19(9), 1411-1418.
15. Artymovich, K & Appledorn, DM. A multiplexed method for kinetic measurements of apoptosis and proliferation using live-content imaging. Apoptosis and Cancer: Methods and Protocols, 1219, 35-42, 2014, 2014. Methods in Molecular Biology, 2015, 1219, 35-42.
16. Hoare, M et al. NOTCH1 mediates a switch between two distinct secretomes during senescence. Nature Cell Biology, 2016, 18, 979-992.
17. Lahtela, J et al. A high-content cellular senescence screen identifies candidate tumor suppressors, including EPHA3. Cell Cycle, 2013, 12(4), 625-634.

Vascularization

18. Wolfe, A et al. Pharmacologic characterization of a kinetic in vitro human co-culture angiogenesis model using clinically relevant compounds. Journal of Biomolecular Screening, 2013, 18(10), 1234-1245.
19. Falcon, BL et al. Development and characterization of a high-throughput in vitro cord formation model insensitive to VEGF inhibition. Journal of Hematology & Oncology, 2013, 6, 31.
20. Yang M et al. Lysyl oxidase assists tumor initiating cells to enhance angiogenesis in hepatocellular carcinoma. International Journal of Oncology, 2019, 54, 1398-1408.

21. Egbivwie N et al. FGFR1 Expression and Role in Migration in Low and High Grade Pediatric Gliomas. Frontiers in Oncology, 13 March 2019.
22. Kim, TK et al. Heat shock protein 70-1A is a novel angiogenic regulator. Biochemical and Biophysical Research Communications, 2016, 469(2), 222-228.
23. Li, J et al. Piezo1 integration of vascular architecture with physiological force. Nature, 2014, 515(7526), 279-282.
24. Strese, S et al. The novel alkylating prodrug melflufen (J1) inhibits angiogenesis in vitro and in vivo. Biochemical Pharmacology, 2013, 86(7), 888-895.
25. Neshatian, M et al. Determining the Size Dependence of Colloidal Gold Nanoparticle Uptake in a Tumor-like Interface (Hypoxic). Colloids and Interface Science Communications, 2014, 1, 57-61.
26. Sonke, E et al. Inhibition of endogenous hydrogen sulfide production in clear-cell renal cell carcinoma cell lines and xenografts restricts their growth, survival and angiogenic potential. Nitric Oxide, 2015, 49, 26-39.

Invasion and metastasis

27. Vinci M et al. Functional diversity and co-operativity between subclonal populations of paediatric glioblastoma and diffuse intrinsic pontine glioma cells. Nature Medicine, 2018, 24(8), 1204-1215.
28. Härmä, V et al. A comprehensive panel of three-dimensional models for studies of prostate cancer growth, invasion and drug responses. PLoS One, 2010, 5(5), e10431.
29. Mitra M et al. Alternative polyadenylation factors link cell cycle to migration. Genome Biology, 2018, 19, 176.
30. O'Clair, L et al. Visualize Chemotaxis in Real Time: Kinetic, Automated, Image-Based Cell Migration Assay. Genetic Engineering & Biotechnology News, 2017, 37, 7.
31. Sartorius, CA et al. Estrogen promotes the brain metastatic colonization of triple negative breast cancer cells via an astrocyte-mediated paracrine mechanism. Oncogene, 2016, 35(22), 2881-2892.
32. Brix DM et al. Release of transcriptional repression via ErbB2-induced, SUMO directed phosphorylation of myeloid zinc finger-1 serine 27 activates lysosome redistribution and invasion. Oncogene, 2019, 38, 3170-3184.
33. Härmä, V et al. Quantification of Dynamic Morphological Drug Responses in 3D Organotypic Cell Cultures by Automated Image Analysis. PLoS One, 2014, 9(5), e96426.
34. Clarke, K et al. Inference of Low and High-Grade Glioma Gene Regulatory Networks Delineates the Role of Rnd3 in Establishing Multiple Hallmarks of Cancer. PLoS Genetics, 2015, 11(7), e1005325.
35. Gujral, TS et al. Noncanonical Frizzled2 Pathway Regulates Epithelial-Mesenchymal Transition and Metastasis. Cell, 2014, 159, 844-856.
36. Mannion AJ et al. CD99 regulates cancer cell transendothelial migration and endothelial cell function via CDC42 and actin remodelling. bioRxiv, 2019, 760934.
37. Circu, ML et al. A Novel High Content Imaging-Based Screen Identifies the Anti-Helminthic Niclosamide as an Inhibitor of Lysosome Anterograde Trafficking and Prostate Cancer Cell Invasion. PLoS ONE, 2016, 11(1), e0146931.
38. Hulkower, KI & Herber, RL. Cell Migration and Invasion Assays as Tools for Drug Discovery. Pharmaceutics, 2011, 3(4), 107-124.
39. Neri, S et al. Cancer cell invasion driven by extracellular matrix remodeling is dependent on the properties of cancer-associated fibroblasts. Journal of Cancer Research and Clinical Oncology, 2016, 142(2), 437-446.

Metabolic rewiring

40. Serguienko, A et al. Metabolic reprogramming of metastatic breast cancer and melanoma by let-7a microRNA. Oncotarget, 2015, 6(4), 2451-2465.
41. Bettum, IJ et al. Metabolic reprogramming supports the invasive phenotype in malignant melanoma. Cancer Letters, 2015, 366(1), 71-83.
42. Deblois, G et al. ERR mediates metabolic adaptations driving lapatinib resistance in breast cancer. Nature Communications, 2016, 7, 12156.
43. Ferguson, J et al. Glucose availability controls ATF4-mediated MITF suppression to drive melanoma cell growth. Oncotarget, 2017, 8(20), 32946-32959.
44. Del Nagro, C et al. Depletion of the central metabolite NAD leads to oncosis-mediated cell death. Journal of Biological Chemistry, 2014, 289(51), 35182-35192.

Immune modulation

45. Aarreberg LD et al. Interleukin-1b Induces mtDNA Release to Activate Innate Immune Signaling via cGAS-STING. Molecular Cell, 2019, 74(4), 801–815, e6.
46. Wolf-Dennen K at al. Exosomal communication by metastatic osteosarcoma cells modulates alveolar macrophages to an M2 tumor-promoting phenotype and inhibits tumoricidal functions. OncoImmunology, 2020, 9(1), 1747677.
47. Foster, AE et al. Regulated expansion and survival of chimeric antigen receptor-modified T cells using small molecule-dependent inducible MyD88/CD40. Molecular Therapy, 2017, 25(9), 2176-2188.
48. Lau, J et al. Tumour and host cell PD-L1 is required to mediate suppression of anti-tumour immunity in mice. Nature Communications, 2017, 8, 14572.
49. Boudousquie, C et al.Polyfunctional response by ImmTAC (IMCgp100) redirected CD8(+) and CD4(+) T cells. Immunology, 2017, 152(3), 425-438.
50. Rubin J et al. Mebendazole stimulates CD14+ myeloid cells to enhance T-cell activation and tumour cell killing. Oncotarget, 2018, 9(56), 30805-30813.

51. Laubreton, D et al. The fully synthetic MAG-Tn3 therapeutic vaccine containing the tetanus toxoid-derived TT830-844 universal epitope provides anti-tumor immunity. Cancer Immunology, Immunotherapy, 2016, 65(3), 315-325.
52. Dobson, CC et al. Oncolytic virus synergizes with Smac mimetic compounds to induce rhabdomyosarcoma cell death in a syngeneic murine model. Oncotarget, 2017, 8(2), 3495-3508.

An abetting microenvironment

53. Kasashima, H et al. Bone marrow-derived stromal cells are associated with gastric cancer progression. Journal of Cancer, 2015, 113(3), 443-452.
54. Kucerova, L et al. Altered features and increased chemosensitivity of human breast cancer cells mediated by adipose tissue-derived mesenchymal stromal cells. BMC Cancer, 2013, 13(1), 535.
55. Kasashima, H et al. Lysyl oxidase-like 2 (LOXL2) from stromal fibroblasts stimulates the progression of gastric cancer. Cancer Letters, 2014, 354(2), 438-446.
56. Arutyunyan, IV et al. Angiogenic Potential of Multipotent Stromal Cells from the Umbilical Cord: an In Vitro Study. Experimental Biology and Medicine, 2016, 161(1), 141-149.
57. Tokumoto, MW et al. Identification of tumour-reactive lymphatic endothelial cells capable of inducing progression of gastric cancer. Journal of Cancer, 2015, 113(7), 1046-1054.
58. Joensuu, K et al. Angiogenic potential of human mesenchymal stromal cell and circulating mononuclear cell co-cultures is reflected in the expression profiles of proangiogenic factors leading to endothelial cell and pericyte differentiation. Journal of Tissue Engineering and Regenerative Medicine, 2017, 1-9 (ePub ahead of print).
59. Neri, S et al. Cancer cell invasion driven by extracellular matrix remodeling is dependent on the properties of cancer-associated fibroblasts. Journal of Cancer Research and Clinical Oncology, 2016, 142(2), 437-446.
60. Thayanithy, V et al. Tumor-stromal cross talk: direct cell-to-cell transfer of oncogenic microRNAs via tunneling nanotubes. Translational Research, 2014, 164(5), 359-365.

Reports

BioTechniques

2D and 3D *in vitro* assays to quantify the invasive behavior of glioblastoma stem cells in response to SDF-1α

Vashendriya VV Hira[1], Barbara Breznik[1], Cornelis JF Van Noorden[1,2], Tamara Lah[1] & Remco J Molenaar*[,1,2,3]

*[1]Department of Genetic Toxicology & Cancer Biology, National Institute of Biology, Ljubljana, Slovenia; [2]Department of Medical Biology, Cancer Center Amsterdam, Amsterdam UMC at The Academic Medical Center, Amsterdam, The Netherlands; [3]Department of Medical Oncology, Cancer Center Amsterdam, Amsterdam UMC at The Academic Medical Center, Amsterdam, The Netherlands; *Author for correspondence: r.j.molenaar@amsterdamumc.nl*

BioTechniques 69: 339–346 (November 2020) 10.2144/btn-2020-0046

First draft submitted: 14 April 2020; Accepted for publication: 27 July 2020; Published online: 1 September 2020

ABSTRACT

Invasion is a hallmark of cancer and therefore *in vitro* invasion assays are important tools in cancer research. We aimed to describe *in vitro* 2D transwell assays and 3D spheroid assays to quantitatively determine the invasive behavior of glioblastoma stem cells in response to the chemoattractant SDF-1α. Matrigel was used as a matrix in both assays. We demonstrated quantitatively that SDF-1α increased invasive behavior of glioblastoma stem cells in both assays. We conclude that the 2D transwell invasion assay is easy to perform, fast and less complex whereas the more time-consuming 3D spheroid invasion assay is physiologically closer to the *in vivo* situation.

METHOD SUMMARY

We describe 2D transwell invasion assays and 3D spheroid invasion assays for the investigation of effects of the chemoattractant SDF-1α on human glioblastoma stem cells *in vitro* in a quantitative manner using image analysis. In both *in vitro* invasion assays, Matrigel was used as the matrix that glioblastoma stem cells invade. The 2D assay is easy to perform, fast and less complex whereas the 3D assay models the *in vivo* situation more closely.

KEYWORDS:

2D transwell invasion assay ● 3D spheroid invasion assay ● cancer cell ● cellular invasion ● glioblastoma stem cells

Invasive behavior is a hallmark of cancer and a major reason why the disease is hard to eradicate, causing poor patient prognosis [1–3]. Invasive cancer cells migrate through the extracellular matrix (ECM), enabled by the secretion of proteases to degrade the ECM and alterations in the cytoskeleton [4–6].

Multiple *in vitro* assays and models are available to study cellular migration and invasion, such as the scratch assay, 3D bioscaffolds and microfluidic co-cultures [3,7–11]. Frequently used invasion assays are the transwell invasion assay (2D invasion assay) [3,8,12,13] and the spheroid invasion assay (3D invasion assay) [5,12,14–16]. The latter two types of invasion assays are discussed in this article. Both types of *in vitro* invasion assays are relatively easy to perform, fast, reproducible and cheap. Although the 3D invasion assay is more complex than the 2D invasion assay, it is physiologically more relevant because it represents the *in vivo* situation in solid tumors more accurately. In 3D invasion assays, cancer cells not only invade through a matrix, but are also affected by other cancer cells in their direct surroundings. Cancer cells need to change and modify their surrounding environment in order to invade, which is also the case in the *in vitro* invasion assays [1,17]. *In vitro* invasion assays are generally preferred over *in vivo* invasion experiments using fluorescently-labeled cells and intravital imaging in animal models because of ethical concerns and the high costs of animal models. Furthermore, the *in vitro* invasion assays are more controllable, more flexible and easier to modify [1,18,19].

In this article, we describe the *in vitro* 2D transwell invasion assay and the 3D spheroid invasion assay in detail with the use of a brain tumor patient-derived glioblastoma stem cell (GSC) line. GSCs have been used instead of differentiated glioblastoma cells, because they have a higher invasive potential than differentiated glioblastoma cells [20,21]. The presence of cell surface protein L1CAM and the intracellular PI3K/AKT and Notch signaling pathways are involved in the highly elevated invasive potential of GSCs compared with differentiated glioblastoma cells [21,22]. Therefore, GSCs are a suitable cell type to demonstrate cellular invasion. GSCs as well as differentiated glioblastoma cells express CXCR4, a specific receptor for the chemoattractant SDF-1α, which we found to be highly expressed in hypoxic peri-arteriolar GSC niches in glioblastoma patient samples where GSCs are maintained in the tumors and protected from chemotherapy and radiotherapy because of their quiescence [23–25]. Interactions between SDF-1α and CXCR4 have been reported

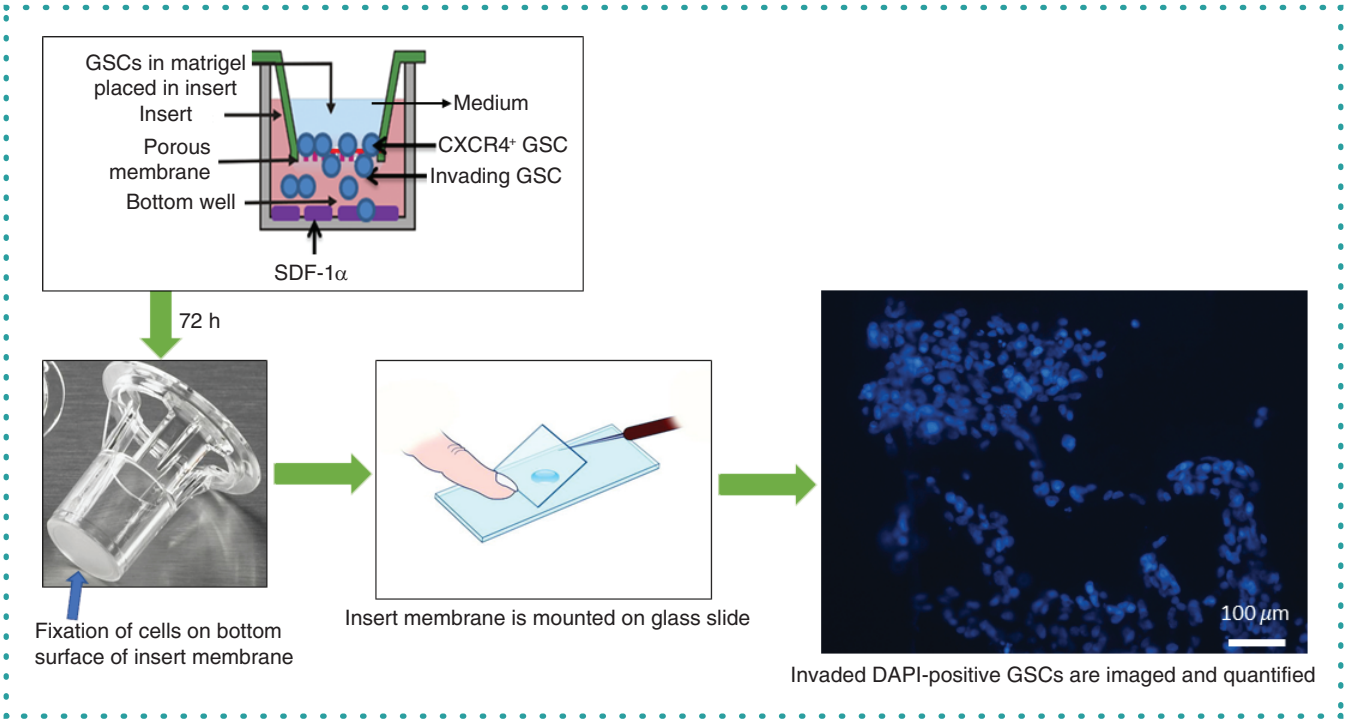

Figure 1. Schematic overview of the 2D transwell invasion assay. CXCR4-positive GSCs in Matrigel-containing medium are placed in the top wells (inserts) in the presence or absence of chemoattractant SDF-1α in the medium in bottom wells. Invaded GSCs accumulate at the bottom surface of the insert membrane (blue arrow). After 72 h, cells on the bottom surface of insert membranes are fixed and the membrane is cut out of the insert. The membrane is mounted on a microscopic slide, followed by imaging and quantification of DAPI-positive GSCs using image analysis. Scale bar = 100 μm. DAPI: 4′,6-diamidino-2-phenylindole; GSC: Glioblastoma stem cell.

to be involved in cellular invasive behavior in glioblastoma [26–29] and the SDF-1α–CXCR4 axis enables invasion of CXCR4-positive glioblastoma cells into SDF-1α-rich niches and transformation into GSCs [23–25].

In the 2D and 3D invasion assays, Matrigel is used as a matrix. In this study we aimed to quantitatively determine the invasive cellular behavior of CXCR4-expressing GSCs in the presence and absence of SDF-1α. In addition, we aimed to assess the advantages and disadvantages of both types of *in vitro* invasion assays.

Materials & methods

Cell culture

NCH421k GSCs [30,31] were a generous gift from Christel Herold-Mende (Heidelberg University, Heidelberg, Germany) and were cultured as non-adherent 3D spheroids in Neurobasal™ medium (Gibco, Life Technologies, CA, USA) containing 1% penicillin/streptomycin (Sigma, MO, USA), 1% L-glutamine (Sigma), 2% B27 (Gibco), 0.08% bFGF (Gibco), 0.01% EGF (Gibco) and 0.01% heparin (Sigma) at 37°C in a 5% CO_2 incubator.

2D transwell invasion assay

The method of the transwell invasion assay is described step by step, to be performed chronologically to reproduce the experiment. NCH421k GSCs growing as 3D spheroids were mechanically resuspended to obtain single cells. Transwell invasion assays as shown in Figure 1 were performed using inserts with 8.0-μm pores (Corning Life Sciences, NY, USA). NCH421k GSCs (80,000 cells/insert) were used that express CXCR4 as described elsewhere [12,24]. Cells were mixed in 0.5 mg/ml Matrigel (Corning) and plated in inserts in a total volume of 50 μl, and the inserts were then placed in 24-well plates (Corning). After incubation for 30 min at 37°C in a 5% CO_2 incubator, 50 μl complete Neurobasal medium was added to the inserts to obtain a total volume of 100 μl. For the experimental condition, 600 μl complete Neurobasal medium containing 10 ng/ml SDF-1α (catalog #: 300-28A; Peprotech, NJ, USA) was added to the bottom wells. As a control, complete Neurobasal medium without SDF-1α was added to the bottom wells. After 72 h, invaded cells that accumulated on the bottom surface of the insert membranes were fixed with 4% paraformaldehyde (Merck, Darmstadt, Germany) for 20 min at room temperature, washed with 1× phosphate-buffered saline (PBS; Gibco) for 10 min and the cell nuclei were stained with the DNA dye 4′,6-diamidino-2-phenylindole (DAPI; Sigma) for 5 min, followed by a washing step with 1× PBS for 10 min. After removing the cells and Matrigel out of the inserts with cotton swabs, the membranes were cut out from the inserts with a scalpel and mounted on microscopic slides using Prolong Gold mounting medium (Life Technologies, CA, USA) for quantification of invaded DAPI-positive cells (Figure 1).

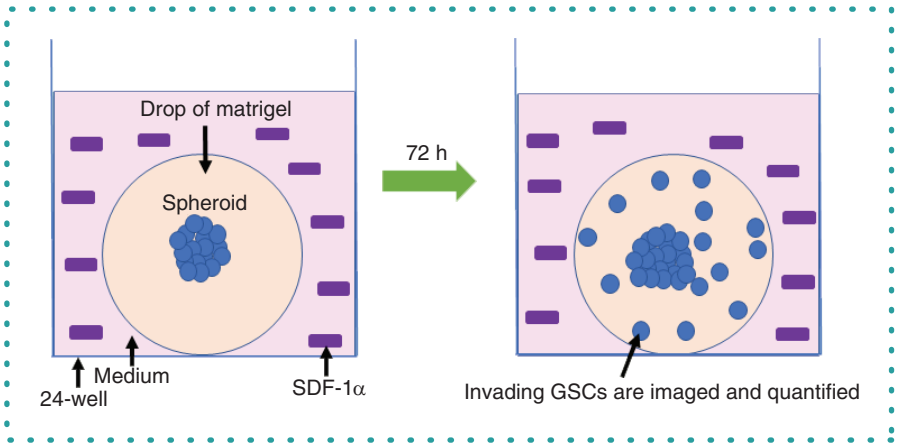

Figure 2. Schematic overview of the 3D spheroid invasion assay. After spheroid preparation in U-bottomed 96 wells, single GSC spheroids are transferred into 24-wells and embedded in a drop of Matrigel. The spheroids are covered with Neurobasal medium in the presence or absence of SDF-1α. After 72 h of incubation at 37°C, images of the spheroids are captured and the GSCs that invade from the spheroid into the Matrigel-containing medium are quantified using image analysis.
GSC: Glioblastoma stem cell.

Images of the membranes were captured using a Nikon Eclipse Ti-E fluorescence inverted microscope and the NIS-Elements AR 4.13.04 software (Nikon, Tokyo, Japan). The total number of cells in ten individual fields per condition was counted using image analysis and the ImageJ software [32,33]. Three experiments were performed, each in triplicate.

Image analysis was performed using ImageJ software and the following tools: → Analyze → Cell counter. Cells were counted by clicking on all DAPI-positive nuclei (Figure 1).

Ki67 expression to determine cell proliferation in transwell invasion assays

In order to determine whether invasion of GSCs is affected by cell proliferation during the transwell invasion assays, transmembranes were stained using the proliferation biomarker Ki67. After fixation of the cells with 4% paraformaldehyde, cell membranes were permeabilized using PBS containing 1% bovine serum albumin and 0.1% Triton-X for 30 min at room temperature. Afterward, transmembranes were incubated with anti-Ki67 antibodies conjugated with fluorescein isothiocyanate (Miltenyi Biotec, CA, USA; catalog number: 130-117-691) in a dilution of 1:50 in PBS at room temperature for 1 h. After one washing step with PBS, transmembranes were stained with DAPI for 5 min, followed by a washing step with 1× PBS for 10 min. Transmembranes were cut out of the inserts and mounted on microscopic slides using Prolong Gold mounting medium for quantification of invaded DAPI-positive and Ki67-positive cells. Images of the transmembranes were taken using a Nikon Eclipse Ti-E inverted microscope and the NIS-Elements AR 4.13.04 software. The total number of cells in ten individual fields per transmembrane was counted using image analysis and Image J software [32,33]. Three experiments were performed, each in triplicate.

Three-dimensional spheroid invasion assay

The method of the spheroid invasion assay is described step by step, to be performed chronologically to reproduce the experiment. NCH421k GSCs were seeded in complete Neurobasal medium containing 4% methylcellulose in U-bottomed 96-well plates with 3000 cells/well (BD Biosciences, CA, USA). The 4% methylcellulose was prepared as follows: 6 g of pure methylcellulose powder (Sigma, catalog # m-0512) was autoclaved and dissolved in 250 ml pre-heated complete Neurobasal medium (60°C) for 20 min using a magnetic stirrer. Then 250 ml complete Neurobasal medium (room temperature) was added, to a final volume of 500 ml, and this solution was mixed for 2 h at 4°C. The final stock solution was aliquoted and cleared by centrifugation (5000×*g*, 2 h, room temperature). Only the clear highly viscous supernatant – approximately 90–95% of the stock solution – was used for the spheroid invasion assay. The cells in U-bottomed 96-well plates were centrifuged at 850 × *g* and 31°C for 90 min and incubated at 37°C in a 5% CO_2 incubator for 72 h to form a single spheroid of similar size in each well. Spheroids were transferred into 24-well plates (Corning) and embedded in 6.0 mg/ml Matrigel (Figure 2). After 30 min of incubation at 37°C in a 5% CO_2 incubator, spheroids were covered with complete Neurobasal medium containing SDF-1α (10 ng/ml). As a control, complete Neurobasal medium without SDF-1α was used to cover the spheroids. Microscopical images were captured after 72 h using a Nikon Eclipse Ti inverted fluorescence microscope and NIS-Elements AR 4.13.04 software. The number of GSCs that invaded from the spheroids into the Matrigel was determined using image analysis and the NIS-Elements software (Figure 2) [32,33]. GSC spheroids with a minimum diameter of 40 μm were considered as spheroids [11]. Three experiments were performed, each in triplicate.

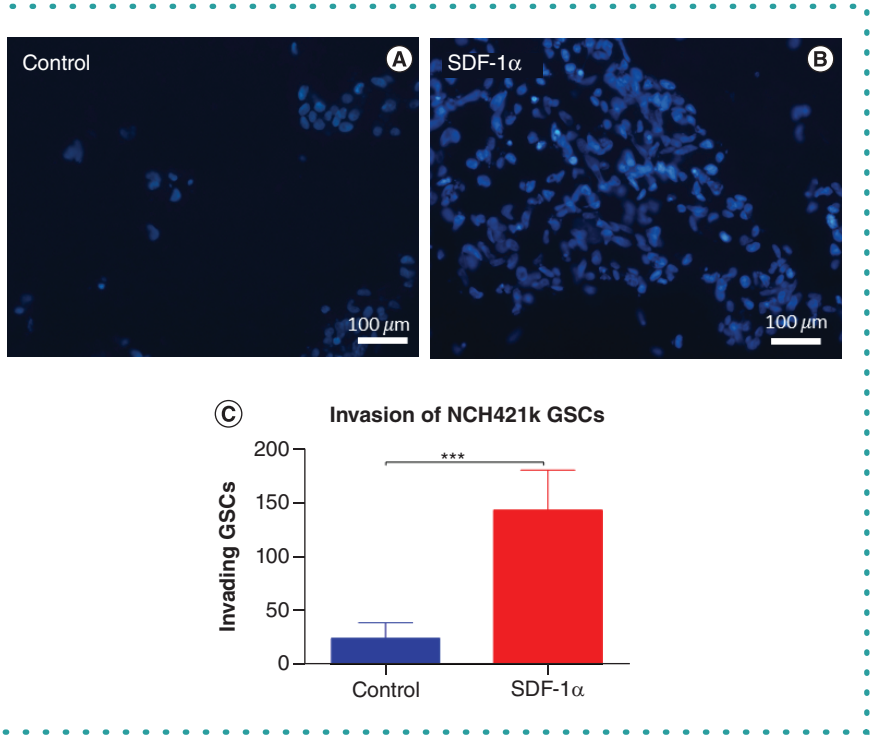

Figure 3. 2D transwell invasion data of CXCR4-positive NCH421k glioblastoma stem cells. GSCs that accumulated on the bottom surface of the insert membranes were imaged at 72 h. DAPI staining was used to show cell nuclei. In the presence of the chemoattractant SDF-1α in bottom wells, a significant increase in the average number of invading GSCs was observed as compared with the control condition without SDF-1α. Bars represent the mean number (± standard error of the mean) of invading NCH421k GSCs after 72 h of incubation in control conditions (empty medium) or in medium containing 10 ng/ml SDF-1α.
Scale bar = 100 μm. ***$p < 0.001$.
DAPI: 4′,6-diamidino-2-phenylindole; GSC: Glioblastoma stem cell.

Statistical analyses

Data was processed in Excel 2013 (Microsoft, WA, USA) and GraphPad Prism 6 (GraphPad, CA, USA) for statistical analyses using one-way analysis of variance; p-values lower than 0.05 were considered to indicate significant differences.

Results & discussion

CXCR4-positive GSCs are attracted to SDF-1α in 2D transwell invasion assays

Transwell invasion assays were performed using CXCR4-positive NCH421k GSCs in Matrigel-containing medium in inserts in the presence or absence of the chemoattractant SDF-1α in the bottom wells. Imaging of DAPI-positive GSCs on the bottom surface of insert membranes was performed at 72 h (Figure 3). Our data demonstrate a significant (sevenfold) increase in the average number of invading GSCs in the presence of SDF-1α (Figure 3B & C) as compared with the control condition, where empty medium was added to the bottom wells (Figure 3A & C). Only cells that had accumulated on the bottom surface of insert membranes were included as no cells were found in the bottom wells.

CXCR4-positive GSCs invade into Matrigel in the presence of SDF-1α in 3D spheroid invasion assays

In the 3D invasion assay, spheroids of CXCR4-positive NCH421k GSCs were embedded in Matrigel and covered with medium with or without SDF-1α (Figure 4). At 72 h, imaging was performed and the number of GSCs that invaded out of the spheroid was quantified. Our data demonstrate that the presence of SDF-1α resulted in a 1.8-fold higher number of GSCs invading from the spheroid into the Matrigel-containing medium (Figure 4B & C), as compared with the control condition (Figure 4A & C).

Proliferation of GSCs is not affected during invasion assays

To determine whether or not proliferation of GSCs is affected during invasion assays, antibodies against the proliferation biomarker Ki67 were used to detect proliferating cells on the membrane of inserts in 2D transwell invasion assays (Figure 5A). Our data demonstrate that proliferation of NCH421K GSCs was not affected; the percentage of Ki67-positive GSCs did not differ between control conditions and the wells where SDF-1α was added (Figure 5A). In the 3D spheroid invasion assays, we assessed that cells that invaded out of spheroids were always single cells and not clusters of cells (Figure 5B), confirming that GSC proliferation did not take place during invasion.

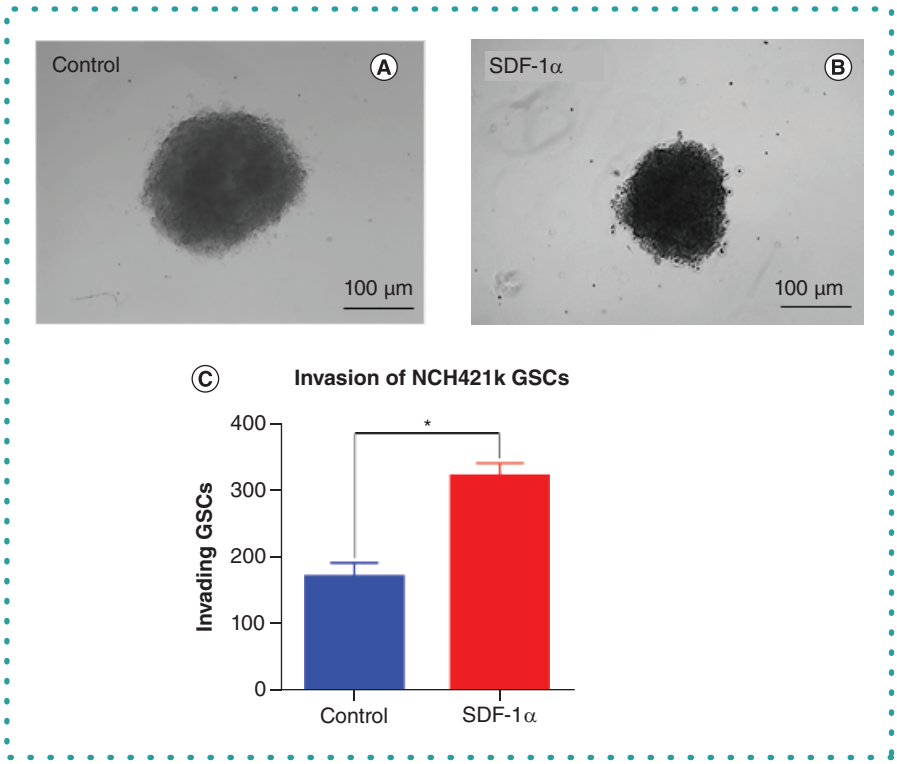

Figure 4. 3D spheroid invasion data of CXCR4-positive NCH421k glioblastoma stem cells. GSC spheroids were embedded in a drop of Matrigel that was covered with empty medium **(A)** or medium containing SDF-1α **(B)**. **(C)** Higher numbers of GSCs invaded from the spheroid in the presence of SDF-1α as compared with the control condition. Bars represent the mean number (± standard error of the mean) of invading NCH421k GSCs after 72 h from the spheroids into the Matrigel in control conditions (empty medium) or in medium containing 10 ng/ml SDF-1α. Scale bar = 100 µm.
*$p < 0.05$.
GSC: Glioblastoma stem cell.

Taken together, our data indicate that SDF-1α attracts CXCR4-positive GSCs in 2D transwell invasion assays and induces invasion of CXCR4-positive GSCs into the Matrigel in 3D spheroid invasion assays. Proliferation is not affected during invasion of GSCs in either type of *in vitro* invasion assay.

In this article, we describe two quantitative assays for the evaluation of GSC invasion *in vitro* – the 2D transwell invasion assay and a 3D spheroid invasion assay – and assess the advantages and disadvantages of each.

Our data demonstrate that both *in vitro* invasion assays are feasible experimental methods to investigate the cellular invasive behavior of cancers with invasive properties, such as glioblastoma. As an example, we demonstrate that CXCR4-positive GSCs are attracted toward SDF-1α in bottom wells in the 2D transwell invasion assays (Figure 3) and in Matrigel-containing medium around spheroids in the 3D spheroid invasion assay (Figure 4). GSCs invaded out of spheroids as single cells (Figures 4 & 5B), as reported in our previous study [12]. We also demonstrate that cell proliferation is not affected in either type of *in vitro* invasion assay (Figure 5). This is in line with studies that reported the 'go or grow' hypothesis, which states that cancer cells either invade or proliferate, because cellular invasion and proliferation do not occur simultaneously [34,35].

The major advantages of the 2D transwell and 3D spheroid invasion assays for the *in vitro* evaluation of GSC invasion are that they are technically easy to perform, relatively cheap and reproducible [3]. They can also be applied to other types of cancer (stem) cells and are now also used for drug testing, to determine whether drugs can inhibit the invasive behavior of cancer (stem) cells and their spheroid formation ability [36–41]. Chemotaxis, such as attraction between CXCR4 and SDF-1α, can be studied in an accurate manner using both assays [12]. In both assays, the presence of SDF-1α clearly results in increased invasive behavior of CXCR4-positive GSCs (Figures 3 & 4). Another advantage of 2D transwell and 3D spheroid invasion assays is that qualitative data are obtained by imaging (differences in numbers of invading GSCs can be clearly observed microscopically) and quantitative data are obtained using image analysis, which is relatively easy to perform and accurate at the same time. Alternatively, a quantitative microscopic analysis has been described for the 3D spheroid assay in which the distance of invading cells from the spheroid or invasive area is determined [15,42].

Both *in vitro* invasion assays can be performed in more complicated experimental settings by using multiple cell types – for example, CXCR4-positive GSCs in the inserts and SDF-1α-producing cells in the bottom wells, such as mesenchymal stem cells (MSCs) that are known to infiltrate glioblastoma tumors and are major SDF-1α producers [24]. Compared with experiments with exogenous SDF-1α

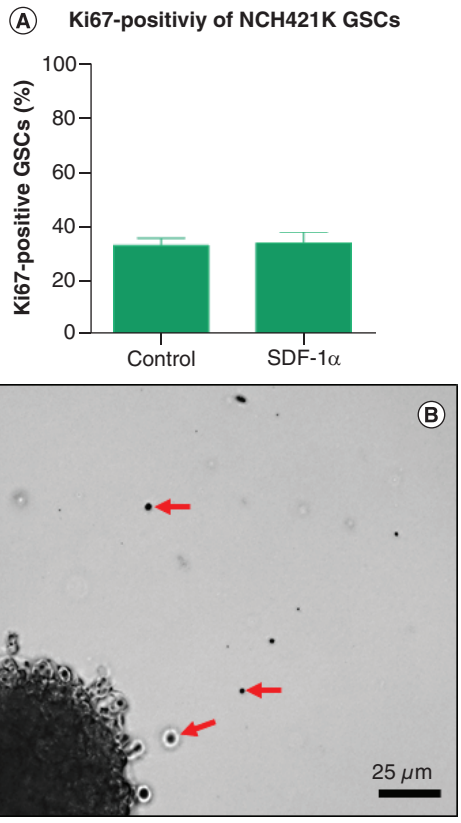

Figure 5. Proliferation of NCH421k glioblastoma stem cells was not affected during invasion assays. In the 2D transwell invasion assay, Ki67 staining was performed on GSCs that accumulated on the bottom surface of insert membranes to detect proliferating GSCs in transwell invasion assays. Imaging was performed after 72 h. **(A)** No differences were found between the percentages of proliferating Ki67-positive GSCs in control conditions and in the presence of SDF-1α in bottom wells. **(B)** NCH421k GSCs that invaded out of the spheroid in 3D spheroid invasion assays were single cells, which confirms that invading GSCs are not proliferating. Bars represent the mean number (± standard error of the mean) of invading NCH421k GSCs in the 2D transwell invasion assay after 72 h of incubation in control conditions (empty medium) or in medium containing 10 ng/ml SDF-1α. Scale bar = 25 μm. GSC: Glioblastoma stem cell.

present in the bottom wells, such experiments are both more biologically relevant (because SDF-1α is produced by MSCs in GSC niches *in vivo*) and cheaper (fewer reagents are needed because MSCs produce SDF-1α). However, it should be noted that MSCs produce a plethora of chemokines, not only SDF-1α [12,43]. Thus, to determine whether the obtained effect was caused by MSC-secreted SDF-1α, control experiments need to be performed using selective CXCR4 inhibitors like plerixafor [44]. In the 3D spheroid invasion assays, spheroid co-cultures of different fluorescently-labeled cell types can also be used to study cancer cell invasion into the 3D matrix [14]. A disadvantage of these two invasion methodologies is that the tumor microenvironment is not accurately reproduced [3,8]. More advanced and expensive *in vitro* 3D invasion methods are now available, such as 3D microfluidic co-culture systems that allow the construction of a 3D tumor microenvironment, real-time cell tracking, evaluation of interactions between different cell types, mimicking of blood flow and studies of phenomena such as cell proliferation and invasion [3,8,11,45–47]. The most true-to-nature systems are the 3D tumor organoids, in which the tumor complexity (i.e., tumor structures including blood vessels, stroma, ECM) is intact and tumor heterogeneity is present. Organoids can be used for drug testing as well for the investigation of phenomena such as cellular invasive behavior [48–55]. In future research, we aim to introduce 3D tumor organoids as a model to study glioblastoma invasion and interactions between glioblastoma cells/GSCs with other cell types in the tumor microenvironment, but both 2D transwell invasion assay and 3D spheroid invasion assay will continue to be used as well because of their own advantages. The 2D transwell invasion assay is a faster method and is less complex than the 3D spheroid invasion assay. However, it is more expensive than the 3D invasion assay because of the costs of inserts. Therefore, we suggest that the 2D transwell assay is applied first to determine whether the hypothesized chemoattractant-receptor interactions are involved in the process of cellular invasion. Afterward, cellular invasion can be studied using the more time-consuming 3D spheroid invasion assays that are more complex and closer to the *in vivo* situation. A limitation of the present study is that both *in vitro* invasion assays have been performed with the use of a single GSC line only. The application of this protocol to additional patient-derived GSC lines in the future may enable the optimization of this methodology for individual cell lines.

Besides the SDF-1α–CXCR4 axis, various other signaling axes are involved in the invasive behavior of GSCs, such as the intracellular PI3K/AKT and Notch signaling pathways [21,22]. In addition, proteases such as matrix metalloproteinases (e.g., MMP-2, MMP-9 and MMP-13), membrane-type matrix metalloproteinases and cathepsins, which degrade the ECM, are also involved in increased cancer cell invasion [5,6,56–58]. Pro-invasion soluble factors secreted from non-cancerous cells such as endothelial cells and immune cells in the tumor microenvironment [25,56,59–61] have also been reported to be involved in the invasive behavior of GSCs.

In conclusion, both 2D transwell invasion assays and 3D spheroid invasion assays are accurate and reproducible *in vitro* methodologies to study GSC invasion and are also applicable to other types of cancer. We conclude that the 2D transwell invasion assay is faster and less complex and is therefore more suitable for the initial experimental determination of specific chemoattractant receptor-mediated cellular invasion, which can then be studied using the more time consuming and complex 3D spheroid invasion assay that is physiologically closer to the *in vivo* situation than the 2D transwell invasion assay.

Future perspective

The described *in vitro* invasion assays are excellent experimental tools for translational research to increase our understanding of glioblastoma biology and to facilitate the development of novel therapies that inhibit invasion of GSCs. The methodological principles are not exclusive for glioblastoma and can also be applied to other types of cancer (stem) cells. In addition, novel therapies designed on the basis of these methodologies can work synergistically with current therapeutic approaches such as chemotherapy, radiotherapy and/or immunotherapy.

Author contributions

Study conception: V Hira, B Breznik, R Molenaar. Experiments: V Hira, B Breznik. Analysis: V Hira, B Breznik. Manuscript drafting: V Hira, B Breznik, R Molenaar. Manuscript editing: all authors. Supervision: C Van Noorden, T Lah, R Molenaar. Funding: T Lah, R Molenaar. Final approval of the manuscript: all authors.

Financial & competing interests disclosure

This study was financially supported by the Dutch Cancer Society (KWF; UVA 2014-6839 and UVA 2016-10460). V Hira was supported by the IVY Interreg Fellowship 2018, R Molenaar was supported by the Fondation pour la Recherche Nuovo-Soldati 2019, T Lah was supported by the Slovenian Research Agency (Program P10245) and the European Program of Cross-Border Cooperation for Slovenia-Italy Interreg TRANS-GLIOMA (Program 2017) and B Breznik was supported by postdoctoral grant of Slovenian Research Agency (Project Z3-1870). The authors have no other relevant affiliations or financial involvement with any organization or entity with a financial interest in or financial conflict with the subject matter or materials discussed in the manuscript apart from those disclosed.

No writing assistance was utilized in the production of this manuscript.

Ethical conduct of research

The study was approved by the National Medical Ethics Committee of the Republic of Slovenia (approval no. 0120-190/2018/4).

References

1. Galarza S, Kim H, Atay N, Peyton SR, Munson JM. 2D or 3D? How cell motility measurements are conserved across dimensions *in vitro* and translate *in vivo*. *Bioeng. Transl. Med.* 5(1), e10148 (2020).
2. Carmeliet P, Jain RK. Angiogenesis in cancer and other diseases. *Nature* 407(6801), 249–257 (2000).
3. de Gooijer MC, Guillen Navarro M, Bernards R, Wurdinger T, van Tellingen O. An experimenter's guide to glioblastoma invasion pathways. *Trends Mol. Med.* 24(9), 763–780 (2018).
4. Lefranc F, Brotchi J, Kiss R. Possible future issues in the treatment of glioblastomas: special emphasis on cell migration and the resistance of migrating glioblastoma cells to apoptosis. *J. Clin. Oncol.* 23(10), 2411–2422 (2005).
5. Gole B, Huszthy PC, Popovic M *et al.* The regulation of cysteine cathepsins and cystatins in human gliomas. *Int. J. Cancer* 131(8), 1779–1789 (2012).
6. Lah TT, Duran Alonso MB, Van Noorden CJ. Antiprotease therapy in cancer: hot or not? *Expert Opin. Biol. Ther.* 6(3), 257–279 (2006).
7. Bellail AC, Hunter SB, Brat DJ, Tan C, Van Meir EG. Microregional extracellular matrix heterogeneity in brain modulates glioma cell invasion. *Int. J. Biochem. Cell Biol.* 36(6), 1046–1069 (2004).
8. Rao SS, Lannutti JJ, Viapiano MS, Sarkar A, Winter JO. Toward 3D biomimetic models to understand the behavior of glioblastoma multiforme cells. *Tissue Eng. Part B Rev.* 20(4), 314–327 (2014).
9. Friedl P, Sahai E, Weiss S, Yamada KM. New dimensions in cell migration. *Nat. Rev. Mol. Cell Biol.* 13(11), 743–747 (2012).
10. Heffernan JM, Overstreet DJ, Le LD, Vernon BL, Sirianni RW. Bioengineered scaffolds for 3D analysis of glioblastoma proliferation and invasion. *Ann. Biomed. Eng.* 43(8), 1965–1977 (2015).
11. Sart S, Tomasi RF, Amselem G, Baroud CN. Multiscale cytometry and regulation of 3D cell cultures on a chip. *Nat. Commun.* 8(1), 469 (2017).
12. Hira VV, Verbovsek U, Breznik B *et al.* Cathepsin K cleavage of SDF-1alpha inhibits its chemotactic activity towards glioblastoma stem-like cells. *Biochim. Biophys. Acta* 1864(3), 594–603 (2017).
13. Gont A, Daneshmand M, Woulfe J, Lavictoire SJ, Lorimer IA. PREX1 integrates G protein-coupled receptor and phosphoinositide 3-kinase signaling to promote glioblastoma invasion. *Oncotarget* 8(5), 8559–8573 (2017).
14. Breznik B, Motaln H, Vittori M, Rotter A, Lah Turnsek T. Mesenchymal stem cells differentially affect the invasion of distinct glioblastoma cell lines. *Oncotarget* 8(15), 25482–25499 (2017).

15. Moriconi C, Palmieri V, Di Santo R *et al.* INSIDIA: a FIJI macro delivering high-throughput and high-content spheroid invasion analysis. *Biotechnol. J.* 12(10), (2017).
16. Corcoran A, De Ridder LI, Del Duca D *et al.* Evolution of the brain tumour spheroid model: transcending current model limitations. *Acta Neurochir.* 145(9), 819–824 (2003).
17. Decaestecker C, Debeir O, Van Ham P, Kiss R. Can anti-migratory drugs be screened *in vitro*? A review of 2D and 3D assays for the quantitative analysis of cell migration. *Med. Res. Rev.* 27(2), 149–176 (2007).
18. Benjamin DC, Hynes RO. Intravital imaging of metastasis in adult zebrafish. *BMC Cancer* 17(1), 660 (2017).
19. Hirata E, Girotti MR, Viros A *et al.* Intravital imaging reveals how BRAF inhibition generates drug-tolerant microenvironments with high integrin beta1/FAK signaling. *Cancer Cell* 27(4), 574–588 (2015).
20. Kallenberg K, Goldmann T, Menke J *et al.* Glioma infiltration of the corpus callosum: early signs detected by DTI. *J. Neurooncol.* 112(2), 217–222 (2013).
21. Cheng L, Wu Q, Guryanova OA *et al.* Elevated invasive potential of glioblastoma stem cells. *Biochem. Biophys. Res. Commun.* 406(4), 643–648 (2011).
22. Molina JR, Hayashi Y, Stephens C, Georgescu MM. Invasive glioblastoma cells acquire stemness and increased Akt activation. *Neoplasia* 12(6), 453–463 (2010).
23. Hira VV, Ploegmakers KJ, Grevers F *et al.* CD133+ and nestin+ glioma stem-like cells reside around CD31+ arterioles in niches that express SDF-1alpha, CXCR4, osteopontin and Cathepsin K. *J. Histochem. Cytochem.* 63(7), 481–493 (2015).
24. Hira VVV, Breznik B, Vittori M *et al.* Similarities between stem cell niches in glioblastoma and bone marrow: rays of hope for novel treatment strategies. *J. Histochem. Cytochem.* 68(1), 33–57 (2020).
25. Aderetti DA, Hira VVV, Molenaar RJ, van Noorden CJF. The hypoxic peri-arteriolar glioma stem cell niche, an integrated concept of five types of niches in human glioblastoma. *Biochim. Biophys. Acta Rev. Cancer* 1869(2), 346–354 (2018).
26. Zagzag D, Lukyanov Y, Lan L *et al.* Hypoxia-inducible factor 1 and VEGF upregulate *CXCR4* in glioblastoma: implications for angiogenesis and glioma cell invasion. *Lab. Invest.* 86(12), 1221–1232 (2006).
27. Ehtesham M, Winston JA, Kabos P, Thompson RC. CXCR4 expression mediates glioma cell invasiveness. *Oncogene* 25(19), 2801–2806 (2006).
28. Monteiro AR, Hill R, Pilkington GJ, Madureira PA. The role of hypoxia in glioblastoma invasion. *Cells* 6(4), 45 (2017).
29. Hong X, Jiang F, Kalkanis SN *et al. SDF-1* and *CXCR4* are up-regulated by VEGF and contribute to glioma cell invasion. *Cancer Lett.* 236(1), 39–45 (2006).
30. Podergajs N, Motaln H, Rajcevic U *et al.* Transmembrane protein CD9 is glioblastoma biomarker, relevant for maintenance of glioblastoma stem cells. *Oncotarget* 7(1), 593–609 (2016).
31. Kolosa K, Motaln H, Herold-Mende C, Korsic M, Lah TT. Paracrine effects of mesenchymal stem cells induce senescence and differentiation of glioblastoma stem-like cells. *Cell Transplant.* 24(4), 631–644 (2015).
32. Schneider CA, Rasband WS, Eliceiri KW. NIH image to ImageJ: 25 years of image analysis. *Nat. Methods* 9(7), 671–675 (2012).
33. Chieco P, Jonker A, De Boer BA, Ruijter JM, Van Noorden CJ. Image cytometry: protocols for 2D and 3D quantification in microscopic images. *Prog. Histochem. Cytochem.* 47(4), 211–333 (2013).
34. Horing E, Harter PN, Seznec J *et al.* The 'go or grow' potential of gliomas is linked to the neuropeptide processing enzyme carboxypeptidase E and mediated by metabolic stress. *Acta Neuropathol.* 124(1), 83–97 (2012).
35. Hatzikirou H, Basanta D, Simon M, Schaller K, Deutsch A. 'Go or grow': the key to the emergence of invasion in tumour progression? *Math. Med. Biol.* 29(1), 49–65 (2012).
36. Bahmad HF, Chamaa F, Assi S, Chalhoub RM, Abou-Antoun T, Abou-Kheir W. Cancer stem cells in neuroblastoma: expanding the therapeutic frontier. *Front. Mol. Neurosci.* 12, 131 (2019).
37. Bahmad HF, Cheaito K, Chalhoub RM *et al.* Sphere-formation assay: three-dimensional *in vitro* culturing of prostate cancer stem/progenitor sphere-forming cells. *Front. Oncol.* 8, 347 (2018).
38. Bahmad HF, Elajami MK, El Zarif T, Bou-Gharios J, Abou-Antoun T, Abou-Kheir W. Drug repurposing towards targeting cancer stem cells in pediatric brain tumors. *Cancer Metastasis Rev.* 39(1), 127–148 (2020).
39. Bahmad HF, Mouhieddine TH, Chalhoub RM *et al.* The Akt/mTOR pathway in cancer stem/progenitor cells is a potential therapeutic target for glioblastoma and neuroblastoma. *Oncotarget* 9(71), 33549–33561 (2018).
40. Bahmad HF, Poppiti RJ. Medulloblastoma cancer stem cells: molecular signatures and therapeutic targets. *J. Clin. Pathol.* 73(5), 243–249 (2020).
41. Mouhieddine TH, Nokkari A, Itani MM *et al.* Metformin and Ara-a effectively suppress brain cancer by targeting cancer stem/progenitor cells. *Front. Neurosci.* 9, 442 (2015).
42. Gole B, Duran Alonso MB, Dolenc V, Lah T. Post-translational regulation of cathepsin B, but not of other cysteine cathepsins, contributes to increased glioblastoma cell invasiveness *in vitro*. *Pathol. Oncol. Res.* 15(4), 711–723 (2009).
43. Motaln H, Turnsek TL. Cytokines play a key role in communication between mesenchymal stem cells and brain cancer cells. *Protein Pept. Lett.* 22(4), 322–331 (2015).
44. Hira VVV, Van Noorden CJF, Molenaar RJ. CXCR4 antagonists as stem cell mobilizers and therapy sensitizers for acute myeloid leukemia and glioblastoma? *Biology (Basel)* 9(2), 31 (2020).
45. Chonan Y, Taki S, Sampetrean O, Saya H, Sudo R. Endothelium-induced three-dimensional invasion of heterogeneous glioma initiating cells in a microfluidic coculture platform. *Integr. Biol.* 9(9), 762–773 (2017).
46. Fernandes JT, Chutna O, Chu V, Conde JP, Outeiro TF. A novel microfluidic cell co-culture platform for the study of the molecular mechanisms of Parkinson's disease and other synucleinopathies. *Front. Neurosci.* 10, 511 (2016).
47. Gao Y, Majumdar D, Jovanovic B *et al.* A versatile valve-enabled microfluidic cell co-culture platform and demonstration of its applications to neurobiology and cancer biology. *Biomed. Microdevices* 13(3), 539–548 (2011).
48. Jacob F, Salinas RD, Zhang DY *et al.* A patient-derived glioblastoma organoid model and biobank recapitulates inter- and intra-tumoral heterogeneity. *Cell* 180(1), 188–204.e22 (2020).
49. Clevers H. Modeling development and disease with organoids. *Cell* 165(7), 1586–1597 (2016).
50. Bian S, Repic M, Guo Z *et al.* Genetically engineered cerebral organoids model brain tumor formation. *Nat. Methods* 15(8), 631–639 (2018).
51. Ogawa J, Pao GM, Shokhirev MN, Verma IM. Glioblastoma model using human cerebral organoids. *Cell Rep.* 23(4), 1220–1229 (2018).
52. da Silva B, Mathew RK, Polson ES, Williams J, Wurdak H. Spontaneous glioblastoma spheroid infiltration of early-stage cerebral organoids models brain tumor invasion. *SLAS Discov.* 23(8), 862–868 (2018).
53. Linkous A, Balamatsias D, Snuderl M *et al.* Modeling patient-derived glioblastoma with cerebral organoids. *Cell Rep.* 26(12), 3203–3211.e5 (2019).
54. Hubert CG, Rivera M, Spangler LC *et al.* A three-dimensional organoid culture system derived from human glioblastomas recapitulates the hypoxic gradients and cancer stem cell heterogeneity of tumors found *in vivo*. *Cancer Res.* 76(8), 2465–2477 (2016).
55. Chen HI, Song H, Ming GL. Applications of human brain organoids to clinical problems. *Dev. Dyn.* 248(1), 53–64 (2019).
56. Roos A, Ding Z, Loftus JC, Tran NL. Molecular and microenvironmental determinants of glioma stem-like cell survival and invasion. *Front. Oncol.* 7, 120 (2017).
57. Inoue A, Takahashi H, Harada H *et al.* Cancer stem-like cells of glioblastoma characteristically express MMP-13 and display highly invasive activity. *Int. J. Oncol.* 37(5), 1121–1131 (2010).
58. Mook OR, Frederiks WM, Van Noorden CJ. The role of gelatinases in colorectal cancer progression and metastasis. *Biochim. Biophys. Acta* 1705(2), 69–89 (2004).
59. Vollmann-Zwerenz A, Leidgens V, Feliciello G, Klein CA, Hau P. Tumor cell invasion in glioblastoma. *Int. J. Mol. Sci.* 21(6), 1932 (2020).
60. Xia S, Lal B, Tung B, Wang S, Goodwin CR, Laterra J. Tumor microenvironment tenascin-C promotes glioblastoma invasion and negatively regulates tumor proliferation. *Neuro Oncol.* 18(4), 507–517 (2016).
61. Wurth R, Bajetto A, Harrison JK, Barbieri F, Florio T. CXCL12 modulation of CXCR4 and CXCR7 activity in human glioblastoma stem-like cells and regulation of the tumor microenvironment. *Front. Cell. Neurosci.* 8, 144 (2014).

Reports

BioTechniques

Isolation of spheroid-forming single cells from gastric cancer cell lines: enrichment of cancer stem-like cells

Jong Won Lee [‡,1,2], Jae Sook Sung[‡,2], Young Soo Park[2], Seok Chung[4] & Yeul Hong Kim [*,1,2,3]

[1]Brain Korea 21 Plus Project for Biomedical Science, Korea University College of Medicine, Seoul 02841, Republic of Korea ; [2]Cancer Research Institute, Korea University, Seoul 02841, Republic of Korea; [3]Division of Medical Oncology, Department of Internal Medicine, Korea University Medical Center, Korea University College of Medicine, Seoul 02841, Republic of Korea; [4]School of Mechanical Engineering, College of Engineering, Korea University, Seoul 02841, Republic of Korea; [‡]These authors contributed equally to this work

BioTechniques 65: 197-203 (October 2018) 10.2144/btn-2018-0046

First draft submitted: 11 April 2018; Accepted for publication: 13 July 2018

ABSTRACT

Isolation of spheroid-forming cells is important to investigate cancer stem cell (CSC) characteristics. However, conventional tumor spheroid culture methods have not proven suitable because the aggregated spheroids generally maintain their original heterogeneity and harbor multiple cells with various characteristics. Here we cultured spheroids using a polydimethylsiloxane microwell-based method and a limiting dilution protocol. We then isolated and enriched for CSCs that formed single cell-derived spheroids from gastric cancer cell lines. Cells from the microwell demonstrated higher self-renewal, increased expression of stem cell markers and resistance to apoptosis compared with spheroid cells made by the traditional method. This novel approach allows efficient cancer stem cell isolation and represents a step forward in cancer stem cell studies.

METHOD SUMMARY

This microwell-based spheroid culture method provides the following advantages over the traditional spheroid culture platforms: it is ready for co-culture without direct cell-to-cell contact; allows easy growth medium changes in the device due to the shear-free structure; and provides unlimited throughput, given that 361 cell spheroids can be obtained from a single device.

KEYWORDS

cancer stem cells • gastric cancer • spheroids

Cancer stem cells (CSCs) have been hypothesized to drive tumor initiation, metastasis and chemoresistance. The American Association for Cancer Research defines CSCs as subpopulations of cells within a tumor that possess the capacity for self-renewal and that differentiate into heterogeneous lineages of cancer cells that constitute a tumor [1] . Emerging evidence suggests that CSCs contribute to disease recurrence after completion of initial treatment [2] .

To form spheroids, candidate cells are seeded in culture dishes under special nonadherent conditions in serum-free medium. This approach has been used to isolate gastric CSCs in most studies [3, 4]. Many studies have reported that the capability of CSCs to form spheroid structures is acquired in various solid tumors [5–9] . Hanging drop culture, surface topology, microwells and microfluidic devices have all been developed as techniques for studying the formation of aggregated multicellular spheroids [10–13]. Nevertheless, these methods have not proven suitable for isolation of specific cells from a heterogeneous cell population because the aggregated spheroids generally maintain their original heterogeneity and harbor multiple cells with various characteristics [14].

Here, we used a limiting dilution protocol [15] in concert with a microwell-based spheroid culture plate to isolate spheroid-forming single cells. Spheroid-forming cells were selected by their capacity for anchorage-independent growth. The selected spheroid cells proliferated without forming agglomerates or cell-to-cell contacts. The ability of a single cell to generate a spheroid is considered indicative of self-renewal ability and is therefore consistent with a CSC phenotype [7] . Using gastric cancer cell lines, we isolated single cell-derived spheroid cells. These spheroids were clear and round and were composed of tightly bound cells; moreover, they were not isolated by the traditional culture method. We also examined whether these cells exhibited distinct stemness gene expression or apoptotic resistance properties compared with spheroid cells isolated by the traditional culture method.

MATERIALS & METHODS

Cell lines & culture conditions

The human gastric cancer cell lines SNU-638 and SNU-484 were obtained from the Korean Cell Line Bank (Seoul, Korea). Cells were maintained in RPMI-1640 medium (HyClone, MA, USA) supplemented with 10% FBS (HyClone), 25 mM 4-(2-hydroxyethyl)-1-piperazine ethanesulfonic acid (HEPES; Invitrogen, CA, USA), 25 mM $NaHCO_3$ (Invitrogen), and 1% penicillin/streptomycin (HyClone). Cells were grown at 37°C in a humidified incubator with 5% CO_2 until the monolayers reached confluence.

Spheroid culture

For traditional 3D tumor spheroid culture, 500 cells were seeded onto each poly 2-hydroxyethyl methacrylate (PolyHEMA)-coated (to prevent attachment) 24-well plate as previously described [3,16].

The 'C-Well' microwell plate (Incyto, Chonan, Korea) was made of polydimethylsiloxane (PDMS), had 361 microwells, and was 29 × 29 mm^2. Each well had an inner diameter of 500 µm and a depth of 500 µm. Seeding density was calculated as number of cells per volume for single cell occupancy in each microwell. For microwell-based spheroid culture, 5 × 10^3 parent cells were seeded onto the microwell, which was placed in a 60-mm petri dish (SPL, Pocheon, Korea). After 30 min, the medium was refreshed to remove any cells that had landed outside the microwells. We confirmed the spheroid that derived from a single cell with microscopic observation. For spheroid culture, serum-free RPMI-1640 medium containing 1% B-27 supplement (Invitrogen), 10 ng/ml human recombinant fibroblast growth factor-basic (Invitrogen), 20 ng/ml human recombinant epidermal growth factor (Invitrogen), 10 mM HEPES (Invitrogen), and 1% penicillin/streptomycin (HyClone) was used. The medium was changed every 4 days. After 2 weeks, spheroids were examined using an Olympus CK40 optical microscope (Olympus, Tokyo, Japan) and images were captured with a Canon EOS 600D CCD Camera (Canon, Tokyo, Japan). For the second passage, spheroids were dissociated into single cells using trypsin-EDTA and mechanical disruption with a pipette. The resulting cells were then suspended in spheroid culture medium and plated onto a new microwell to allow spheroid reformation.

Viability

On day 14 of culture, the spheroids were stained using a fluorescence-based live/dead cell viability assay kit (Invitrogen) according to the manufacturer's instructions. The medium was replaced with medium containing ethidium homodimer-1 and calcein AM, after which the cells were incubated overnight at 37°C. Spheroids were examined using an Olympus DP 71 microscope (Olympus) and an LSM 700 laser scanning microscope (Zeiss, Oberkochen, Germany) to evaluate cellular viability.

Quantitative reverse transcription real-time PCR

Total RNA was prepared using TRIzol (MRC, OH, USA) according to the manufacturer's instructions. For quantitative RNA analysis, 1 µg of total RNA was reverse transcribed using M-MLV reverse transcriptase (Invitrogen) to produce cDNA. Amplification was performed in a CFX Real-Time PCR Detection System (Bio-Rad, CA, USA) using iQ SYBR Green Supermix (Bio-Rad). For quantitative real-time PCR analysis, the expression level of each mRNA of interest was normalized to the GAPDH mRNA expression levels. The following primer sequences were used:

OCT4: forward 5'-GCAGCGACTATGCACAACGA-3', reverse 5'-CCAGAGTGGTGACGGAGACA-3'; *SOX2*, forward 5'-CATCACCCACAG-CAAATGACA-3', reverse 5'-GCTCCTACCGTACCACTAGAACTT-3'; *NANOG*, forward 5'-AATACCTCAGCCTCCAGCAGATG-3', reverse 5'-TGCGT-CACACCATTGCTATTCTTC-3'; *GAPDH*, forward 5'-CAGCCTCAAGATCATCAGCAATG-3', reverse 5'-TCATGAGTCCTTCCACGATACCA-3'.

Western blot analysis

For western blot analysis, parent cells were harvested from cells plated at 70–80% confluence. To collect whole cell extracts, parent and spheroid cells were lysed using PRO-PREP™ (iNtRON Biotechnology, Seongnam, Korea) according to the manufacturer's instructions. Protein concentrations were determined using the BCA assay (Bio-Rad), after which 30 ug of protein was loaded onto an 8% SDS-PAGE gel. After electrophoresis was carried out, the resolved proteins were transferred to a polyvinylidene difluoride membrane. The membranes were blocked in PBS with 0.1% Tween-20 and 5% nonfat milk for 1 h. After incubation at 4°C overnight with primary antibodies, goat anti-mouse (Bio-Rad) or goat anti-rabbit (Santa Cruz Biotechnology, TX, USA) secondary antibodies conjugated with horseradish peroxidase were added to the membranes at a 1:5000 dilution and incubated for 1 h at room temperature. Immunoreactive bands were detected using the ECL Western Blot Detection system (Amersham Biosciences, CA, USA); images were captured using a Chemi-Doc imager (Bio-Rad). The following concentrations were used for primary antibodies: anti-OCT4, 1:1000 (Abcam); anti-SOX2, 1:1000 (Cell Signaling); anti-NANOG, 1:1000 (Cell Signaling); and anti-beta-actin, 1:10,000 (Sigma Aldrich).

Immunofluorescence

Spheroid cells were washed with PBS and fixed with 4% paraformaldehyde for 10 min. The fixed cells were permeabilized with 0.3% Triton X-100 in PBS for 30 min and then blocked in 5% BSA in PBS for 1 h. Next, the cells were incubated with PE Mouse Anti-Human CD44 (BD Pharmingen, CA, USA) or PE Mouse Anti-Human CD54 (BD Pharmingen) in blocking solution for 1 h according to the supplier's instructions, after which the cells were washed three times with PBS-T. Nuclei were stained with Hoechst 33342 (Thermo Fisher, MA, USA) and the slides were mounted in mounting medium (Dako). Cells were analyzed on an LSM 700 laser scanning microscope (Zeiss).

Apoptosis assay

Spheroid cells were stained using an annexin V-FITC apoptosis detection kit (BD Pharmingen) according to the supplier's instructions. The stained cells were analyzed using a FACSCalibur machine (BD Biosciences, CA, USA) and gated according to forward scatter and side scatter to analyze similar cell populations. Annexin V-positive and PI-negative cells were considered early apoptotic cells, while annexin V-positive and PI-positive cells were considered necrotic cells.

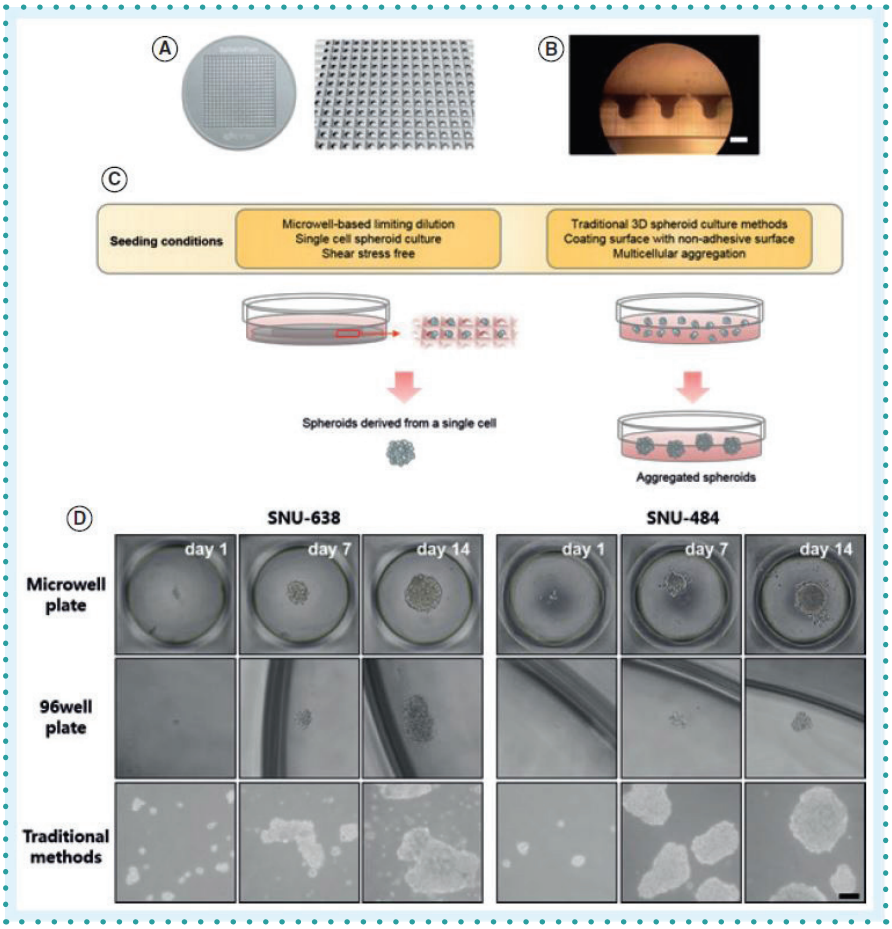

Figure 1. Figure 1. Microwell-based chip approach for generating single cell-derived spheroids. (A) Illustration of the microwell-based spheroid culture chip. The chip was made of polydimethylsiloxane and had 361 microwells in a 29 × 29 mm2 area. Each well size was 500 µm (inner diameter) × 500 µm (depth). (B) Magnified cross-sectional image of the microwell-based chip (vertical axis, 10x magnification, scale bar = 500 µm). (C) Schematic illustration of the microwell-based and traditional spheroid culture methods. Growth medium can be readily changed in the microwell due to the shear stress-free structure. (D) Sequential microscopic images of spheroid cells from SNU-638 and SNU-484 cells cultured by the microwell-based, nonadherent 96-well culture plate and traditional spheroid culture methods. Representative phase contrast images from day 1 to day 14 are shown of spheroids (40x magnification, scale bar = 100 µm).

Soft agar colony-formation assay

Soft agar assays were constructed in 60 mm dish. Briefly, 5 × 103 cells were resuspended in 2 ml with final concentration of 1x media containing 0.3% agarose (Amresco, OH, USA), and then paved on a 2-ml base layer containing 0.6% agar. The plates were incubated for 14–21 days at 37°C, 5% CO_2 condition, then stained with 0.01% crystal violet, 10% methanol solution for 1 h (Sigma). Assays were repeated a total of three times.

Xenograft model

Xenograft studies were approved by the Institutional Animal Care and Use Committee (IACUC) of Korea University College of Medicine (IACUC approval No. KOREA-2017-0108). 6-week-old male nude mice were purchased from Orient Bio Animal Center (Seongnam, Korea). Nude mice were injected with a suspension of parent of spheroid cells subcutaneously into the flank.

Statistical analysis

Data are expressed as means ± standard deviations. At least three experiments were performed independently for each type of experiment to ensure reproducibility. Statistical differences among the experimental groups were evaluated by analysis of variance, followed by Student's t-test. p-values less than 0.05 were considered statistically significant.

RESULTS & DISCUSSION

Single cell-derived spheroids isolated using microwell-based culture method with gastric cancer cells

Due to the disadvantages of traditional 3D spheroid screening culture methods, we performed a limiting dilution protocol using a microwell spheroid culture chip to isolate spheroid-forming single cells from mixed populations. The microwell-based chip was made from PDMS (Figure 1A). In Figure 1B, the side of the small wells on the microwell was magnified ten times, enabling the consistency of the chamber shape to be observed. Figure 1C displays a schematic diagram of the culture process and of the process of spheroid isolation from single cells without shear stress. By using a microwell, cell loss was minimized when changing the culture medium. To test the effectiveness of spheroid isolation using the microwell, we used the chip with SNU-638 and SNU-484 cells. On the microwell, several cells formed round spheroids with clear boundaries; these spheroids are hereafter referred to as single cell-derived spheroids (SS; Figure 1D, top). SS#1 had

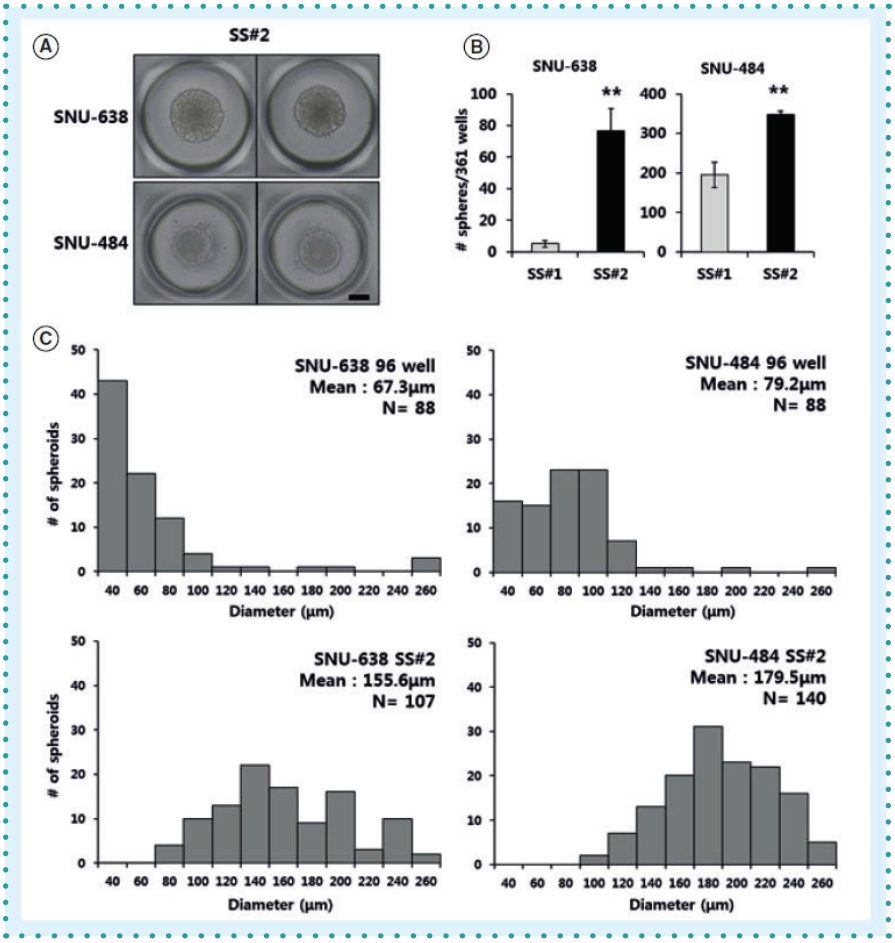

Figure 2. Isolation of single cell-derived spheroid cells generated from SNU-638 and SNU-484 cells. (A) Microscopic images of a second-passage spheroid formed from a single SS#1 cell after another 2 weeks in culture (40x magnification, scale bar = 100 µm). (B) Spheroid-forming efficiency as calculated from single dissociated spheroid cells. The single cells were counted in 361-microwells. Error bars represent standard deviation. **$p < 0.01$ compared with the SS#1 group ($n = 4$). (C) Size distribution of spheroids cultured on the microwell and on the 96-well plates.

clear boundaries, were compact, and were tightly adhered to each other, hindering the distinction of individual cells from each other. However, a small portion of these two populations of gastric cancer cells formed irregular spheroids with poor cell-to-cell adhesion by the traditional 3D tumor spheroid culture method; these spheroids are referred to as tumor spheroids (TS; Figure 1D, bottom). Approximately two- to three-fold more TS#1 spheroids were formed compared with the spheroids formed from the microwell. We hypothesized that the TS#1 spheroids were composed of mixed cell populations that formed agglomerates and irregularly shaped spheroids lacking self-renewal ability. In addition, SS#1 spheroids could be detected in the microwell but not on the nonadherent 96-well plates (Figure 1D, middle). The use of the microwell enables precise single-cell seeding and also enables the exclusion of cells under shear stress from agglomerates. Next, we compared the self-renewal capability of spheroids isolated from the traditional method with that of spheroids isolated from the microwell-based culture method.

Single cell-derived spheroids show self-renewal ability & uniformity

We measured the numbers and diameters of spheroids isolated from both methods to examine the self-renewal potential of each spheroid type. SS#1 spheroids were separated into single cells and seeded at the same concentration on a new microwell. Divided single cells from SS#1 spheroids proliferated on SS#2 spheroids in the same clear, round forms (Figure 2A). The percentage of spheroid-forming cells in the second passage increased from 1.4 to 21.1% (five to 76 in 361 microwells) for SNU-638 cells and from 54 to 96.1% (195 to 347 in total 361 microwells) for SNU-484 cells (Figure 2B). The increased number of spheroids with clear boundaries in the second culture passage provides definitive evidence for the self-renewal capacity of these spheroids. It also indicates that the spheroids were enriched with CSC properties.

In addition, examination of the SS#2 results showed that the spheroids formed from the microwell were more uniform in size compared with spheroids formed from nonadherent surface-coated 96-well plates. The average diameters of SS#2 spheroids from SNU-638 and SNU-484 cells were 155.6 and 179.5 µm, respectively (Figure 2C). However, the majority of the spheroids from 96-well plates remained small, with mean diameters of 67.3 and 79.2 µm in the two cell lines, respectively. Spheroid uniformity is critical for obtaining reproducible experimental results, since size affects cellular characteristics [17]. Therefore, applying the microwell-based culture method to spheroid isolation was advantageous for long-term culture approaches, since it could be performed in shear-stress free conditions and produced uniform spheroids.

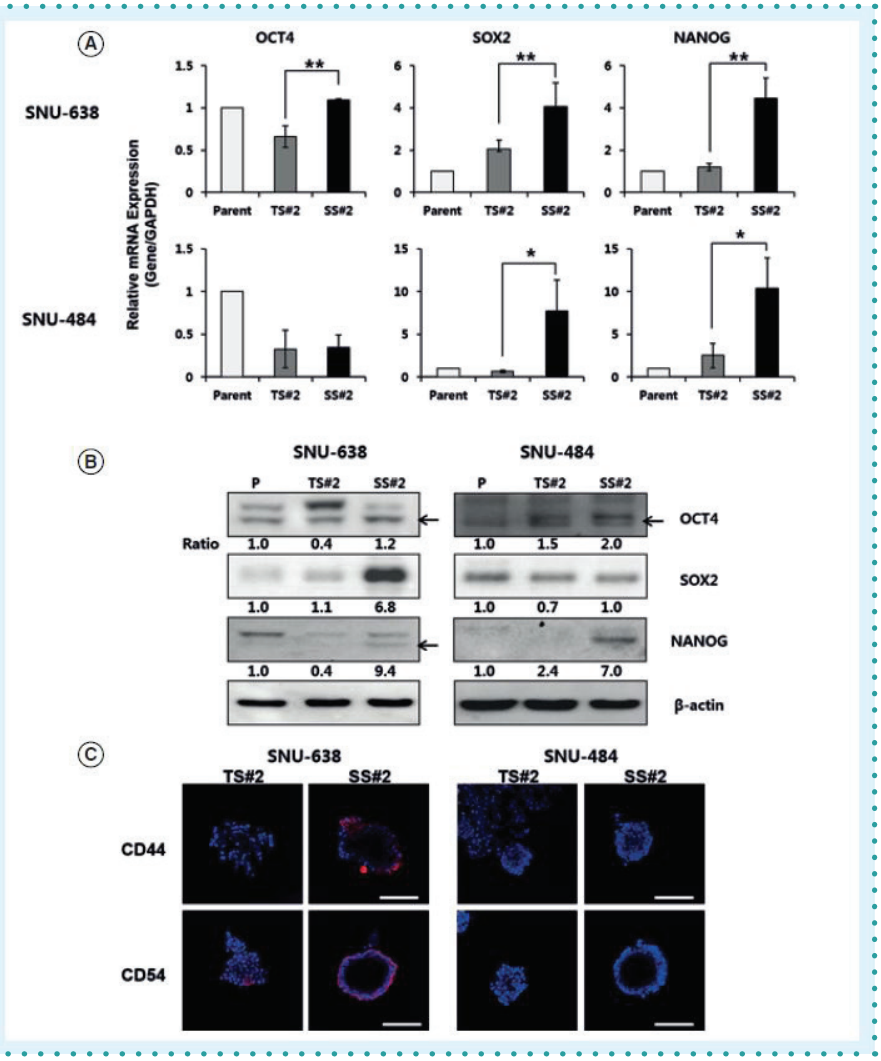

Figure 3. Cancer stem cell-like properties of spheroid cells derived from SNU-638 and SNU-484 cells. (A) mRNA expression of stemness markers in parent and spheroid cells as measured by qRT-PCR. Each data point represents the mean of three replicates. Error bars represent standard deviation. **p < 0.01; *p < 0.05 compared to the parent group (n = 3). Expression levels were normalized to that of GAPDH. (B) Western blot analysis of stemness proteins; beta-actin was used as a loading control. Band intensity was measured with a densitometer and values are expressed relative to that of the loading control. (C) Immunofluorescence images of TS#2 and SS#2 spheroids stained with anti-CD44 or anti-CD54 antibodies (red color). The blue signal represents nuclear DNA staining by Hoechst 33342 (20x magnification, scale bar = 100 μm).

Expression levels of candidate CSC markers are upregulated in single cell-derived spheroids

Many studies have demonstrated that CSCs are characterized by the upregulation of three stem cell-specific transcription factors, OCT4, SOX2 and NANOG [3,18]. We thus examined whether the spheroids expressed genes that have been postulated to play key roles in CSCs. The transcription levels of SOX2 and NANOG in SS#2 spheroids were four- and ten-fold higher than those in the parental cells, respectively (Figure 3A). However, the levels in TS#2 spheroids were not significantly increased compared with the levels in the parental cells. Also, OCT4 transcription was not detected in either TS#2 or SS#2 spheroids. Consistent with these results, the protein levels of SOX2 and NANOG, but not OCT4, were increased in SS#2 spheroids (Figure 3B). These data suggest that among those three genes, SOX2 and NANOG are the key factor conferring 'stemness' characteristics in spheroid-forming ability as previous studies reported [19,20]. Furthermore, higher expression levels of those genes in SS#2 than TS#2 demonstrate that our novel method isolated more homogeneous spheroid cells with stem-like characteristics.

In gastric cancer, CD44 was first identified as a potential gastric CSC marker [7,21]. Also, LGR5 and D54 have been reported to act as a gastric CSC marker [22–24]. To assess the expression level of those markers, we performed immunocytochemical staining of TS#2 and SS#2 spheroids. CD44 and CD54 expression were remarkably up-regulated in SS#2 spheroids compared with TS#2 spheroids from SNU-638 cells (Figure 3C). There was no significant difference between SS#2 and TS#2 spheroids derived from SNU-484 cells. LGR5 was not detectable in both cell lines (data not shown). These results suggest that more cells in SS#2 spheroids than in TS#2 spheroids have stem cell-like properties.

Colony-forming & tumorigenic ability of single cell-derived spheroids

The above results suggested that the derived spheroids are composed of mixed cell populations, including non-CSCs, as previously reported [25]. To test this hypothesis, the percentages of dead and apoptotic cells in both TS#2 and SS#2 spheroids were measured using a live/dead cell viability assay kit and an annexin V-FITC apoptosis detection kit, respectively, according to the manufacturers' instructions. These assays revealed that TS#2 spheroids included more dead cells than SS#2 spheroids; these results held true for spheroids ▶

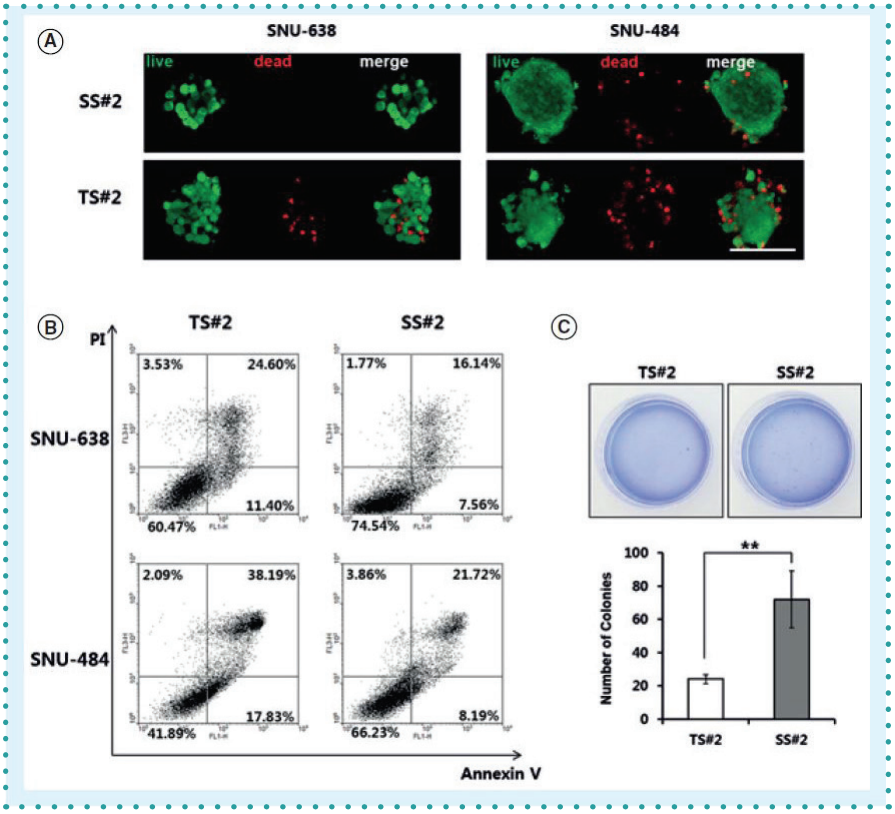

Figure 4. Viability and colony-forming ability of single-cell-derived spheroid cells using SNU-638 and SNU-484 cells. (A) Selected fluorescence images of TS#2 and SS#2 cells. Live cells are green and dead cells are red (20x magnification, scale bar = 100 µm). (B) Representative data from an annexin-V/PI staining assay to assess apoptosis in parental and SS#2 cells. At least three independent experiments were performed, each obtaining similar results. Q3, normal; Q4, annexin V-positive (i.e., the early apoptotic population); Q1, PI positive; and Q2, annexin-V/PI positive (i.e., the late apoptotic population). (C) Representative photographs of colonies in soft agar in 60-mm dishes. Each number of colonies formed per well is presented as the mean of three replicates. Error bars represent standard deviation.
**$p < 0.01$, compared with the parent group ($n = 3$).

derived from SNU-638 cells and in spheroids derived from SNU-484 cells (Figure 4A). FACS analysis showed that approximately 40% of the cells in the TS#2 spheroids were apoptotic and necrotic (Figure 4B). By contrast, the SS#2 spheroids were composed of less than 25% apoptotic and necrotic cells. Taken together, our results indicate that the cells in the SS#2 spheroids were more resistant to apoptosis than those in the TS#2 spheroids.

Single-cell-derived spheroids are resistant to apoptosis

We next investigated anchorage-independent growth by assessing colony formation on soft agar, which is the gold standard assay for cellular transformation *in vitro* [26]. For SNU-638-derived spheroids, the SS#2 spheroids formed softer agar colonies compared with the TS#2 spheroids (Figure 4C). However, neither SS#2 nor TS#2 spheroids derived from SNU-484 cells formed colonies, despite extended periods of time in culture (data not shown). In addition, we tested the tumorigenicity of isolated spheroid cells *in vivo*. The SNU-638 cell line did not show tumorigenic ability in both parent and spheroid cells, until 8 weeks from injection despite one million cells injected (data not shown). The spheroids from the SNU-484 cell line developed into a larger size of tumor than the parental cells (data not shown). Therefore, the latent population among the cells could be identified with a simple culture material.

In this study, we used a limiting dilution protocol integrated with a microwell-based spheroid culture chip to isolate spheroid-forming cells from a single cell. Various 3D, multicellular, spheroid-forming methods, such as the hanging drop assay and the use of hydrogels, have been employed to evaluate CSCs [10–12,27]. However, due to the rarity of CSCs, these methods are hindered by poor single-cell seeding and low throughput [28]. In these methods, it is also difficult to change the culture medium for long-term culture without significant cell loss during passage. Additionally, these methods may result in the formation of spheroids containing many cells that are not CSCs. A recent report showed that CSC-like cells protect non-CSCs from anoikis and also promote tumor growth [25]. As spheroid bodies themselves display marked cellular heterogeneity, experiments using spheroids should be interpreted as studies of mixed cell populations, not as purified CSCs [29]. Therefore, we propose that forming spheroids from a single cell on a microwell-based culture chip is the most suitable approach for isolating and evaluating CSCs.

This is the first study demonstrating that single cell-derived spheroids from gastric cancer cells can be isolated using an elastomeric microwell-based culture method. We also showed that spheroids from the microwells have larger populations of cells with stem cell-like properties compared with spheroids formed by conventional tumor spheroid culture methods. The microwell-based spheroid culture method provides the following advantages over the hanging drop method and the other developed spheroid culture platforms: an extended culture period of 10–30 days due to easy medium changes; ready for co-culture without direct cell-to-cell contact [30]; easy generation of size-controlled cell spheroids; easy growth medium changes in the device due to the shear-free and stress-free structure [31]; ready application to various cell types; and unlimited throughput, given that 361 cell spheroids can be obtained from a single device.

Moreover, the microwell mimics the *in vivo* environment and contains CSC-secreted factors [32]. One recent study reported that round spheroids showed a signature of high mRNA expression for secreted molecules, which activate cell cycle-related signaling pathways and their downstream transcriptional regulators [33]. This finding supports the idea that the microwell is more effective at mimicking the *in vivo* environment by sharing the medium. Therefore, we hypothesize that round spheroids may be acquired only in a microwell, but not in independent 96-well plates (Figure 1D). Additionally, the microwell facilitates independent CSC growth and avoids agglomeration with non-CSCs. Taken together, our microwcell-based spheroid culture method is an efficient and suitable approach for isolating spheroid cells with stem-like characteristics on the single-cell level.

AUTHOR CONTRIBUTIONS

JWL designed the study and performed the experiments, gathered data and wrote the manuscript. JSS and YSP designed experimental approaches, and critically reviewed the data. SC constructed the microwell that was used for isolation of spheroidforming single cells. YHK performed general oversight of the work.

FINANCIAL & COMPETING INTERESTS DISCLOSURE

This study was supported by a grant from the National Research Foundation of Korea (NRF), which is funded by the Korean government (MEST) (No. 2010-0020986). The authors have no other relevant affiliations or financial involvement with any organization or entity with a financial interest in or financial conflict with the subject matter or materials discussed in the manuscript apart from those disclosed.

No writing assistance was utilized in the production of this manuscript.

OPEN ACCESS

REFERENCES

1. Clarke MF, Dick JE, Dirks PB *et al.* Cancer stem cells – perspectives on current status and future directions: AACR Workshop on cancer stem cells. *Cancer Res.* 66(19), 9339–9344 (2006).
2. Xu ZY, Tang JN, Xie HX *et al.* 5-fluorouracil chemotherapy of gastric cancer generates residual cells with properties of cancer stem cells. *Int. J. Biol. Sci.* 11(3), 284–294 (2015).
3. Liu J, Ma L, Xu J *et al.* Spheroid body-forming cells in the human gastric cancer cell line MKN-45 possess cancer stem cell properties. *Int. J. Oncol.* 42(2), 453–459 (2013).
4. Zhang X, Hua R, Wang X *et al.* Identification of stem-like cells and clinical significance of candidate stem cell markers in gastric cancer. *Oncotarget* 7(9), 9815–9831 (2016).
5. Fang D, Nguyen TK, Leishear K *et al.* A tumorigenic subpopulation with stem cell properties in melanomas. *Cancer Res.* 65(20), 9328–9337 (2005).
6. Wright MH, Calcagno AM, Salcido CD, Carlson MD, Ambudkar SV, Varticovski L. *Brca1* breast tumors contain distinct $CD44^+/CD24^-$ and $CD133^+$ cells with cancer stem cell characteristics. *Breast Cancer Res.* 10(1), R10 (2008).
7. Takaishi S, Okumura T, Tu S *et al.* Identification of gastric cancer stem cells using the cell surface marker CD44. *Stem Cells* 27(5), 1006–1020 (2009).
8. Todaro M, Alea MP, Di Stefano AB *et al.* Colon cancer stem cells dictate tumor growth and resist cell death by production of interleukin-4. *Cell Stem Cell* 1(4), 389–402 (2007).
9. Monterey MD, Szerlip NJ, Mathupala SP. Lowcost media formulation for culture of brain tumor spheroids (neurospheres). *BioTechniques* 55(2), 83–88 (2013).
10. Wong SF, No da Y, Choi YY, Kim DS, Chung BG, Lee SH. Concave microwell based sizecontrollable hepatosphere as a three-dimensional liver tissue model. *Biomaterials* 32(32), 8087–8096 (2011).
11. Kelm JM, Timmins NE, Brown CJ, Fussenegger M, Nielsen LK. Method for generation of homogeneous multicellular tumor spheroids applicable to a wide variety of cell types. *Biotechnol. Bioeng.* 83(2), 173–180 (2003).
12. Foty R. A simple hanging drop cell culture protocol for generation of 3D spheroids. *J. Vis. Exp.* (51) (2011).
13. Napolitano AP, Dean DM, Man AJ *et al.* Scaffoldfree three-dimensional cell culture utilizing micromolded nonadhesive hydrogels. *BioTechniques* 43(4), 494, 496–500 (2007).
14. Brophy CM, Luebke-Wheeler JL, Amiot BP *et al.* Rat hepatocyte spheroids formed by rocked technique maintain differentiated hepatocyte gene expression and function. *Hepatology* 49(2), 578–586 (2009).
15. Rota LM, Lazzarino DA, Ziegler AN, LeRoith D, Wood TL. Determining mammosphere-forming potential: application of the limiting dilution analysis. *J. Mammary Gland Biol. Neoplasia* 17(2), 119–123 (2012).
16. Song Z, Yue W, Wei B *et al.* Sonic hedgehog pathway is essential for maintenance of cancer stem-like cells in human gastric cancer. *PLoS One* 6(3), e17687 (2011).
17. Mehta G, Hsiao AY, Ingram M, Luker GD, Takayama S. Opportunities and challenges for use of tumor spheroids as models to test drug delivery and efficacy. *J. Control. Rel.* 164(2), 192–204 (2012).
18. Wang AM, Huang TT, Hsu KW *et al.* Yin Yang 1 is a target of microRNA-34 family and contributes to gastric carcinogenesis. *Oncotarget* 5(13), 5002–5016 (2014).
19. Yoon C, Cho SJ, Aksoy BA et al. Chemotherapy resistance in diffuse-type gastric adenocarcinoma is mediated by RhoA activation in cancer stem-like cells. *Clin. Cancer Res.* 22(4), 971–983 (2016).
20. Yoon C, Park DJ, Schmidt B *et al.* CD44 expression denotes a subpopulation of gastric cancer cells in which Hedgehog signaling promotes chemotherapy resistance. *Clin. Cancer Res.* 20(15), 3974–3988 (2014).
21. Lau WM, Teng E, Chong HS *et al.* CD44v8–10 is a cancer-specific marker for gastric cancer stem cells. *Cancer Res.* 74(9), 2630–2641 (2014).
22. Wang B, Chen Q, Cao Y *et al.* LGR5 is a gastric cancer stem cell marker associated with stemness and the EMT signature genes NANOG, NANOGP8, PRRX1, TWIST1, and BMI1. *PLoS One* 11(12), e0168904 (2016).
23. Chen X, Wei B, Han X *et al.* LGR5 is required for the maintenance of spheroid-derived colon cancer stem cells. Int. J. Mol. Med. 34(1), 35–42 (2014).
24. Chen T, Yang K, Yu J *et al.* Identification and expansion of cancer stem cells in tumor tissues and peripheral blood derived from gastric adenocarcinoma patients. *Cell Res.* 22(1), 248–258 (2012).
25. Kim SY, Hong SH, Basse PH *et al.* cancer stem cells protect non-stem cells from anoikis: bystander effects. *J. Cell. Biochem.* 117(10), 2289–2301 (2016).
26. Rotem A, Janzer A, Izar B *et al.* Alternative to the soft-agar assay that permits high-throughput drug and genetic screens for cellular transformation. *Proc. Natl Acad. Sci. USA* 112(18), 5708–5713 (2015).
27. Wang Y, Wang J. Mixed hydrogel bead-based tumor spheroid formation and anticancer drug testing. *Analyst* 139(10), 2449–2458 (2014).
28. Chen YC, Ingram PN, Fouladdel S *et al.* Highthroughput single-cell derived sphere formation for cancer stem-like cell identification and analysis. *Sci. Rep.* 6, 27301 (2016).
29. Schatton T, Frank MH. The *in vitro* spheroid melanoma cell culture assay: cues on tumor initiation? *J. Invest. Dermatol.* 130(7), 1769–1771 (2010).
30. Halldorsson S, Lucumi E, Gomez-Sjoberg R, Fleming RMT. Advantages and challenges of microfluidic cell culture in polydimethylsiloxanedevices. *Biosens. Bioelectron* 63, 218–231 (2015).
31. Wang Y, Kim MH, Tabaei SR *et al.* Spheroid formation of hepatocarcinoma cells in microwells: experiments and Monte Carlo simulations. *PLoS One* 11(8), e0161915 (2016).
32. Singh M, Mukundan S, Jaramillo M, Oesterreich S, Sant S. Three-dimensional breast cancer models mimic hallmarks of size-induced tumor progression. *Cancer Res.* 76(13), 3732–3743 (2016).
33. Park MC, Jeong H, Son SH *et al.* Novel morphologic and genetic analysis of cancer cells in a 3D microenvironment identifies STAT3 as a regulator of tumor permeability barrier function. *Cancer Res.* 76(5), 1044–1054 (2016).

SARTORIUS

White Paper

April 5, 2019

Keywords or phrases:
Immunology, Live-Cell Analysis, Immuno-phenotyping, NETosis, Phagocytosis, Immune Cell Killing, Antibody Internalization, Macrophage, T Cell

Ten Applications of Live-Cell Analysis in Immunology

Del Trezise
Essen BioScience Ltd., a Sartorius Company, Welwyn Garden City AL7 3AX UK

Abstract

The main *in vitro* methods for immunologists to analyze cells of the immune system are flow cytometry, PCR and various forms of ELISA (e.g., ELISPOT). Together, these techniques allow measurement of different cell populations at the molecular and functional level ("immuno-phenotyping") and quantification of immune responses, for example, cytokine release. While these platforms are extremely powerful, they provide little insight into morphology and the spatial interactions of cells. Moreover, as 'end-point' measures, they are not well suited to report on changes in biology over time.

Over recent years, real-time live-cell analysis has become an enabling research method for immunologists, addressing many of the limitations described above. Here, we review 10 functional bio-assay "applications" that illustrate the breadth, depth and value of this approach.

What is Live-Cell Analysis?

Live-cell analysis is the real-time quantification of behavior from living cells using time-lapse imaging (hours to weeks). The technique comprises:

1. Acquisition of images repeatedly from the same cells over time
2. Maintenance of the cells in a stable physiological environment that is unperturbed throughout the experiment
3. Image analysis and data visualization on the fly to provide a real-time view of dynamic changes in the biology (Figure 1)

Purpose-built live-cell analysis systems, such as Incucyte® Live-Cell Analysis Systems (Sartorius), can automatically gather, analyze, and display images and time-course data from over 2000 parallel experiments (e.g., 6 x 384-well micro-plates). The system resides within a standard cell incubator, and uniquely, the optical path moves (rather than the cell plate) so that high quality images of non-adherent cells can be captured without disturbing them. A suite of optimized live-cell reagents, protocols and software modules complete the 'integrated solution', such that live-cell analysis is turnkey and accessible to the everyday scientist.

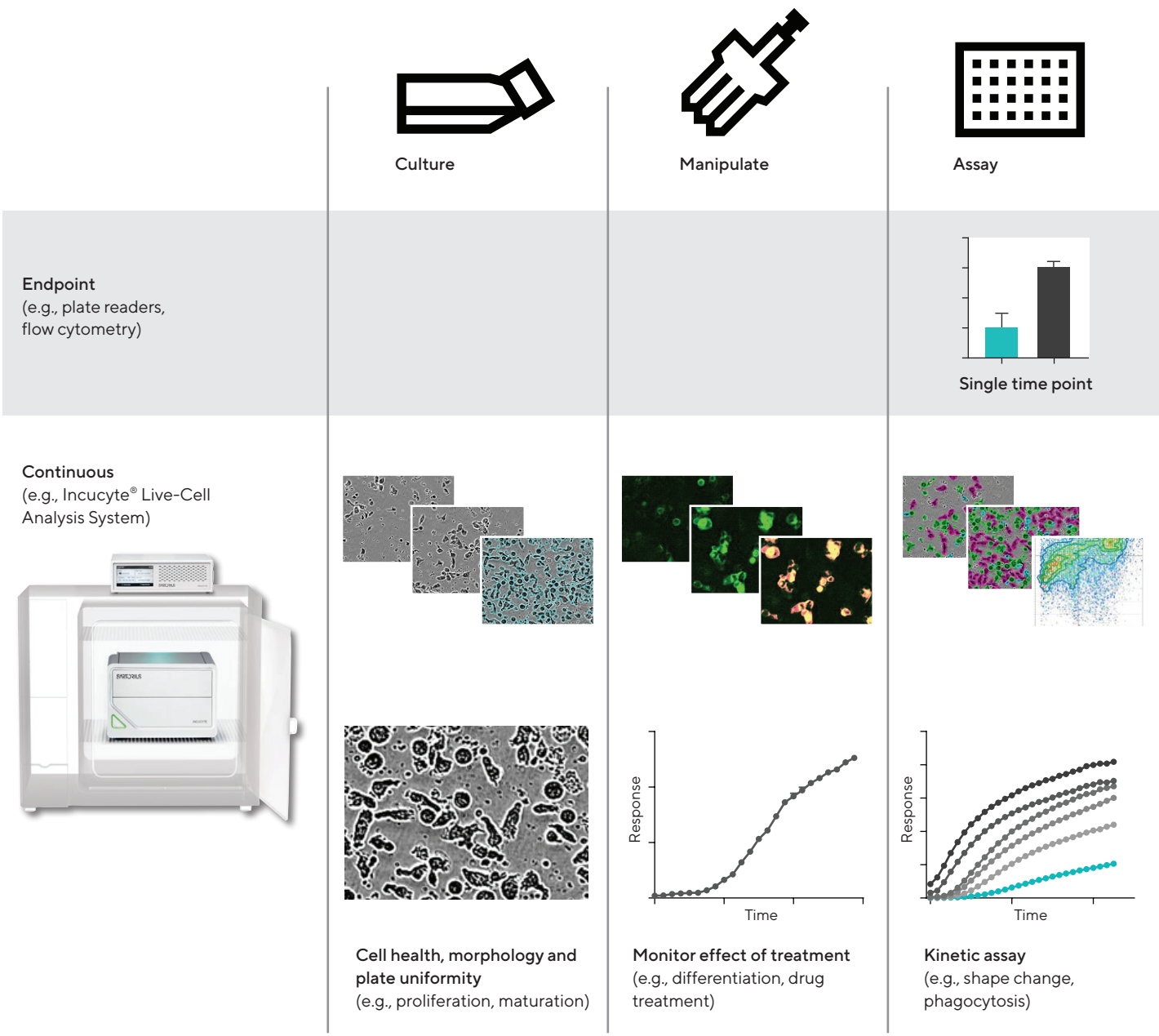

Figure 1: Workflow, QC and cell health. Comparison of continuous live-cell analysis and endpoint workflows. For live-cell analysis, images and data are collected in real time from within the cell incubator, throughout the culture, manipulation, and kinetic assay phases.

Applications in Immunology

Live-cell analysis is applicable to both the generalized biology of immune cells, such as proliferation, activation, differentiation, surface protein dynamics and cell heath, as well as more specialized functions including cytolysis (immune cell killing), phagocytosis, NETosis and chemotaxis. The approach is amenable to all types of immune cells, including T cells, B cells, macrophages, neutrophils, as well as dendritic cells, and can be used with monocultures, co-cultures and more advanced 3D cell models.

1. Proliferation and Counting

Immune cells can be enumerated non-invasively with live-cell analysis in a number of different ways. First, area measurements (% confluence of phase contrast images) can be used as a good proxy of the number of cells (Figure 2). At least up to 80% confluence, this metric is a robust indicator as evidenced by a high correlation with direct cell counting (Sceptre, Millipore) and ATP luminescence measurements. This correlation can weaken in densely packed cultures, or if individual cell areas change over time. Alternatively, fluorescent labels can be used, such as nuclear–targeted fluorescent proteins (e.g., Incucyte® Nuclight Lentivirus) or non-perturbing dyes (e.g., Incucyte® Cytolight Rapid Dye). Nuclear counting provides an accurate measure of cell number even when cells are packed in, and fluorescent labels can be used to identify different cells in co-cultures.

In a recent development, label-free cell counts can be obtained using new image segmentation tools (Incucyte® Cell-by-Cell Analysis). Metrics, such as size and eccentricity, are calculated at the individual cell level for all the cells in the field of view and displayed using 'dot plot' tools that are similar to those used in flow cytometry. This powerful technique provides accurate cell counts and greater insight into the distribution of single cell parameters in the population. Whichever method is applied, the assays yield full time-course data, valuable morphological insight, and can be miniaturized to 96- and/or 384-well formats providing sufficient throughput for industrial discovery purposes.

2. Identification and Immuno-Phenotyping

Fluorescently-labeled antibodies (Abs) to CD-surface markers are widely used in flow cytometry for identifying and classifying immune cells ("immuno-phenotyping"). At least 15 discrete subtypes of human T cells have been described based on these profiles (e.g., CD4+, CD8+, etc.). Methods have now been developed for live-cell analysis using the same principal. Rather than using directly-labeled Abs, the preferred approach is to conjugate the anti-CD Ab to an isotype matched fluorescent Fc-targeting Fab fragment (e.g., Incucyte® Fabfluor-488 Dye). This can be done with a simple one-step mix protocol. A non-perturbing background fluorescence suppressing dye is used in the assay to help

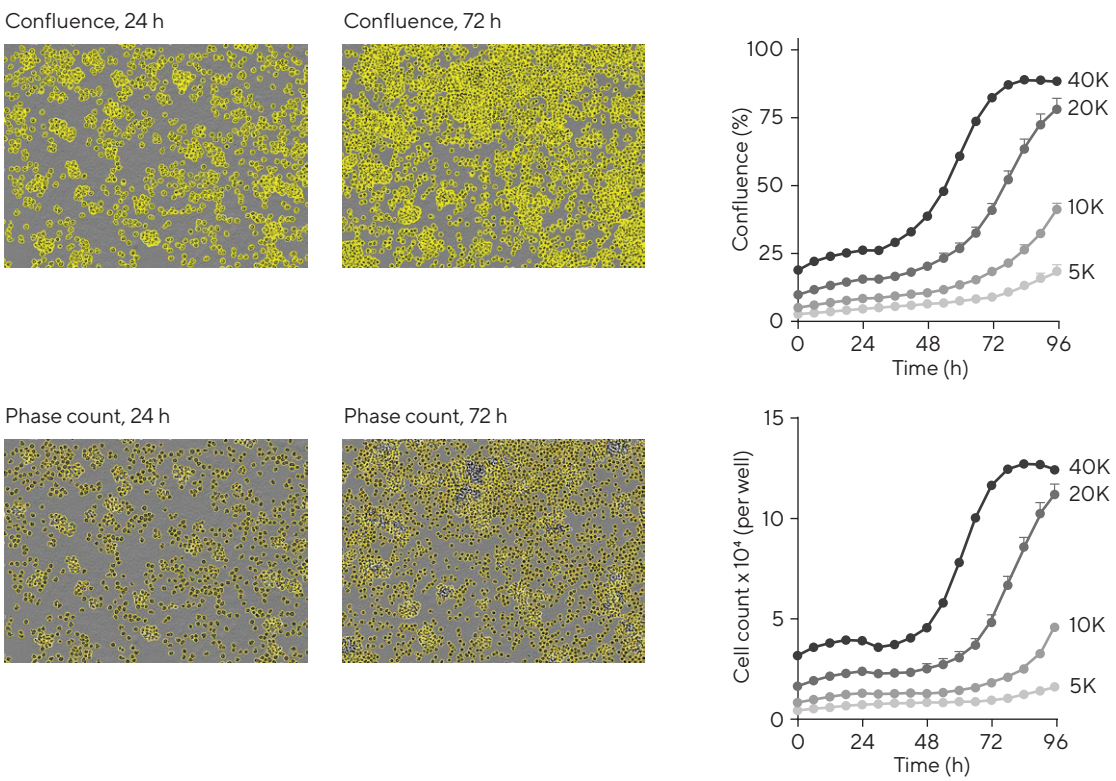

Figure 2: Assessment of cell proliferation. Images show Ramos B cells with either confluence phase masking or individual cell masking using Incucyte® Cell-by-Cell Analysis Software Module at 24 and 72 h post-platings. Analysis of images by either method enables the production of proliferation plots (right column) with similar growth profiles.

improve the 488 nM fluorescent signal window. The Fabfluor-488 labeled Ab and suppressor are then added directly to the cells, and only cells that express the surface marker will fluoresce. Subsets of cells can then be readily identified and quantified over time.

In the simplest immuno-phenotyping application, the percentage of marker positive cells (e.g., CD4+, CD8+) can be determined and morphological attributes can be associated with different subsets. Changes in the proportions of cells over time can be measured. More useful, perhaps, is the possibility to observe the interactions between cell subsets in the culture—for example, in a PBMC-based immune-cell killing assay, the physical interactions of CD8+ cytotoxic T cells with their tumor targets can be visualized (Section 5).

3. Activation and Differentiation

Differentiation and activation of immune cells are critical steps in the development of immunity and the immune response. Cells are expanded and primed for their effector functions via receptor signaling pathways, which culminate in gene expression, differentiation, and phenotypic changes. Live-cell analysis is well suited to studying the complex and dynamic nature of these events. In a simple case, we assessed chemokine-induced activation of human neutrophils (Figure 3). Cell-by-cell analysis techniques demonstrated time- and concentration-dependent changes in area, shape (eccentricity) and the surface expression of CD11b (integrin aM, part of the complement C3 receptor—quantified using a Fabfluor-488/Ab complex) in response to CXCL8. The time courses of these changes were similar (0–6 h) and the EC_{50} values for the increase in eccentricity and CD11b expression were 0.63 nM and 0.22 nM, respectively. CXCL8-induced activation was attenuated by an anti-CXCL8 antibody.

In a further illustration, we probed stimuli-induced differentiation of human THP-1 monocytes to macrophages. In both control (untreated) and stimulated THP-1 cells, no changes in the ubiquitous cell surface marker CD45 were observed throughout the 3 d time-course of the experiment. CD45 can be considered a stable 'housekeeping' protein in this regard. THP-1 cells showed little expression of CD11b, CD14

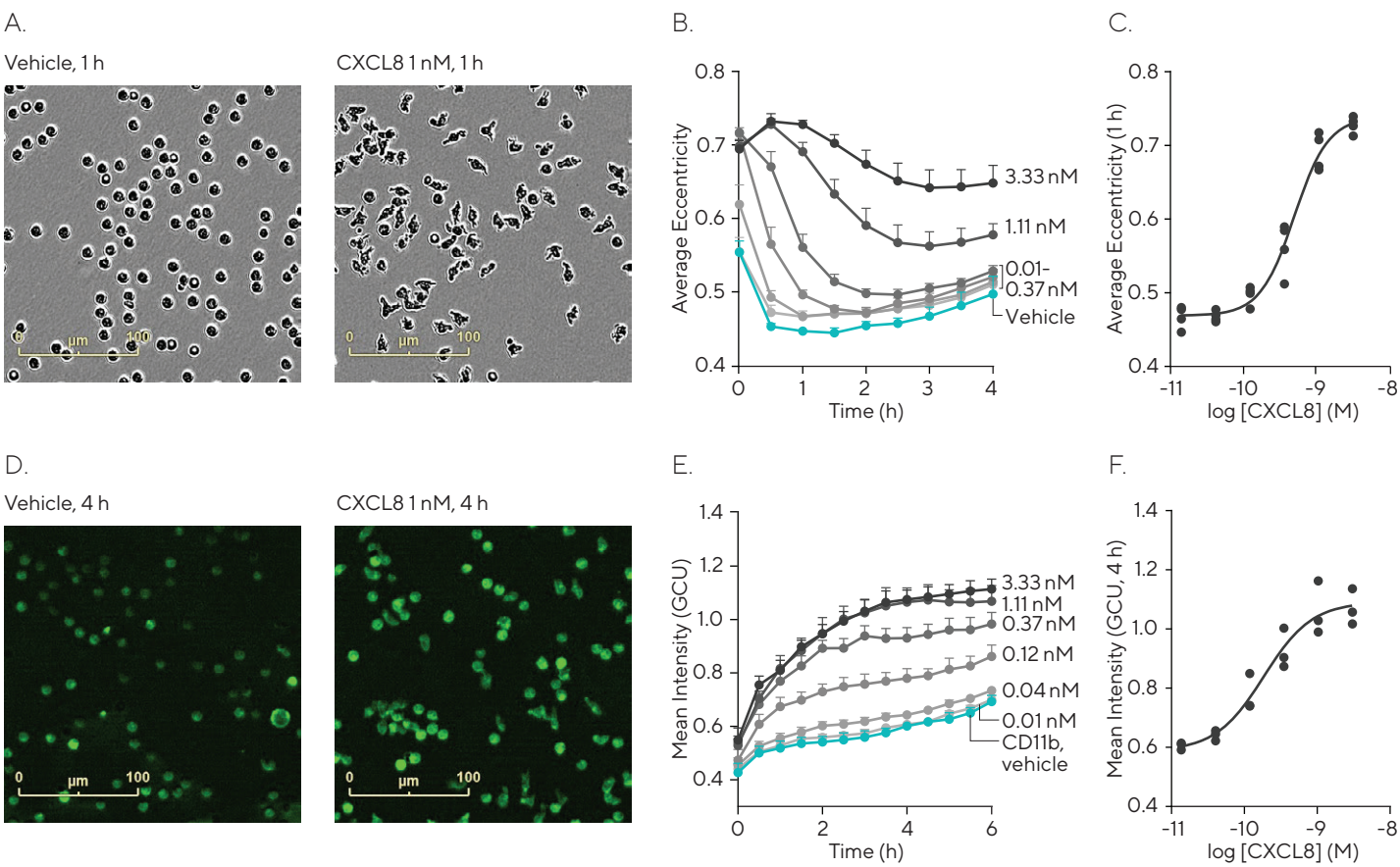

Figure 3: Quantification of neutrophil activation. Freshly isolated human neutrophils were seeded (40K/well) in Matrigel® (50 µg/mL) coated 96-well plates and treated with increasing concentrations of CXCL8 in the presence of Fabfluor-488 labeled CD11b antibody (1 µg/mL). Images were captured every 30 min (20X) and analyzed using Incucyte® Cell-by-Cell Analysis Software. Images (A and D) show the change in morphology and CD11b expression induced by CXCL8 (1 nM). Morphology was quantified as a change in eccentricity and CD11b expression as mean intensity. Data demonstrates a rapid, concentration dependent increase in eccentricity with CXCL8 with an EC_{50} of 0.63 nM (B and C), in combination with an increase in CD11b expression with and EC_{50} of 0.22 nM (E and F). Data shown as mean of at least 3 separate donors ± SEM.

(an endotoxin receptor), and CD40 (a co-stimulatory protein) for up to 72 h under control conditions. All three CD markers could be upregulated to different extents over 12–72 h with specific differentiation agents, i.e., vitamin D3, IFNγ + mCSF, IFNγ + LPS, Phorbol Myristate Acetate (PMA). Most notably, PMA upregulated CD11b and CD40, but not CD14, while vitamin D3 increased expression of CD11b and CD14 in a time-dependent manner (Figure 4). Vitamin D3 did not upregulate CD40. From close inspection of the cell images, only PMA produced a marked change in morphology, yielding large, flattened, adherent "macrophage-like" cells. Only those cells treated with PMA were able to phagocytose pHrodo®-labeled apoptotic Jurkat cells (Section 6).

Together, these data illustrate how temporal changes in surface protein markers, morphology, and function can be associated using a single method, and highlight characteristic response profiles to individual differentiation stimuli.

4. Health and Apoptosis

The applications above can also be duplexed with apoptosis or cell health readouts using fluorogenic dyes that are optimized for live-cell analysis. For example, cellular apoptosis can be measured both via externalized phosphotidyl-serine (Incucyte® Annexin V Dye) and Caspase 3/7 activity (Incucyte® Caspase 3/7 Dye; Zhang, *et al.*, 1997; Cen, *et al.*, 2008; Daya, *et al.*, 2010). Cell impermeant DNA binding fluoroprobes (e.g., Incucyte® Cytotox Red Dye) can be used to detect loss of integrity of the cell membrane. The real-time readout of live-cell analysis provides insight into the time-course of apoptosis, cell death, and their relationship to cell proliferation in dividing cultures (Artymovich and Appledorn, 2014).

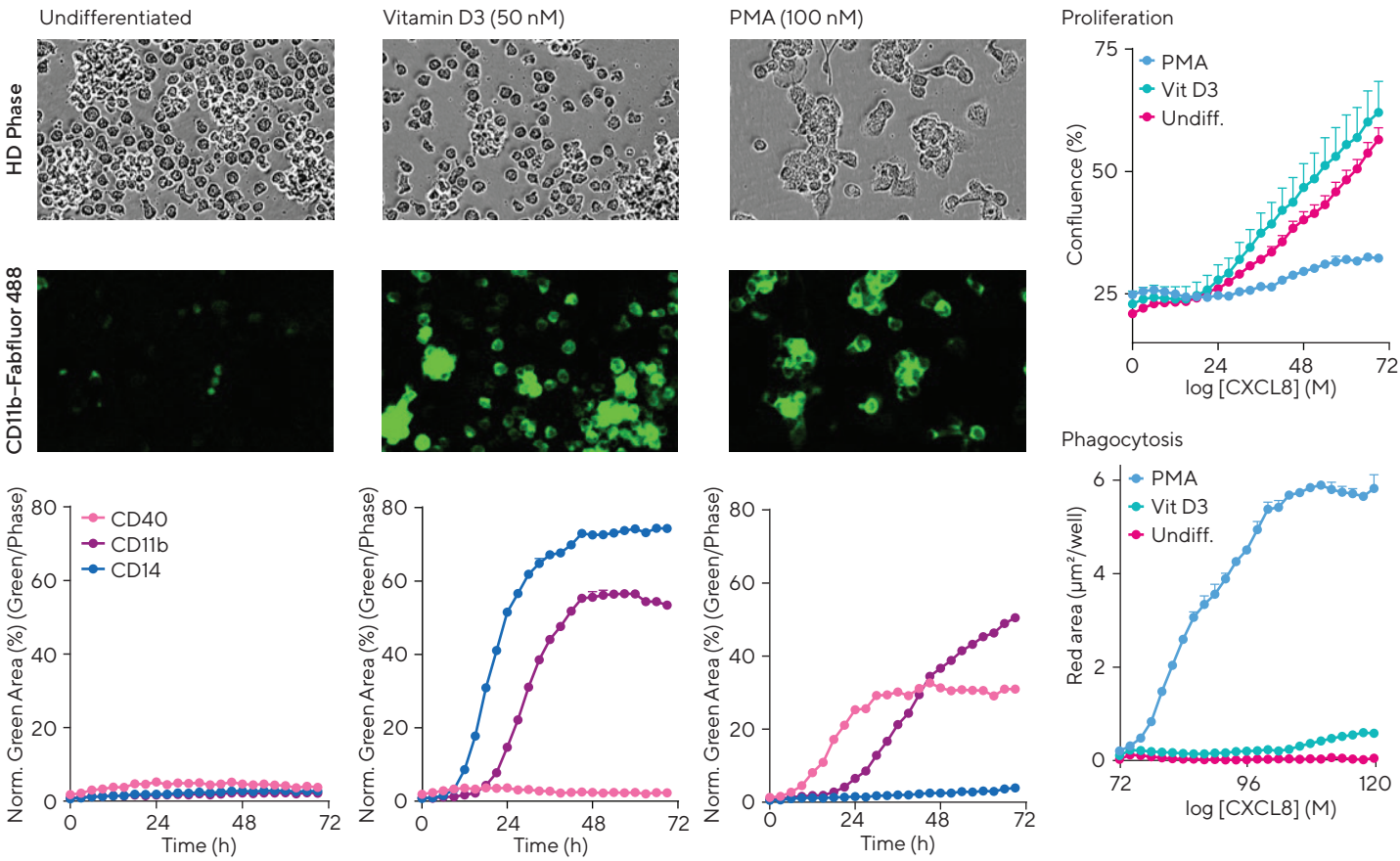

Figure 4: Multiplex cell surface marker, phagocytic activity, and proliferation measurements plus visualization of morphology to study differentiation. THP-1 monocytes were exposed to media (undifferentiated), vitamin D3 or PMA in the presence of Incucyte® Fabfluor-488 Dye complexed to CD11b, CD14 or CD40. PMA showed a marked change in cell morphology (HD phase contrast images) compared to media alone or vitamin D3 treated cells. The kinetic graphs highlight differential and time-dependent surface protein expression in response to the various treatments. Interestingly, PMA, but not media or vitamin D3, yields a decrease in cell proliferation (confluence) and concordant increase in phagocytic potential as measured by efferocytosis of apoptotic Jurkat cells labeled with pHrodo® Red Cell Labeling Kit for Incucyte®.

5. Immune Cell Killing (Cytolysis)

Cytotoxic T cells (CTLs), natural killer (NK) cells and certain neutrophils have the ability to kill infected or malignant cells. While the killing mechanisms may differ (e.g., release of cytokines, cytotoxic granules or ROS, Fas/FasL interactions), ultimately these immune defenders inactivate unwanted cells through cell lysis. Cytolysis assays typically involve measuring the release of either a pre-loaded detector (e.g., Cr51) or a cellular enzyme (e.g., LDH) from the dying target cells. If apoptotic mechanisms are involved, biochemical assays for annexin V or caspase 3/7 activation may be employed. The key challenges are: (1) high background signals; (2) discriminating contaminating signals that may arise from the effector (killing) cells; and (3) knowing when to measure the killing end point.

Live-cell analysis offers a number of approaches to cytolysis measurement. Most simply, target cells can be labeled with a fluorescent protein (e.g., RFP), and as they are lysed, monitored for a loss in red fluorescence. For example, THP-1 cells were stably transfected with a nuclear targeted RFP and plated on 96-well plates. Addition of pre-activated PBMCs (anti-CD3/IL-2, 72 h), caused a rapid and time-dependent lysis of the THP-1 cells and ultimately a complete loss of the RFP signal. The rate of cytolysis was dependent on the number of PBMCs (ratios 1:1 to 1:10). The cytolysis signal was validated by inspection of the cell images, showing membrane disruption, loss of motility and shrinkage of the target cell. A similar assay principle can be applied to killing of tumor spheroids. In Figure 5, Incucyte® Nuclight Red A549 tumor cells were formed and grown as 3D spheroids in ultra-low attachment plates for 3 days prior to the addition of PBMCs. Over time the PBMCs lysed the spheroids and ablated the red fluorescence signal.

This format can be extended to directly measure apoptosis of the target cells in the second fluorescence channel (McCormack, *et al.*, 2013). Providing that the effector cells are smaller than the target cells, any apoptotic signal arising from the PBMCs can be excluded by size gating of the fluorescent objects. To illustrate this, CD8+ cytotoxic T cells were co-cultured on 96-well plates with Incucyte® Nuclight Red A549 cells in the presence of Incucyte® Caspase 3/7 Dye (5 mM). The T cells were activated within the co-culture to kill via the addition of anti-CD3/IL-2. In this example, it took approximately 48 h for the T cell-killing to commence—a concomitant rise in (size-gated) apoptotic nuclei (green Caspase 3/7 labeling) and fall in red cell number (cytolysis) was observed verifying apoptotic-mediated cell death.

These methods are exceptionally useful for characterizing the phenotypic effects of checkpoint inhibitors, CAR-T cells, bi-specific antibodies, and other immune-based therapies.

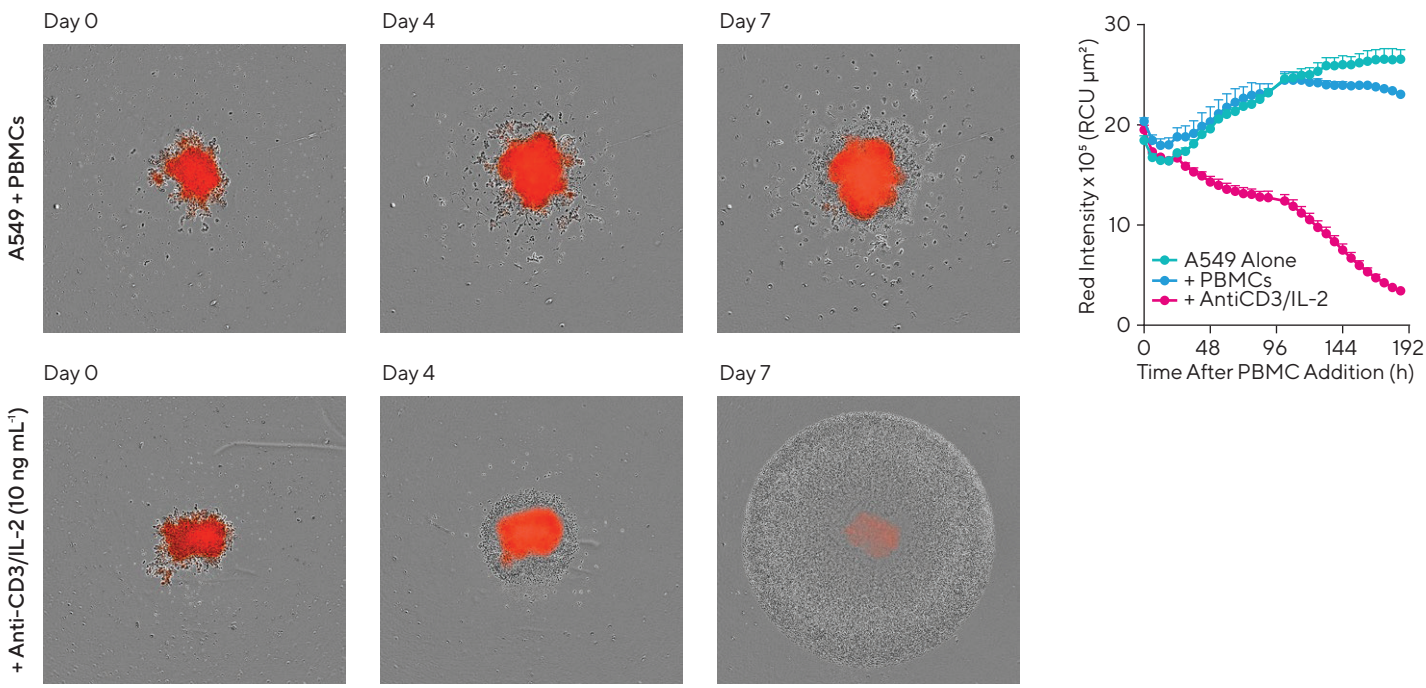

Figure 5: Impact of activated PBMCs on tumor spheroid proliferation. A549 tumor cells stably expressing Incucyte® Nuclight Red Lentivirus were seeded in a round bottom ULA 96-well plate (2,500 cells/well) and allowed to form spheroids for 3 d. Once formed, spheroids were co-cultured with freshly isolated PBMCs (E:T, 2.5:1) in the presence or absence of an Anti-CD3 and IL-2 antibody cocktail (10 ng/mL of each). Incucyte® HD phase and fluorescence images compare the effect of PBMCs on spheroid proliferation in the absence (non-activated, top panel) and presence (activated, bottom panel) of Anti-CD3 and IL-2 antibodies. Note the marked loss of fluorescence intensity in spheroids in the presence of activated PBMCs. Time course plot shows spheroid cytotoxicity quantified as a loss of fluorescence intensity over time. Data were collected over 7 d at 6 h intervals. Each data point represents mean ± SEM, n = 3 wells.

6. Phagocytosis and Cell Clearance

Phagocytosis is a specific form of cellular endocytosis by which microorganisms (e.g., microbial pathogens) and unwanted cells (e.g., foreign, dying) are inactivated and removed from the body. The professional phagocytes of the immune system are macrophages, neutrophils, Kuppfer cells, microglia and immature dendritic cells. Assays for phagocytosis typically require the detection of a fluorescent label on the microorganism or cell as it is internalized. To be useful, it is important to distinguish between phagocytosis and non-specific cellular uptake and/or surface-bound, non-internalized label. Live-cell analysis methods have been developed using pH-sensitive dye labels (e.g., pHrodo®) that are conjugated to bacterial wall proteins or target cells. When the protein or target cell is phagocytosed and enters the acidic environment of the phagosome, the resulting increase in dye fluorescence is measured over time.

In the first example, the phagocytosis of *Escherischia coli* by mouse J774.1 macrophages was measured by adding pHrodo®-green labeled *E. coli* bioparticles. Intracellular fluorescence increased over time (24 h) as the bioparticles were internalized (Figure 6). In control experiments, no fluorescence was observed in either the absence of bioparticles or if non-phagocytic cells (e.g., A549) were used (data not shown). The signal could be ablated by inhibitors of phagocytosis including cytochalasin D and latruculin A. From close inspection of the cell images and time-lapse movies, the fluorescence signal was restricted to the cytoplasm (presumably phagolysosome). Moreover, the engulfment of bioparticles via the formation of phagocytic cups in the cell membrane could be clearly observed.

To exemplify phagocytosis of mammalian cells ("efferocytosis"), we characterized anti-CD47 antibody-mediated engulfment of CD47+ CCRF-CEM T-lymphocytes by mouse bone-marrow derived macrophages. CD47 is a transmembrane "don't-eat-me" signaling protein that enables tumor cells to evade clearance by neighboring phagocytes. Blocking CD47 allows phagocytes to identify and clear tumor cells and is a promising new approach for immunotherapy. Anti-CD47 Ab (0.04–5 mg mL), but not IgG-control, produced time- and concentration-dependent

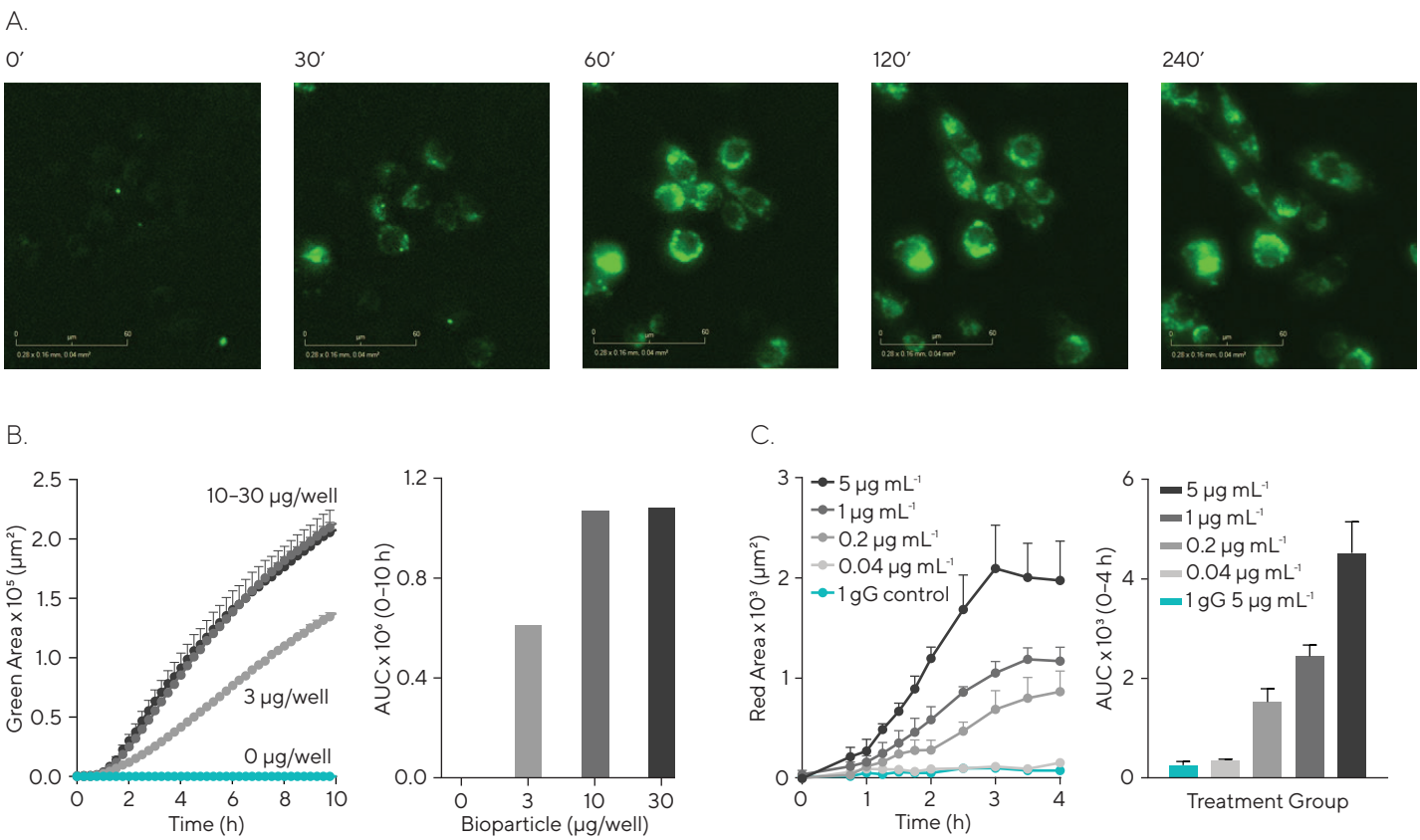

Figure 6: Kinetically monitor and quantify phagocytosis. Temporal visualization of J774A.1 mouse macrophages phagocytosing pHrodo® Green *E. coli* Bioparticles® for Incucyte® over 4 h. Images (A) verify the presence of fluorescent punctate (phagosomal) labeled structures in the cytosol but not in the nucleus. J774A.1 mouse macrophages were also exposed to increasing concentrations of pHrodo® Green *S. aureus* Bioparticles® for Incucyte®. Note that phagocytosis is bioparticle quantity-dependent (B). Viable T lymphoblast cells CCRF-CEM were labeled with the pHrodo® Red Cell Labeling Kit for Incucyte® and exposed to either anti-CD47 monoclonal antibody or IgG isotype control. The anti-CD47 antibody binds to the 'don't eat me' signal on CCRF-CEM cells to promote macrophage mediated phagocytosis. In the presence of anti-CD47, target cells were engulfed by bone marrow-derived macrophages, increasing the fluorescent signal and producing a concentration-dependent effect (C). The presence of isotype control IgG had no effect on engulfment at all concentrations tested.

engulfment of CCRF-CEMs (30 min–6 h, Figure 6C). Apoptotic CCRF-CEM cells (camptothecin, 10 mM) were also engulfed. In both cases, the signal window was large, and engulfment could be verified by visualization. This functional assay is amenable to screening for novel CD47 modulators and modifiers of cellular phagocytosis.

7. NETosis

NETosis is a specialized form of programmed cell death and one of several mechanisms by which the body defends against infection. When neutrophils encounter invading pathogens, they release a mixture of antimicrobial proteins and chromatin to trap and degrade microbes. Live-cell analysis can be used to automatically visualize and quantify these extracellular traps, or NETs, in real time using a fluorescent DNA-binding reagent (Gupta, *et al.*, 2017).

When neutrophils are treated with NETosis inducing stimulants (e.g., PMA, ionomycin), a rapid rise in fluorescence occurs, which appears as a cloud or halo of degraded DNA outside of the cell boundary (Figure 7). Degradation of the nuclei and loss of cell motility is observed. By duplexing this measurement with either phosphotidylserine (PS) externalization or reactive oxygen species (ROS) detectors, different mechanisms of NETosis can be elucidated. Real time data analysis is also helpful in determining the most appropriate time-points for complementary biochemical analyses, such as the presence of extracellular myeloperoxidase (MPO) in the NETs. Gupta concluded that live-cell analysis is "a powerful tool to assess neutrophil physiology and NETosis, as well as to swiftly develop and test novel neutrophil targets".

8. Chemotaxis

Chemotaxis is the directional movement of cells in response to a chemical stimulus and is an essential component of immune responses. Neutrophils, monocytes, T cells, macrophages and microglia are all drawn toward pathogens and inflammatory stimuli in this way. Chemotaxis can be measured with live-cell analysis, using specialized Incucyte® Clearview 96-Well Plates (e.g., Taylor, *et al.*, 2016; He, *et al.*, 2018). These novel transwell consumables incorporate precision, laser-drilled pores in each well for cells to move through. Unlike traditional Boyden chamber transwell assays, cells can be visualized and quantified as they move toward the chemoattractant. As with the earlier applications, this approach affords the full time-course of biology with morphological insight. As another upside, considerably fewer (5- to 10-fold less) cells are required compared to Boyden chambers.

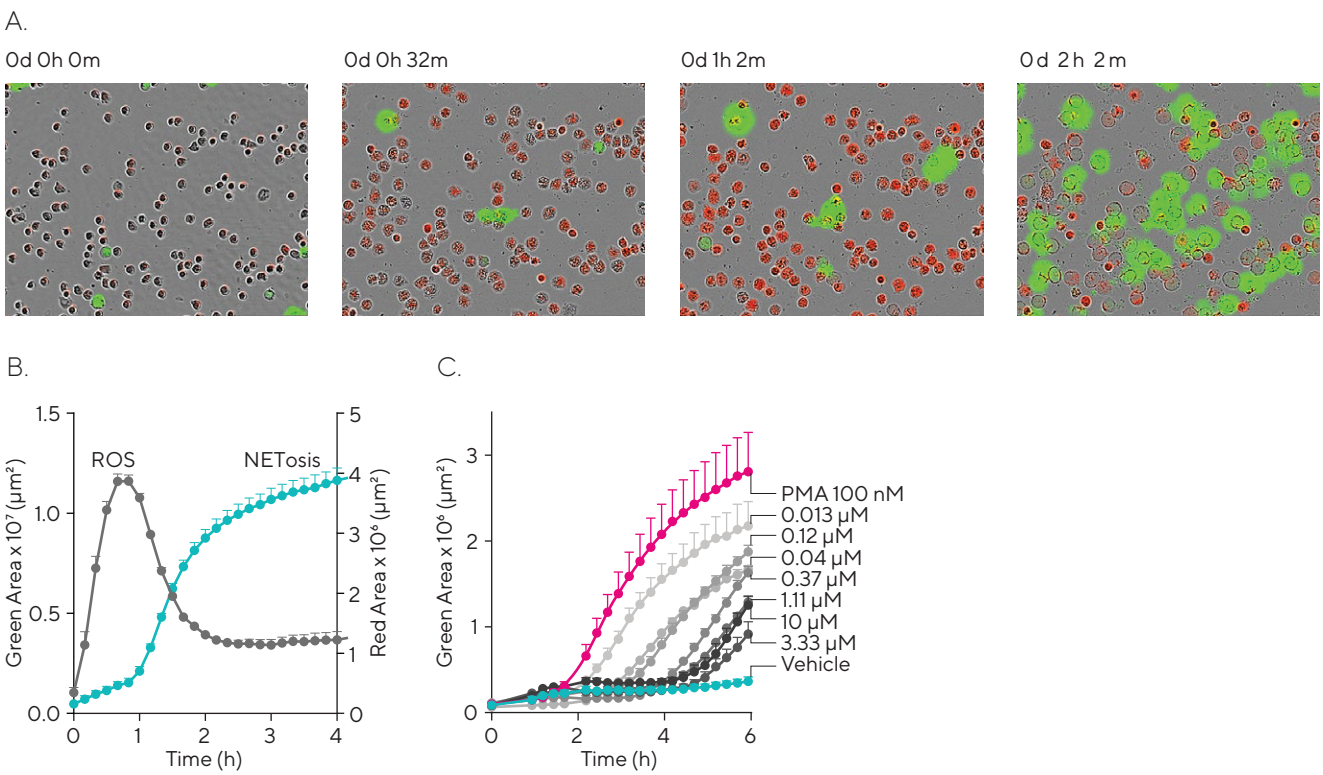

Figure 7: Quantification of NETosis. Freshly isolated human neutrophils were treated with PMA (100 nM) in the presence of Incucyte® Cytotox Green Dye (250 nM) and CellROX® Deep Red (5 µM, Thermo Scientific). Phase and fluorescence images show (A) the transient production of reactive oxygen species (ROS, red, 0–2 h), decondensation of nuclei (30–60 min) and increase in extracellular DNA (green, > 1 h). PMA produces a rapid, transient increase in ROS production (red area), with subsequent (post-1 h) NETosis production (green area, B). DPI, a known ROS inhibitor, induces attenuation of NETs in a time- and concentration-dependent manner (C).

9. Viral Infection

Measuring the infectivity and replication of viruses in mammalian cells *in vitro* is critical to our understanding of viral disease and for screening new anti-viral drugs, vaccines, and immune-cell adjuvants. In contrast to traditional plaque assays and focus-forming assays, live-cell analysis can automatically quantify viral spread and replication over time by counting the number and extent of cells infected with fluorescent protein (e.g., GFP)–tagged viral constructs. Viral titers can be determined accordingly.

This approach has been published for a range of viruses including Foot and Mouth Disease, Chikungunya, and HCMV (Forrest, *et al.*, 2014; Stevenson, *et al.*, 2014; Tulloch, *et al.*, 2014; Herod, *et al.*, 2016a, b; Stewart, *et al.*, 2015; Joubert, *et al.*, 2016). Oncolytic viruses have also been analyzed in this way (Berghauser, *et al.*, 2015). The images and time-lapse movies provide insight into the spread of the virus, and for cytopathic viruses, the degree of bystander cell death via apoptosis | necrosis can be measured. One interesting advantage of the live-cell analysis workflow is that once the virus or replicon is added to the cells, the assay does not require the cell plates to leave the cell incubator. Thus, even highly infectious viruses can be safely analyzed in appropriate biocontainment facilities without exposing the operator to potential hazard.

10. Antibody Internalization

Monoclonal antibodies (mAb) and antibody-drug conjugates (ADCs) are widely used to target immune cells, particularly in immuno-oncology and auto-immune diseases. A key property of these biologics is the extent and rate of internalization into different cells, which governs their efficacy, safety and pharmacodynamic profile.

Live-cell analysis can be used to quantify Ab internalization measurements in an industrialized 96-well format. Internalization of the Ab into the acidic lysozyme is detected using a pH-sensitive fluorescent label along similar lines to the phagocytosis measurements (Section 6). Labeling is realized via an Fc-binding fragment (Incucyte® Fabfluor-pH Dye) single step, no wash protocol that provides efficient, high throughput sample preparation. To illustrate this, six commercially available CD71 (transferrin receptor) Abs were labeled with Incucyte® Fabfluor-pH Dye, serially diluted (1:2, 4.6–10,000 ng mL^{-1}) and added to HT-1080 osteosarcoma cells. Three of the Abs produced a large internalization signal with detection < 50 ng mL^{-1}, while the other three were internalized weakly with signal only visible at higher concentrations. A mean Z′ value of 0.82 was calculated from control wells indicating a microplate assay with high precision and robustness (Figure 8).

The demonstration that different Abs to the same surface protein have distinct internalization profiles highlights the importance of such measurements. Increasingly, quantifying and comparing the internalization rates of different Ab-drug candidates and production batches will become a critical step in the biopharmaceutical selection and optimization process.

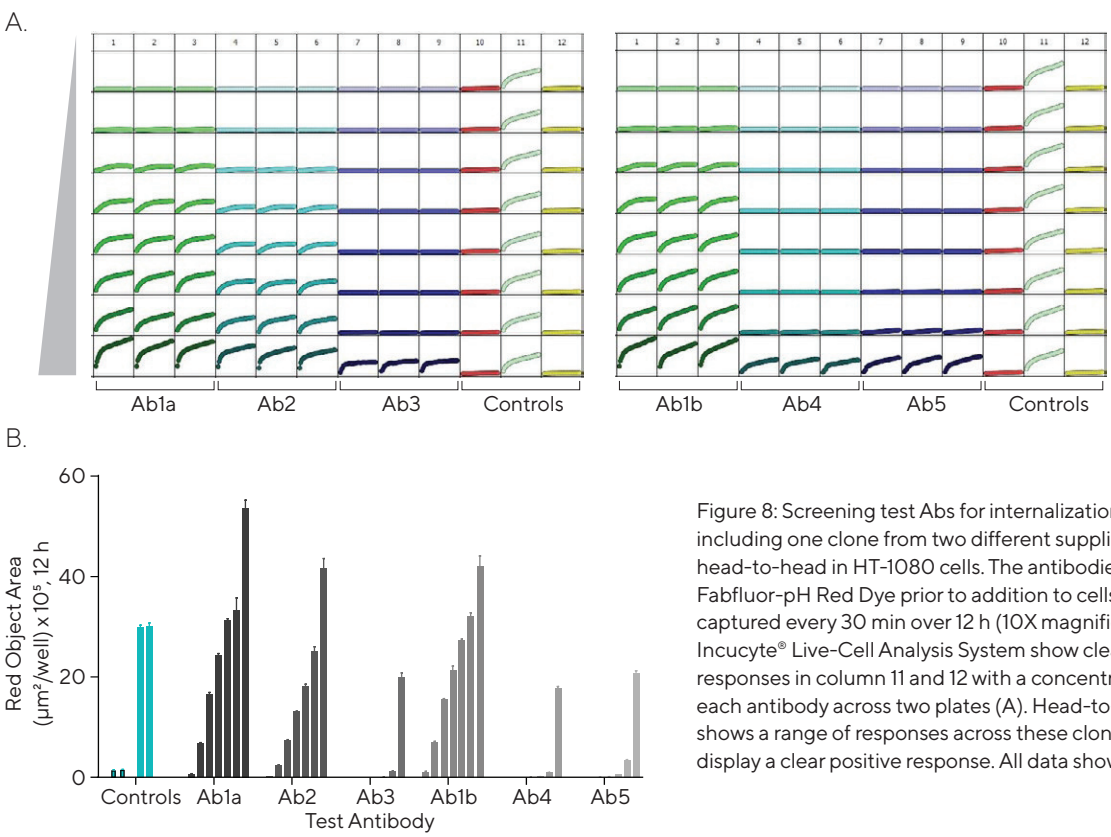

Figure 8: Screening test Abs for internalization. Six different CD71 antibodies, including one clone from two different suppliers (clone 1a and 1b), were tested head-to-head in HT-1080 cells. The antibodies were labeled with Incucyte® Fabfluor-pH Red Dye prior to addition to cells, and the internalization signal captured every 30 min over 12 h (10X magnification). Plate views taken from Incucyte® Live-Cell Analysis System show clear positive and negative control responses in column 11 and 12 with a concentration-dependent response for each antibody across two plates (A). Head-to-head analysis of antibody data shows a range of responses across these clones (B) control responses at 12 h display a clear positive response. All data shown as mean of eight wells.

Summary and Perspective

From the ten examples described, live-cell analysis is applicable to a wide range of generalized and specialized immune cell measurements. A key and common feature is that the cells remain unperturbed throughout the duration of the experiment. As such, the method readily lends itself to coupling with other analytical techniques. For example, the supernatants from cells in live-cell analysis experiments can be sampled and measured for analytes such as cytokines, and cells can be lifted at the end of the experiment and probed using flow cytometry, PCR and/or other methods.

The ability to study immune-cell biology over time in a completely non-perturbing way addresses a major limitation of most other assay approaches that provide only single time point measures. The deep biological insight and validation provided through cell images and time-lapse-movies, along with enhanced productivity through automated image capture and processing, positions live-cell analysis as a powerful approach for the study of immune cell biology.

References

Proliferation, Counting, Cell Health, and Apoptosis

- Zhang G, Gurtu V, Kain SR, Yan G. **Early detection of apoptosis using a fluorescent conjugate of annexin V.** *Biotechniques,* 23(3);525-531 (1997)
- Cen H, Mao F, Aronchik I, Fuentes RJ, Firestone GL. **Devd-Nucview 488: A Novel Class of Enzyme Substrates for Real-Time Detection of Caspase-3/7 Activity in Live Cells.** *FASEB J,* 22(7);2243-2252 (2008)
- Daya S, Roberts M, Isherwood B, Ingleston-Orme A, Caie P, Teobald I, Eagle R, Carragher N. **Integrating an Automated *in vitro* Combination Screening Platform with Live-Cell and Endpoint Phenotypic Assays to Support the Testing of Drug Combinations.** *SBS 16th Annual Conference and Exhibition* (2010)
- Artymovich K, Appledorn DM. **A Multiplexed Method for Kinetic Measurements of Apoptosis and Proliferation Using Live-Content Imaging.** *Apoptosis and Cancer: Methods and Protocols,* 1219;35-42 (2014)

Immune Cell Killing (Cytolysis)

- McCormack E, Adams KJ, Hassan NJ, Kotian A, Lissin NM, Sami M, Muji´c M, Osdal T, Gjertsen BT, Baker D, Powlesland AS, Aleksic M, Vuidepot A, Morteau O, Sutton DH, June CH, Kalos M, Ashfield R, Jakobsen BK. **Bi-specific TCR-anti CD3 redirected T cell targeting of NY-ESO-1- and LAGE-1-positive tumors.** *Cancer Immunol Immunother,* 62(4);773-785 (2013)

Phagocytosis and Cell Clearance

- Kapellos TS, Taylor L, Lee H, Cowley SA, James WS, Iqbal AJ, Greaves DR. **A novel real-time imaging platform to quantify macrophage phagocytosis.** *Biochem Pharmacol,* 116;107-19 (2016)

NETosis

- Gupta S, Chan DW, Zaal K, Kaplan M. **A high throughput real-time imaging technique to quantify NETosis and distinguish mechanisms of cell death in human neutrophils.** *J Immunol,* 200(2);869-879 (2018)

Chemotaxis

- Taylor L, Brodermann, MH, McCaffary, D, Iqbal, AJ Greaves, DR. **Netrin-1 reduces monocyte and macrophage chemotaxis towards the complement component C5a.** *PLoS ONE,* 11(8);e0160685 (2016)
- He Y, Yao X, Taylor N, Bai Y, Lovenberg T, Bhattacharya A. **RNA sequencing analysis reveals quiescent microglia isolation methods from postnatal mouse brains and limitations of BV2 cells.** *J Neuroinflammation,* 15;153 (2018)

Viral Infection

- Forrest S, Lear Z, Herod MR, Ryan M, Rowlands DJ, Stonehouse NJ. **Inhibition of the FMDV sub-genomic replicon by RNA aptamers.** *J Gen Virol,* 95(12);2649-2657 (2014)
- Stevenson EV, Collins-McMillen D, Kim JH, Cieply SJ, Bentz GL, Yurochko AD. **HCMV reprogramming of infected monocyte survival and differentiation: a Goldilocks phenomenon.** *Viruses,* 6(2);782-807 (2014)
- Tulloch F, Pathania U, Luke GA, Nicholson J, Stonehouse NJ, Rowlands DJ, Jackson T, Tuthill T, Haas J, Lamond AI, Ryan MD**. FMDV replicons encoding green fluorescent protein are replication competent.** *J Virol Methods,* 209;35-40 (2014)
- Herod MR, Loundras EA, Ward JC, Tulloch F, Rowlands DJ, Stonehouse NJ. **Employing transposon mutagenesis to investigate Foot-and-Mouth Disease virus replication.** *J Gen Virol,* 96(12);3507-3518 (2015)
- Herod MR, Ferrer-Orta C, Loundras EA, Ward JC, Verdaguer N, Rowlands DJ, Stonehouse, NJ. **Both cis- and trans-activities of the Foot-and-Mouth Disease virus 3D polymerase are essential for viral RNA replication.** *J Virol,* 90(15);6864-6883 (2016)
- Stewart H, Bartletta C, Ross-Thrieplanda D, Shawb J, Griffin S, Harris M. **A novel method for the measurement of hepatitis C virus infectious titres using the Incucyte® ZOOM and its application to antiviral screening.** *J Virol Methods,* 218;59-65 (2015)
- Joubert PE, Stapleford K, Guivel-Benhassine F, Vignuzzi M, Schwartz O, Albert ML. **Inhibition of mTORC1 enhances the translation of Chikungunya proteins via the activation of the MnK/eIF4E pathway.** *PLoS Pathog,* 11(8);e1005091 (2016)
- Berghauser Pont LM, Kleijn A, Kloezeman JJ, van den Bossche W, Kaufmann JK, de Vrij J, Leenstra S, Dirven CM, Lamfers ML. **The HDAC inhibitors scriptaid and LBH589 combined with the oncolytic virus Delta24-RGD exert enhanced anti-tumor efficacy in patient-derived glioblastoma cells.** *PLoS One,* 10;e0127058 (2015)

Review

Immunotherapy

For reprint orders, please contact: reprints@futuremedicine.com

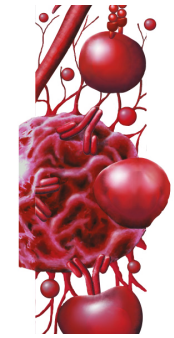

Implications of T cell receptor biology on the development of new T cell therapies for cancer

Ian R Hardy[1], Wolfgang W Schamel[2], Patrick A Baeuerle[1,3], Daniel R Getts[1] & Robert Hofmeister*[,1]

[1]TCR[2] Therapeutics, Inc., 100 Binney St. Suite 710, Cambridge, MA 02142, USA

[2]Department of Immunology, Faculty of Biology, BIOSS Center for Biological Signalling Studies, CIBSS – Centre for Integrative Biological Signalling Studies & Centre for Chronic Immunodeficiency CCI, University of Freiburg, Schänzlestraβe 18,79104 Freiburg, Germany

[3]Institute for Immunology, Ludwig-Maximilians-University Munich, Grosshadernerstr. 9, 82152 Planegg-Martinsried, Germany

*Author for correspondence: robert@tcr2.com

Recently, two chimeric antigen receptor (CAR) T cell therapies were approved based on their remarkable efficacy in patients with hematological malignancies. By contrast, CAR-T cell therapies results in solid tumors have been less promising. To develop the next generation of T cell therapies a better understanding of T cell receptor (TCR) biology and its implication for the design of synthetic receptors is critical. Here, we review current and newly developed forms of T cell therapies and how their utilization of different components of the TCR signaling machinery and their requirement for engagement (or not) of human leukocyte antigen impacts their design, efficacy and applicability as cancer drugs. Notably, we highlight the development of human leukocyte antigen-independent T cell platforms that utilize the full TCR complex as having promise to overcome some of the limitations of existing T cell therapies.

First draft submitted: 3 March 2019; Accepted for publication: 11 December 2019; Published online: 6 January 2020

Keywords: AbTCR • adoptive cell transfer • cancer • CAR • TAC • TCR • therapy • TRuC™

The immune system is a sophisticated defense system that protects our body against pathogens and abnormal or malignant cells. T cells represent a key component of this system by eliminating cancerous and pre-cancerous cells through their ability to discriminate between 'mutated self' and 'self'. This function of T cells is contingent upon the recognition of tumor-associated antigens by the T cell receptor (TCR) [1,2]. Importantly, αβ-TCRs recognize their cognate tumor antigens only when presented on human leukocyte antigen (HLA) molecules. Upon binding, the TCR catalyzes a broad signaling program that results in T cell activation, proliferation, target cell lysis, effector cell differentiation and, ultimately, adaptive immune protection against future relapse [3]. The unique properties of T cells, combined with their amenability to genetic engineering and *ex vivo* expansion, make T cells attractive cancer therapeutics. Here, we discuss the signaling of the natural TCR and the functional differences of various engineered T cell platforms, including adoptive transfer of tumor-infiltrating T cells (TILs), chimeric antigen receptor (CAR)-T cells and HLA-restricted and non-restricted engineered TCR-T cells.

TCR structure & signaling

The TCR is an octameric complex that mediates both antigen recognition and signal transduction [4,5]. In the most common type of T cells, the heterodimer of TCR-α and TCR-β recognizes the peptide-HLA on the surface of other cells. These antigen recognition domains are embedded into a complex of various CD3 signal-transducing subunits, which form hetero- and homo-dimers at a fixed stoichiometry (CD3γ/CD3ϵ, CD3δ/CD3ϵ and CD3ζ/CD3ζ) and initiate T cell activation (Figure 1A) [6,7]. The functional split between the antigen recognition and signal transduction components is a principle shared with other immune receptor complexes including the B cell receptor, NK cell receptors and Fcγ receptors [8]. Diversity of the TCR-αβ sequences is the result of somatic recombination

Future Medicine

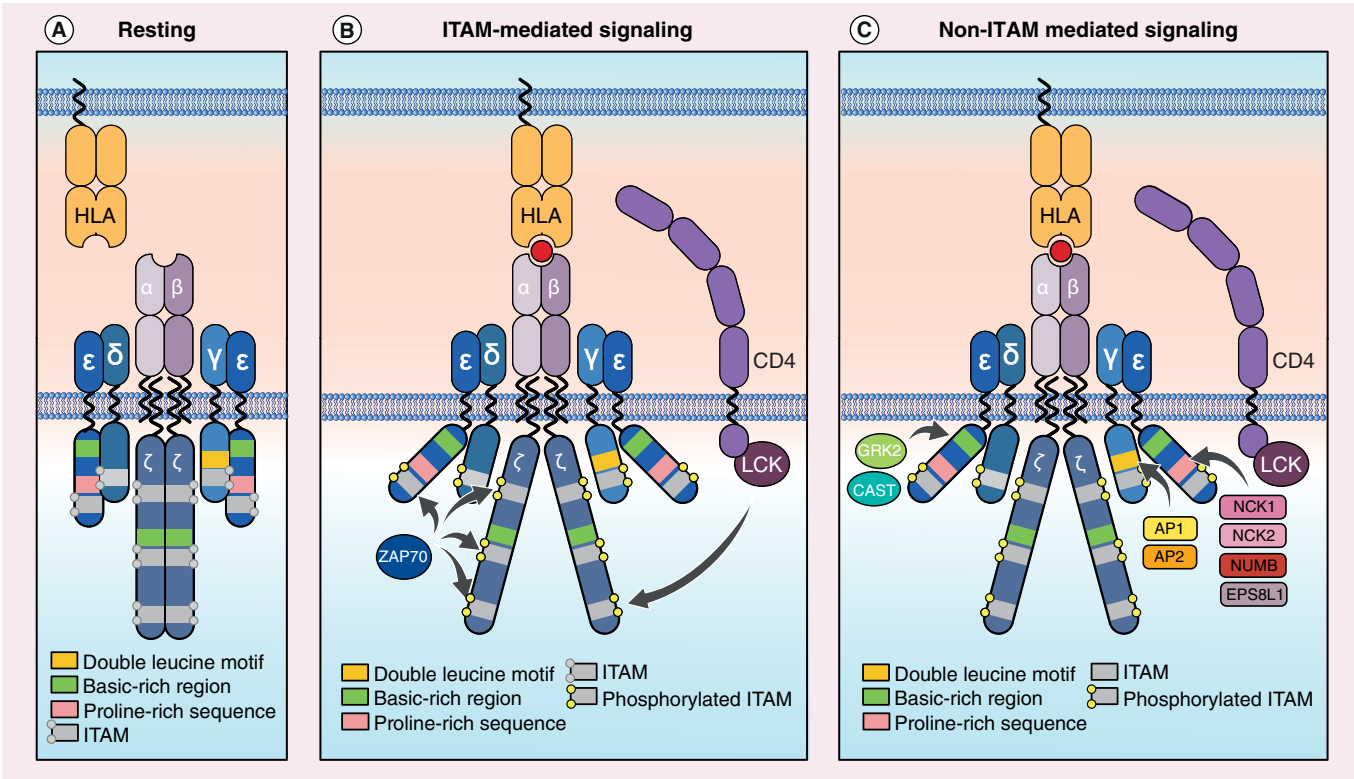

Figure 1. The αβ T cell receptor. (A) The αβ T cell receptor (TCR) is composed of the antigen-binding TCR-αβ dimer and the signal-transducing CD3γ/CD3ϵ, CD3δ/CD3ϵ and CD3ζ/CD3ζ dimers. Each CD3 chain harbors its own specific ITAM sequences (grey boxes). The CD3ϵ and CD3ζ subunits also contain basic-rich sequences (green boxes). In addition, CD3ϵ contains a proline-rich sequence (PRS) (pink boxes), while CD3γ harbors a double leucine motif (yellow box). In the resting state, these docking sites are shielded, which blocks binding of signaling molecules and keeps the TCR silent. **(B)** In the peptide-HLA-bound state, the quaternary structure of the TCR changes. In this state, the cytoplasmic tails of the CD3 subunits get phosphorylated by Lck, which is recruited by CD4 (shown in purple) in $CD4^+$ T cells and or CD8 (not shown) in $CD8^+$ T cells. ITAM phosphorylation facilitates ZAP70 binding, which leads to further phosphorylation of the CD3 signaling complex and recruitment of more canonical, downstream signaling effectors. **(C)** More adapter molecules are recruited to the TCR by other signaling domains outside of the ITAMs. For example, the CD3ϵ PRS binds to the adaptor proteins Nck1, Nck2, Numb, Eps8L1 and related proteins. The double leucine motif of CD3γ binds to AP1 and AP2. GRK2 and CAST have been reported to interact with the basic-rich region of CD3ϵ.
ITAM: Immune-receptor tyrosine-based activation motif.

in the thymus during T cell development of the *TRAC* and *TRBC* gene loci, encoding TCR-α and TCR-β, respectively [9,10]. Therefore, the TCR-αβ repertoire is winnowed during development to ensure appropriate recognition of HLA while pruning out potentially self-reactive TCR specificities [11].

Surface expression of the TCR is highly dependent upon the regulated, stepwise assembly of the TCR complex and its export from the endoplasmic reticulum (ER). Shielding of ER retention signals in the CD3 subunits by the other subunits of the TCR is critical for the translocation of the receptor complex to the T cell surface [12]. Interactions of polar residues in the transmembrane domains of the TCR-αβ and CD3 subunits ensure the correct stoichiometry and stability of the octameric TCR complex [5,12,13].

The TCR-αβ chains themselves have short intracellular domains without signaling function. This necessitates the usage of the invariant CD3γ, CD3δ, CD3ϵ and CD3ζ proteins for intracellular signal transduction [8,14,15]. The cytoplasmic tails of CD3γ, CD3δ and CD3ϵ subunits each contain a single immune-receptor tyrosine-based activation motif (ITAM), while the CD3ζ units contain three ITAMs, summing to ten ITAM motifs in the full TCR, the most among all receptors (Figure 1A) [8,16]. The multiplicity of ITAMs on the TCR has functional consequences. For example, multiple ITAMs increase the probability of T cell activation following TCR ligation and may be the reason for the exquisite sensitivity of T cell activation to be triggered by as few as two peptide-HLA molecules on the surface of target cells [17–19]. The ITAMs within the different CD3 subunits are not redundant or interchangeable. Mice with T cells in which the CD3 complex contained ten ITAMs of a single ITAM sequence,

in lieu of the normal ITAM diversity, had impaired T cell development and reduced surface TCR expression [20]. Likewise, in humans, genetic deficiencies in one or more of the invariant CD3 subunits have also been associated with aberrant thymic cellularity and peripheral T cell deficiency [21].

The TCR exists in two biochemically different states. In the absence of peptide-HLA stimulation, binding of cholesterol to the transmembrane region of the TCR-β keeps the TCR in a resting, inactive state that is not accessible to post-translational modifications of the CD3 subunits [15,22]. Conformational changes upon ligand binding shift the TCR to an active state making the CD3ε PRS and ITAM tyrosines accessible to phosphorylation by the Src family kinases Fyn and Lck, and triggering of downstream signaling (Figure 1B) [22–28].

The coreceptors CD8 or CD4 stabilize the interaction of the TCR with peptide-HLA-I and peptide-HLA-II complexes, respectively, and help to recruit additional Lck molecules to the TCR complex (Figure 1B) [29,30]. The involvement of the coreceptors, although not required for CD3 phosphorylation, increases the TCR sensitivity for ligand-mediated activation [31,32]. Double-phosphorylation of the CD3 ITAMs recruits ZAP70, a central mediator of TCR signals, via its tandem SH2 domains (Figure 1B) [33,34]. Both humans and mice with mutations in *ZAP70* lack T cells or have severely dysfunctional T cells [35,36]. Recruited ZAP70 is then further phosphorylated by Lck, which enables downstream signaling pathways via phosphorylation of LAT and SLP76 [37–39]. The LAT/SLP76 'signalosome' is upstream of several important signaling pathways, including the Erk, NF-AT and NFκB cascades.

Besides ITAMs, other unique motifs in the intracellular domains of CD3γ, CD3δ, CD3ε and CD3ζ are crucial for homeostasis, signaling and function of the TCR complex. For example, the proline-rich sequence (PRS) in CD3ε is required for the recruitment of the adaptor proteins Nck1 and Nck2 that are involved in early TCR signaling and coupling of the TCR to the cytoskeleton (Figure 1C) [26,28,40]. The PRS is also critical for the binding of the adaptor protein Numb to promote TCR degradation as well as recruitment of Eps8L1 and the related proteins Eps8L2, Eps8L3 and Eps8 (Figure 1C) [41,42]. Studies with knock-in mice further highlight the importance of the PRS motif. Substitution of the two central prolines of the CD3ε PRS by alanines greatly reduced TCR-mediated T cell proliferation, tumor lysis and proximal ITAM phosphorylation [43]. In CD3γ, a unique double leucine motif is critical for the binding of the adaptors AP1 and AP2 which mediate TCR internalization after phosphorylation of an upstream serine (Figure 1C) [44]. Moreover, basic-residue rich sequences (BRS) in CD3ε and CD3ζ form complexes with acidic phospholipids in the membrane to control TCR signaling [45–47]. It has been hypothesized that this interaction partially embeds the cytoplasmic tails of CD3ε and CD3ζ in the T cell membrane thereby shielding them from kinases and retaining them in a 'closed' state [46–49]. In CD3ε specifically, the BRS may also interact with GRK2 and CAST, a protein linked to IL-2 production by T cells (Figure 1C) [50,51].

In addition to the well established concept that the cytoplasmic tails of the CD3 subunits are required to trigger the TCR signaling cascade, there is also evidence that the extracellular domains of certain subunits can contribute to TCR signaling. Mutations in the extracellular domain of CD3ε, which are proposed to lock the TCR in a resting state, reduce T cell proliferation and activation [52,53].

At the macromolecular level, upon peptide-HLA binding, the TCR complex and other signaling co-receptors undergo a dramatic reorganization within the T cell membrane to form an immunological synapse [54]. The synapse is characterized by a 'bullseye' surrounded by concentric rings of segregated membrane proteins and intracellular signaling effectors. The degree to which the membrane reorganizations are required for full T cell activation is an area of debate [55]. Regardless, it is clear that clustering, internalization and spatial organization of the TCR are all critical steps to generate a 'signalosome' in support of robust T cell activation [56,57].

T cell therapies for cancer

The isolation of TILs and re-administration to patients after reinvigoration and expansion with IL-2 was one of the earliest approaches to harness the potential of T cells to eradicate cancer [58]. Later, an increased understanding of TCR structure and function opened opportunities for the design and introduction of engineered TCRs and synthetic antigen receptors into T cells isolated from peripheral blood. In the following sections, we discuss and compare various T cell immunotherapeutic approaches. An overview of these platforms is depicted in Figure 2.

TIL therapy

The transfer of TILs for the treatment of melanoma dates back to the 1980s [58,59]. A proportion of TILs recognize tumor-associated antigens with their natural TCR. However, various immune evasion mechanisms hijacked by cancer cells frequently render TILs dysfunctional [60]. These include soluble factors or cell surface ligands with immunosuppressive function that create an inhibitory microenvironment for T cells inside tumors.

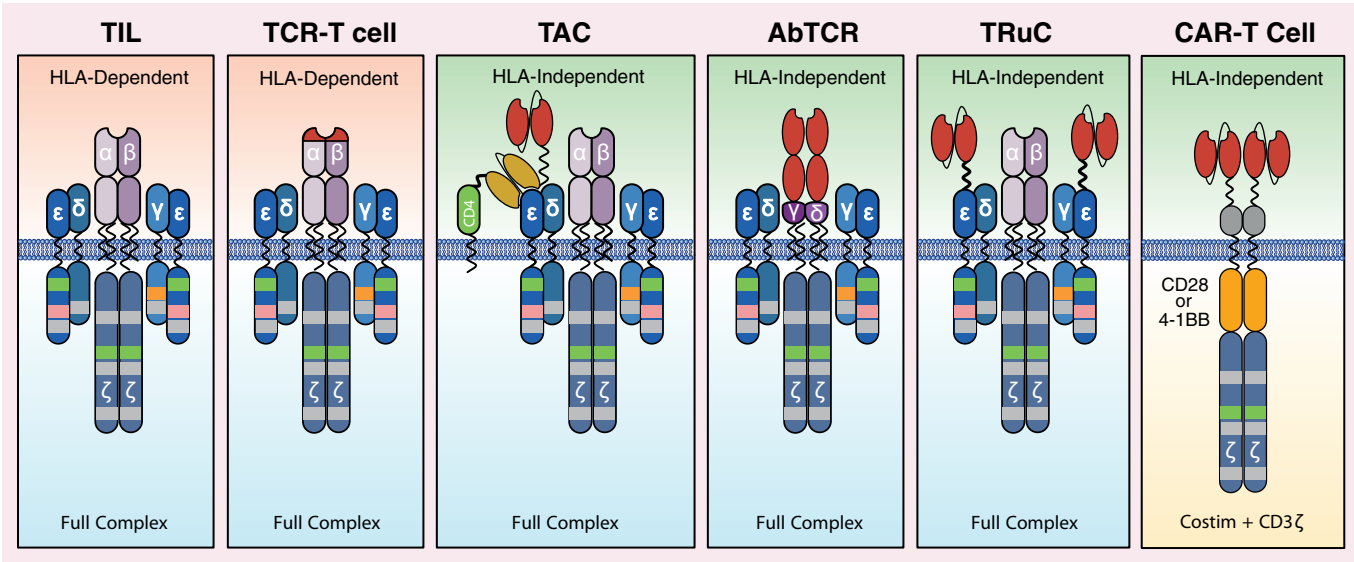

Figure 2. Comparison of T cell therapy approaches. TILs and TCR-T cells utilize all endogenous TCR components and recognize tumor antigen in the context of HLA. TAC, AbTCR and TRuC™ T cells utilize the TCR, but recognize tumor antigens independently of HLA. CAR-T cells bypass the TCR and signal through the CD3ζ chain as the only TCR subunit paired with a costimulatory domain, in orange, which is most commonly CD28 or 4-1BB. Tumor antigen binding, which can be a scFv, single-domain antibodies or Fab fragments, are displayed in red.
AbTCR: Antibody-TCR; TAC: T cell antigen coupler; TCR: T cell receptor; TIL: Tumor-infiltrating T cell; TRuC™: TCR fusion construct.

To harness TILs for cancer therapy, they have to be removed from the suppressive tumor milieu and *ex vivo* reinvigorated by a complicated expansion process. Small fragments of the surgically resected tumor are digested with proteolytic enzymes to obtain a single cell suspension. The suspension is cultured in high-dose IL-2 to stimulate selective expansion of TILs. Expanded TILs are tested for tumor reactivity and, if reactive, entered into a rapid expansion protocol using anti-CD3 and IL-2 to achieve therapeutically effective autologous cell doses for adoptive T cell transfer of cancer patients [61]. Unlike lymphokine activated killer (LAK) cells, which lyse tumors irrespective of HLA restriction, expanded TILs retain restriction to the patient's HLA [62,63]. To date, TIL therapy has been most successful in melanoma, a cancer type with one of the highest known somatic mutation rates and a source for neo-antigen specific T cells [64]. Overall response rates are in the range of 30 to 50% and frequently associated with improved overall survival [65,66]. More recently, encouraging clinical responses were also reported in patients with metastatic cervical cancer. A high disease control rate of 85% was observed with three complete and nine partial responses among 27 evaluated patients [67].

While the clinical responses are encouraging, technical challenges may limit the broader applicability of the adoptive transfer of TILs [68]. Isolation of TILs is not possible for all tumors. To produce enough TIL product, the therapy is limited to tumors with strong T cell infiltrates [69]. Even if enough cells can be manufactured, limited anti-tumor reactivity of the pre-existing T cell repertoire may curb the antitumor response. Recent work has been done to shorten the expansion time of TILs to generate better quality T cells. Still, isolation and expansion of TILs remains a cumbersome and time-consuming process that requires several weeks [65,70,71]. These caveats withstanding, several companies are taking on the task to commercialize TILs for cancer therapy.

Engineered TCR-T cell therapy

With the advancement of new gene transfer methods, such as safer viral vectors, peripheral T cells can be engineered to express TCR-α and TCR-β chains, so-called TCR-T cells, that most commonly recognize predefined tumor-associated peptides derived from differentiation, oncofetal or cancer-testis antigens [72–74]. Peripheral T cells isolated from the blood of the patients are a more readily accessible source of T cells than TILs. HLA-presented peptides are an attractive class of targets because of their tumor-specific expression and the ability to target both cell surface and intracellular proteins. Since the establishment of a proof-of-concept with MART-1 TCRs in melanoma, defined TCRs against a number of other antigens, including gp100, MAGE-A3, MAGE-A4, WT-1 and NY-ESO-1 have been studied in clinical trials [72,75–80]. NY-ESO-1 TCR-T cells are among the most widely tested and have achieved

impressive response rates in melanoma and synovial sarcoma [76,81]. Based on these successes, NY-ESO-1 TCR-T cell trials have been expanded to patients with multiple myeloma, lung, esophageal, breast and bladder cancer [76,82].

While the response rates look promising, TCR-T cell therapies are not without problems. In studies with T cells that target MART1 or gp100, on-target/off-tumor toxicity in eyes and ear were reported [75]. In other cases, affinity maturation of the TCR, needed to increase its potency, resulted in unexpected cross-reactivity with other peptide self-antigens [72,76,78]. In one study with an affinity-matured MAGE-A3 TCR, two patients died due to cardiogenic shock. Follow-up experiments revealed that unlike the original TCR, the affinity-matured version not only recognized MAGE-A3 peptide presented on *HLA-A*01* but also cross-reacted with an unrelated peptide derived from the striated muscle-specific protein titin, also presented on *HLA-A*01* [83]. In another study, T cells carrying a different MAGE-A3 TCR recognizing a peptide on *HLA-A*0201* induced neurotoxicity in three patients due to cross-reactivity with a peptide derived from MAGE-A12, which unlike MAGE-A3, is expressed at low levels in the brain. Two patients died after falling into a coma [78]. In addition to affinity-maturation, mispairing of the engineered TCR-α and TCR-β with endogenous TCR-β and TCR-α can potentially cause off-target binding and unpredictable specificities [84]. To avoid this issue, TCR domain swapping, the expression of TCRγ and TCRδ subunits in αβ T cells or transfer of hybrid receptor units comprising murine constant and human variable TCR regions have been investigated [85,86]. Collectively, the above cases illustrate that pre-defined TCRs need to be optimized very carefully and adequate cross-reactivity screens be implemented for their characterization.

Although new technologies may help to improve the preferential pairing of TCR-α and TCR-β chains in the engineered TCR, HLA restriction remains an issue. Most are directed against antigens presented in the context of *HLA-A*0201*, which in the USA is limited to 27–47% of patients depending upon ethnicity [87,88]. Moreover, immune evasion via loss or downregulation of HLA molecules or of other elements necessary for antigen presentation is a common mechanism of escape from endogenous T cell responses in human cancers that can also limit the success of TCR-T cell and TIL therapies [89,90].

CAR-T cell therapy

CARs are synthetic antigen receptors, which recognize their target antigen independent of HLA. The first-generation of CARs are commonly comprised of an antibody-derived binding domain fused with a hinge and transmembrane domain to intracellular elements of CD3ζ or the FcεR1γ chain [91]. T cells transduced with first-generation CARs targeting a wide variety of antigens (e.g., CAIX, CD19, CD20, CEA, GD2, Her2, PSMA and others) were capable of lysing tumor cells, expanding *in vitro* and producing cytokines but did not demonstrate clinical benefit in patients with hematological or solid tumors [92–102].

To bolster the activity of CAR-T cells, so-called second-generation CARs were developed with an additional costimulatory domain fused to the intracellular domain of CD3ζ (Figure 2) [103]. The addition of the costimulatory domains, most commonly derived from CD28 or 4-1BB/CD137, engage the PI3-kinase subunit p85 or TRAF2, respectively, and couple the CAR to PI3K or NFκB signaling pathways. As a result, CAR-T cells exhibit increased cytokine production, enhanced tumor eradication, and prolonged persistence [104–112].

Second-generation CAR-T cells have shown clinical efficacy in several clinical trials for patients with acute lymphoblastic leukemia (ALL) and diffuse large B-cell lymphoma where they have induced complete remission rates of 80–90% and 40–50%, respectively [113–124]. Based on these impressive results, two CD19-targeted CAR-T cell therapies were recently approved by the US FDA for these indications [125].

However, CD19-targeted CAR-T cell therapies are often associated with severe adverse effects. Frequently, the activation of CAR-T cells upon target engagement results in elevated levels of circulating inflammatory cytokines, onset of fever, hypotension, or hypoxia, known as cytokine-release syndrome (CRS) [126–128]. While CRS can be clinically managed by blockade of IL-6 signaling and glucocorticoids, the cause of neurological toxicities, such as seizures, aphasia, or cerebral edema are less well understood [126–128]. In some cases, neurotoxicity and CRS have been fatal. Despite initial high response rates, long-term follow-up of patients also has shown that in some of these patients responses may not be as durable or complete as initially hoped [129]. In other cases, loss of CD19 antigen expression has limited the durability of response [130]. Despite their successes in hematological malignancies, the performance of CAR-T cells as a monotherapy in solid tumors has been disappointing [131–134]. CAR-T cells likely require additional intervention in solid tumors for efficacy. A recent presentation of an ongoing Phase I study for a mesothelin-targeted CAR in combination with PD1 blockade and local delivery to the tumor site reported promising results with seven partial responses and three complete responses among the 27 patients treated [135].

The choice of costimulatory domain in the second-generation CAR-T cell has divergent impacts on the therapeutic potential and safety of the CAR-T cell. In a study comparing the two clinically approved CAR designs, stimulation through a CD28ζ CAR resulted in faster and higher amplitude changes in downstream signaling events, which correlated with an effector T cell-like phenotype and function [136]. In contrast, 4-1BBζ CAR T cells preferentially expressed T cell memory-associated genes and exhibited sustained anti-tumor activity against established experimental tumors [136]. Clinical experience generally follows these findings as CD19 CAR-T cells with 4-1BB costimulatory domains seem to have delayed expansion kinetics and longer persistence compared with those containing a CD28-derived domain [122,124,137,138].

While the addition of co-stimulatory domains significantly improved CAR-T cell activity and persistence, CARs by design are limited to the signaling domain of the CD3ζ subunit and thus lack important subunits of the native, octameric TCR. These contribute additional ITAMs of the CD3ϵ, CD3γ and CD3δ subunits that may not be redundant to the CD3ζ ITAMs, as well as the CD3ϵ basic-rich region that enables docking of GRK2 and CAST, and the CD3ϵ PRS that recruits to Nck, Numb and Eps8L1 and related proteins to the TCR [20].

Non-HLA-restricted TCR-based therapies

To address the limitations of CAR-T cells and HLA restriction of TCR-T cell therapies, several new platforms that endow the full TCR complex with antibody-derived binding domains have recently emerged. These approaches combine the advantage of an HLA-independent antibody binding domain with the broad and controlled signaling power of the entire TCR complex resulting in a potentially better safety profile and higher activity against solid tumors.

The T cell antigen coupler (TAC) is a synthetic modular fusion protein comprising a tumor antigen-specific scFv and an anti-CD3ϵ binding scFv recombinantly fused to an N-terminally truncated version of CD4 or CD8 (Figure 2) [139]. Upon target engagement, TACs can activate CD3ϵ and thereby co-opt endogenous TCR signaling. In preclinical studies, TAC-T cells induced robust cytokine production and cytotoxicity *in vitro* [139]. When tested in solid tumor models, TAC-T cells outperformed CAR-T cells with increased anti-tumor activity and lower cytokine release, suggesting that engagement of the full TCR circuitry does not require an extra costimulatory domain for efficacy [139].

The antibody–TCR (AbTCR), also called ARTEMIS, presents an alternative way to engage the whole TCR signaling complex independently of HLA. This platform combines an Fab domain derived from an antibody with the heavy and light chains fused independently to portions of the TCRγ and TCRδ subunits (Figure 2). Compared with T cells expressing a CD19-specific CAR, AbTCR-T cells using the identical CD19 binder released less cytokines but showed comparable tumor inhibition in a patient-derived xenograft leukemia model [140]. Like TAC-T cells, AbTCR-T cells function in the absence of costimulatory domains [140]. The AbTCR concept has been also extended to TCR-mimicking antibody binders as illustrated by the fusion with an antibody binding moiety that recognizes an α-fetoprotein derived peptide complexed with HLA [141].

Recently, we have published a novel way to redirect T cells in an HLA-independent manner using recombinant fusion of antigen binding domains to CD3 subunits, which are invariant and obligate components of the TCR complex. The fusion of anti-CD19 scFv to different TCR subunits, including TCR-β, CD3γ and CD3ϵ can effectively reprogram an intact TCR complex to recognize tumor surface antigens without the requirement for HLA matching (Figure 2) [142]. TCR fusion construct (TRuC™) variants become a functional component of the natural TCR complex and can harness the entire TCR signaling cascade to trigger a potent anti-tumor response without requiring an exogenous costimulatory domain. CD19-specific CD3ϵ-based TRuC-T cells had more potent anti-tumor efficacy in leukemia and lymphoma animal models compared with second-generation CAR-T cells [142]. Importantly, TRuC-T cell anti-tumor activity was achieved with significantly lower cytokine release than respective CAR-T cells potentially translating into a better safety profile [142]. Compared the other non-HLA restricted technologies, the flexible design of TRuC platform offers further advantages. Most importantly, the generation of functional TRuC receptors is not restricted to a specific TCR subunit which provides the opportunity to engineer dual targeting TRuC-T cells. For example, binders with different antigen specificities can be tethered to CD3γ and CD3ϵ, respectively, and upon integration into the TCR can simultaneously target two tumor antigens thereby addressing heterogeneous tumor antigen expression and prevent immune escape due to loss of antigen. This may be particularly important in effectively treating solid tumors.

Functional consequences of T cell engineering

Engineered T cells can now be divided into three classes: CAR-T cells that employ of all the TCR subunits only CD3ζ as a surrogate TCR-derived signal, engineered T cells that utilize the entire TCR complex in an HLA-dependent fashion and TRuC-, TAC- and AbTCR-T cells that utilize antibody-like binding to engage the entire TCR in an HLA-independent fashion.

Poor *in vivo* efficacy and lack of persistence of first-generation CAR-T cells illustrated that the CD3ζ chain alone was not sufficient to recapitulate the signaling complexity triggered by the full TCR complex [97,99,100]. The addition of a costimulatory domain in the second-generation CAR significantly improved the anti-tumor activity and persistence of CAR-T cells, but with the cost of deleterious production of cytokines resulting in CRS. The increased potency of the second-generation CAR also has drawbacks for many groups investigating novel CAR targets and construct designs. A combination of supraphysiological surface expression, aggregation due to hinge selection and the propensity for scFvs to oligerimize often results in tonic signaling that limits efficacy at best or drives constitutive activation, T cell exhaustion and additional toxicities at worst [143–146]. Tonic signaling in CARs drives low-level phosphorylation of the CD3ζ ITAMs and recruitment of adaptor molecules like TRAF2, in the case of 4-1BB-containing CARs [147].

Approaches to temper the activity of the CAR is currently under investigation by several groups. In one instance, the reduction of ITAM multiplicity in a CD19-targeted 28ζ CAR by removal of the two most membrane distal ITAM tyrosines skewed T cell differentiation toward less differentiated T cell subsets, enhanced anti-tumor efficacy and increased persistence of the CAR-T cells [148]. These data mirror early experience with murine surrogate CD19 CAR models where deletion of the first and last ITAM tyrosine was required to avoid CAR T cell apoptosis [149]. Similar to ITAM engineering, inactivation of two CD28 subdomains that are tied into apoptotic and differentiation downstream pathways also increased the persistence of CD28ζ CAR-T cells [150]. There are also attempts to harness the TRAC locus for improved CAR expression. Inserting the CAR gene into the TRAC locus not only disrupts the endogenous TCR-α gene and prevents assembly and translocation of the TCR to the cell surface, it also enables the control of CAR expression by the endogenous TCR-α promoter resulting in a reduced expression of CARs relative to strong promoters, such as EF-1α, used in viral vectors. The more homogenous and moderate CAR expression facilitates dynamic CAR surface expression upon antigen encounter and reduces T cell exhaustion that eventually results in enhanced CAR-T cell activity [151].

In contrast to CARs, which seem to require more engineering efforts to find the appropriate balance of activation and inhibition of downstream signals, the TCR contains several autoregulatory mechanisms that are integral to its structure and function. These mechanisms include regulation of expression, degradation, subcellular localization and regulation of the internalization of signaling and non-signaling TCR subunits [152]. In the cell membrane, the activity of the TCR is regulated by its quaternary structure in which the resting TCR is kept in an autoinhibited state, while ligand-binding switches the TCR to an activated state [15,22]. This self-regulated control is missing in the CARs and could potentially explain the common phenomena of tonic signaling in the absence of antigens. Further, the 10 ITAM motifs contained within the entire TCR complex enhance the translation of antigen binding into activation on a populational level [19]. ITAM multiplicity and CD3 diversity is required for the recruitment of certain signaling intermediates and ultimately the catalyzation of effector functions. For example, low ITAM multiplicity can induce cytokine production but is not sufficient to mediating Vav1 interaction, Notch1 recruitment and Myc-dependent proliferation [153]. Interestingly, T cells that utilize the entire TCR secrete less cytokines than CAR-T cells [139,140,142]. In contrast to CAR-T cells, TCR-engineered T cells can also persist in patients with solid tumors for more than a year and acquire a polyfunctional, stem cell memory T cell phenotype [154,155]. It is therefore possible that T cells require the more comprehensive and controlled signaling of a complete TCR complex for maximally therapeutic activity against solid tumors.

Conclusion

To date, clinical trials with CAR-T cell therapies outnumber trials with TCR-T cell therapies, and two CAR-T cell therapies have meanwhile received regulatory approval for their stunning successes in some hematological malignancies [61,156,157]. Nevertheless, the translation of CAR-T cell therapies to solid tumors has been difficult. Surprisingly, TIL-based therapies seem to have lower rates of adverse events while at the same time being more efficacious against solid tumors than CAR-T cell therapies. This discrepancy may reflect a different capacity of engineered T cells to engage the entire TCR signaling machinery compared with the signaling molecules engaged

by the CARs. Unfortunately, the two main modalities of treatment that engage the full TCR, TIL and TCR-T cells, have large-scale production and preclinical development challenges that may limit their applicability.

Here, we define a new emerging class of T cell therapy that combines the advantages of CAR-T cells with those of TIL and TCR-T cell approaches while mitigating their limitations. Unlike TIL and TCR-T cells, non-HLA restricted TCR-based therapies are able to treat a broad selection of patients due to the use of antibody-like antigen engagement. Second, unlike CAR, they have the ability to harness the remarkable and intrinsic properties of TCR complex to modulate therapeutic T cell activity. Taken together, non-HLA restricted TCR-based platforms (e.g., TRuC-, TAC- and AbTCR-T cells) closely follow the activation and autoregulatory paradigm of native TCRs while maintaining HLA-agnosticism. Whether these new modalities can endow new T cell therapies with safer, more effective treatments for solid tumors remains to seen with further preclinical development and results from future clinical trials.

Future perspective

T cell therapies are becoming increasingly complex as investigators augment the persistence, function and safety of engineered T cells. Most strategies to improve CAR-T cells are primarily predicated on a design that can leverage only a fraction of the TCR signaling complexity. Platforms that employ the self-regulatory signaling machinery inherent to the natural TCR may be able to better harness what has evolved as a broad, effective and highly controlled response by T cells against malignant cells. The new approaches discussed in this review will deepen our knowledge about what is required for successful T cell therapy.

Executive summary

The T cell receptor

- The T cell receptor (TCR) is an octameric complex containing variable TCR for antigen recognition and invariant CD3 subunits responsible for signal transduction.
- The CD3 molecules contain ITAMs that are nonredundant and critical for T cell development and function.
- There are other non-ITAM domains within CD3 subunits important for T cell signaling and function.

Tumor-infiltrating T cell therapy

- Tumor-infiltrating T cells (TILs) have been successful against solid tumors with low toxicity.
- Delivery of TIL to patients can be hampered by limited access to tumor tissue, low numbers of isolated TILs, poor expansion and long expansion times.

TCR-T therapy

- TCRs can not only target cell surface antigens, but also a broad repertoire of intracellular antigens not accessible to antibody-based binders.
- Both 'on target' and 'off target' toxicities have been seen with several TCR-T cell therapies.
- Careful optimization of predefined TCRs is required to reduce off-target toxicities.
- Requirement for human leukocyte antigen (HLA) reduces the size of treatable patient populations.

CAR-T cell therapy

- CD19 CAR T cells have had great success in hematological malignancies.
- Improvement of CAR-T cell performance in solid tumors is an area of active research.

Non-HLA restricted TCR-based therapeutics

- Therapies that engage the entire TCR for signaling and T cell activation but are not restricted to HLA for antigen recognition.
- These therapies have lower cytokine release and do not require an additional costimulatory domains for efficacy.

Functional consequences of TCR engineering

- All subunits of the TCR are required for a broad and controlled T cell activation.
- The use of the CD3ζ chain as the only TCR signaling domain in CAR T cells is not sufficient for a comprehensive T cell response requiring additional engineering.
- Addition of costimulatory domains to CARs enhances effector functions and persistence of cells but still does not completely replicate normal TCR-derived signals.

Conclusion

- Newer generations of CARs require additional engineering to reduce toxicities and improve persistence of CAR-T cells in solid tumors.
- More recent HLA-independent approaches that harness the signaling power of the full TCR have the potential to be safer and more efficacious in solid tumors.

Financial & competing interests disclosure

IR Hardy, DR Getts, Robert Hofmeister: Current or former employees of TCR2 Therapeutics, Inc. and hold stocks in the company. PA Baeuerle and WW Schamel are consultants of TCR2 Therapeutics, Inc. and hold stocks in the company. The authors have no other relevant affiliations or financial involvement with any organization or entity with a financial interest in or financial conflict with the subject matter or materials discussed in the manuscript apart from those disclosed.

No writing assistance was utilized in the production of this manuscript.

Author contributions

IR Hardy: conceived, drafted and revised work for intellectual content. WW Schamel: conceived, drafted and revised work for intellectual content. DR Getts: conceived, drafted and revised work for intellectual content. P Baeuerle: conceived, drafted and revised work for intellectual content. R Hofmeister: conceived drafted and revised work for intellectual content.

References

Papers of special note have been highlighted as: • of interest; •• of considerable interest

1. Stone JD, Harris DT, Kranz DM. TCR affinity for p/MHC formed by tumor antigens that are self-proteins: impact on efficacy and toxicity. *Curr. Opin. Immunol.* 33, 16–22 (2015).
2. Ilyas S, Yang JC. Landscape of tumor antigens in T cell immunotherapy. *J. Immunol.* 195(11), 5117–5122 (2015).
3. Klebanoff CA, Gattinoni L, Restifo NP. CD8+ T-cell memory in tumor immunology and immunotherapy. *Immunol. Rev.* 211, 214–224 (2006).
4. Davis MM, Boniface JJ, Reich Z *et al.* Ligand recognition by αβ T cell receptors. *Annu. Rev. Immunol.* 16, 523–544 (1998).
5. Dong , Zheng L, Lin J *et al.* Structural basis of assembly of the human T cell receptor–CD3 complex. *Nature* 573(7775), 546–552 (2019).

• **A report of the 3D structure of the T cell receptor (TCR) and CD3 complex in the membrane with implications for medicines utilizing or targeting the TCR.**

6. Manolios N. Pairwise, cooperative and inhibitory interactions describe the assembly and probable structure of the T-cell antigen receptor. *Embo J.* 10, 1643–1651 (1991).
7. Alarcon B, Gil D, Delgado P, Schamel WWA. Initiation of TCR signaling: regulation within CD3 dimers. *Immunol. Rev.* 191(1), 38–46 (2003).
8. Berry R, Call ME. Modular activating receptors in innate and adaptive immunity. *Biochemistry* 56(10), 1383–1402 (2017).
9. Toyonaga B. Rearrangements of T-cell receptor gene YT35 in human DNA from thymic leukaemia T-cell lines and functional T-cell clones. *Nature* 311(5984), (1984).
10. Sims JE. Complexity of human T-cell antigen receptor β-chain constant- and variable-region genes. *Nature* 312, 541–545 (1984).
11. Ebert PJR, Li Q-J, Huppa JB, Davis MM. Functional development of the T cell receptor for antigen. *Develop. T Cell Immunity* 65–100 (2010).
12. Delgado P, Alarcon B. An orderly inactivation of intracellular retention signals controls surface expression of the T cell antigen receptor. *J. Exp. Med.* 201(4), 555–566 (2005).
13. Call ME, Pyrdol J, Wiedmann M, Wucherpfennig KW. The organizing principle in the formation of the T cell receptor–CD3 complex. *Cell* 111(7), 967–979 (2002).
14. Van Der Merwe PA, Dushek O. Mechanisms for T cell receptor triggering. *Nat. Rev. Immunol.* 11(1), 47–55 (2011).
15. Schamel WW, Alarcon B, Minguet S. The TCR is an allosterically regulated macromolecular machinery changing its conformation while working. *Immunol. Rev.* 291(1), 8–25 (2019).
16. Love PE, Hayes SM. ITAM-mediated signaling by the T-cell antigen receptor. *Cold Spring Harb. Perspect. Biol.* 2(6), a002485 (2010).
17. Purbhoo MA, Irvine DJ, Huppa JB, Davis MM. T cell killing does not require the formation of a stable mature immunological synapse. *Nat. Immunol.* 5(5), 524–530 (2004).
18. Irvine DJ, Purbhoo MA, Krogsgaard M, Davis MM. Direct observation of ligand recognition by T cells. *Nature* 419(6909), 845–849 (2002).
19. James JR. Tuning ITAM multiplicity on T cell receptors can control potency and selectivity to ligand density. *Science signaling* 11 (2018).
20. Bettini ML, Chou PC, Guy CS, Lee T, Vignali KM, Vignali DAA. Cutting Edge: CD3 ITAM diversity is required for optimal TCR signaling and thymocyte development. *J. Immunol.* 199(5), 1555–1560 (2017).

• **A thorough analysis of the non-redunancy of ITAMs of within all the CD3ϵ subunits.**

21. Marin AVM, Garcillán B, Jiménez-Reinoso A *et al.* Human congenital T-cell receptor disorders. *LymphoSign J.* 2(1), 3–19 (2015).
22. Swamy M, Beck-Garcia K, Beck-Garcia E *et al.* A cholesterol-based allostery model of T cell receptor phosphorylation. *Immunity* 44(5), 1091–1101 (2016).

23. Samelson LE, Phillips AF, Luong ET, Klausner RD. Association of the fyn protein-tyrosine kinase with the T-cell antigen receptor. *Proc. Natl. Acad. Sci. USA* 87, 4358–4362 (1990).
24. Veillette A, Bookman MA, Horak EM, Samelson LE, Bolen JB. Signal transduction through the CD4 receptor involves the activation of the internal membrane tyrosine-protein kinase p56lck. *Nature* 338, 257–259 (1989).
25. Schamel WW, Alarcon B, Hofer T, Minguet S. The allostery model of TCR regulation. *J. Immunol.* 198(1), 47–52 (2017).
26. Gil D, Schamel WA, Montoya M, Sánchez-Madrid F, Alarcón B. Recruitment of Nck by CD3 epsilon reveals a ligand-induced conformational change essential for T cell receptor signaling and synapse formation. *Cell* 109, 901–912 (2002).
27. Minguet S, Schamel WW. A permissive geometry model for TCR–CD3 activation. *Trends Biochem. Sci.* 33(2), 51–57 (2008).
28. Minguet S, Swamy M, Alarcon B, Luescher IF, Schamel WW. Full activation of the T cell receptor requires both clustering and conformational changes at CD3. *Immunity* 26(1), 43–54 (2007).
29. Veillette A, Bookman MA, Horak EM, Bolen JB. The CD4 and CD8 T cell surface antigens are associated with the internal membrane tyrosine-protein kinase p56lck. *Cell* 55, 301–308 (1988).
30. Barber EK, Dasgupta JD, Schlossman SF, Trevillyan JM, Rudd CE. The CD4 and CD8 antigens are coupled to a protein-tyrosine kinase (p56lck) that phosphorylates the CD3 complex. *Proc. Natl Acad. Sci. USA* 86, 3277–3281 (1989).
31. Artyomov MN, Lis M, Devadas S, Davis MM, Chakraborty AK. CD4 and CD8 binding to MHC molecules primarily acts to enhance Lck delivery. *Proc. Natl Acad. Sci. USA* 107(39), 16916–16921 (2010).
32. Potter TA, Rajan TV, Dick RF, Bluestone JA. Substitution at residue 227 of H-2 class I molecules abrogates recognition by CD8-dependent, but not CD8-independent cytotoxic T lymphocytes. *Nature* 337, 73–75 (1989).
33. Iwashima M, Irving BA, Van Oers NS, Chan AC, Weiss A. Sequential interactions of the TCR with two distinct cytoplasmic tyrosine kinases. *Science* 263, 1136–1339 (1994).
34. Wang H, Kadlecek TA, Au-Yeung BB *et al.* ZAP-70: an essential kinase in T-cell signaling. *Cold Spring Harb. Perspect. Biol.* 2(5), a002279 (2010).
35. Arpaia E, Shahar M, Dadi H, Cohen A, Rolfman CM. Defective T cell receptor signaling and CD8+ thymic selection in humans lacking Zap-70 kinase. *Cell* 76(5), 947–958 (1994).
36. Sakaguchi N, Takahashi T, Hata H *et al.* Altered thymic T-cell selection due to a mutation of the *ZAP-70* gene causes autoimmune arthritis in mice. *Nature* 436, 454–460 (2003).
37. Jackson JK, Motto DG, Sun Q *et al.* Molecular cloning of SLP-76, a 76-kDa tyrosine phosphoprotein associated with Grb2 in T Cells. *J. Biol. Chem.* 270(13), (1994).
38. Wardenburg JB, Fu C, Jackman JK *et al.* Phosphorylation of SLP-76 by the ZAP-70 protein-tyrosine kinase Is required for T-cell receptor function. *J. Biol. Chem.* 271(33), 19641–19644 (1996).
39. Wange RL, Malek SN, Desiderio S, Samelson LE. Tandem SH2 domains of ZAP-70 bind to T cell antigen receptor and CD3e from activated Jurkat T cells. *J. Biol. Chem.* 268(26), 19797–19801 (1993).
40. Paensuwan P, Hartl FA, Yousefi OS *et al.* Nck binds to the T cell antigen receptor using Its SH3.1 and SH2 domains in a cooperative manner, promoting TCR functioning. *J. Immunol.* 196(1), 448–458 (2016).
41. Kesti T, Ruppelt A, Wang JH *et al.* Reciprocal regulation of SH3 and SH2 domain binding via tyrosine phosphorylation of a common site in CD3epsilon. *J. Immunol.* 179(2), 878–885 (2007).
42. Martin-Blanco N, Jimenez Teja D, Bretones G *et al.* CD3epsilon recruits Numb to promote TCR degradation. *Int. Immunol.* 28(3), 127–137 (2016).
43. Borroto A, Arellano I, Blanco R *et al.* Relevance of Nck-CD3 epsilon interaction for T cell activation *in vivo*. *J. Immunol.* 192(5), 2042–2053 (2014).
44. Lauritsen JP, Boding L, Buus TB *et al.* Fine-tuning of T-cell development by the CD3gamma di-leucine-based TCR-sorting motif. *Int. Immunol.* 27(8), 393–404 (2015).
45. Deford-Watts LM, Dougall DS, Belkaya S *et al.* The CD3 zeta subunit contains a phosphoinositide-binding motif that is required for the stable accumulation of TCR–CD3 complex at the immunological synapse. *J. Immunol.* 186(12), 6839–6847 (2011).
46. Xu C, Gagnon E, Call ME *et al.* Regulation of T cell receptor activation by dynamic membrane binding of the CD3epsilon cytoplasmic tyrosine-based motif. *Cell* 135(4), 702–713 (2008).
47. Aivazian D, Stern LJ. Phosphorylation of T cell receptor ζ is regulated by a lipid dependent folding transition. *Nature* 7, 1023–1026 (2000).
48. Zhang H, Cordoba SP, Dushek O, Van Der Merwe PA. Basic residues in the T-cell receptor zeta cytoplasmic domain mediate membrane association and modulate signaling. *Proc. Natl Acad. Sci. USA* 108(48), 19323–19328 (2011).
49. Zimmermann K, Eells R, Heinrich F *et al.* The cytosolic domain of T-cell receptor zeta associates with membranes in a dynamic equilibrium and deeply penetrates the bilayer. *J. Biol. Chem.* 292(43), 17746–17759 (2017).

50. Deford-Watts LM, Young JA, Pitcher LA, Van Oers NS. The membrane-proximal portion of CD3 epsilon associates with the serine/threonine kinase GRK2. *J. Biol. Chem.* 282(22), 16126–16134 (2007).

51. Yamazaki T, Haman Y, Tashiro H *et al.* CAST, a novel CD3e-binding protein transducing activation signal for interleukin-2 production in T cells. *J. Biol. Chem.* 274, 18173–18180 (1999).

52. Martínez-Martín N, Risueño RM, Morreale A *et al.* Cooperativity between T cell receptor complexes revealed by conformational mutants of CD3ϵ. *Sci. Signal.* 2(83), ra43 (2009).

53. Blanco R, Borroto A, Schamel W, Pereira P, Alarcon B. Conformational changes in the T cell receptor differentially determine T cell subset development in mice. *Sci. Signal.* 7(354), ra115 (2014).

54. Monks CRF, Freiberg BA, Kupfer H, Sciaky N, Kupfer A. Three-dimensional segregation of supramolecular activation clusters in T cells. *Nature* 395, 82–86 (1998).

55. Friedman RS, Beemiller P, Sorensen CM, Jacobelli J, Krummel MF. Real-time analysis of T cell receptors in naive cells *in vitro* and *in vivo* reveals flexibility in synapse and signaling dynamics. *J. Exp. Med.* 207(12), 2733–2749 (2010).

56. Metz PJ, Arsenio J, Kakaradov B *et al.* Regulation of asymmetric division and CD8+ T lymphocyte fate specification by protein kinase Czeta and protein kinase Clambda/iota. *J. Immunol.* 194(5), 2249–2259 (2015).

57. Larghi P, Williamson DJ, Carpier JM *et al.* VAMP7 controls T cell activation by regulating the recruitment and phosphorylation of vesicular Lat at TCR-activation sites. *Nat. Immunol.* 14(7), 723–731 (2013).

58. Rosenberg SA, Packard BS, Aebersold PM *et al.* Use of tumor-infiltrating lymphocytes and interleukin-2 in the immunotherapy of patients with metastatic melanoma. *N. Engl. J. Med.* 319(25), 1676–1680 (1988).

59. Rosenberg SA, Spiess P, Lafreniere R. A new aproach to the adoptive immunotherapy of cancer with tumor-infiltrating lymphocytes. *Science* 233, 1318–1321 (1986).

60. Rosenberg SA, Sherry RM, Morton KE *et al.* Tumor progression can occur despite the induction of very high levels of self/tumor antigen-specific CD8+ T cells in patients with melanoma. *J. Immunol.* 175(9), 6169–6176 (2005).

61. Geukes Foppen MH, Donia M, Svane IM, Haanen JB. Tumor-infiltrating lymphocytes for the treatment of metastatic cancer. *Mol. Oncol.* 9(10), 1918–1935 (2015).

62. Lafreniere R, Rosenberg SA. Successful immunotherapy of murine experimental hepatic metastates with lymphokine-activated killer cells and recombinant interleukin 2. *Cancer Res.* 45, 3735–3741 (1985).

63. Kawakami Y, Eliyahu S, Sakaguchi K *et al.* Identification of the immunodominant peptides of the MART-1 human melanoma antigen recognized by the majority of HLA-A2-restricted tumor infiltrating lymphocytes. *J. Exp. Med.* 180, 347–352 (1994).

64. Lawrence MS, Stojanov P, Polak P *et al.* Mutational heterogeneity in cancer and the search for new cancer-associated genes. *Nature* 499(7457), 214–218 (2013).

65. Besser MJ, Shapira-Frommer R, Itzhaki O *et al.* Adoptive transfer of tumor-infiltrating lymphocytes in patients with metastatic melanoma: intent-to-treat analysis and efficacy after failure to prior immunotherapies. *Clin. Cancer Res.* 19(17), 4792–4800 (2013).

66. Rosenberg SA, Yang JC, Sherry RM *et al.* Durable complete responses in heavily pretreated patients with metastatic melanoma using T-cell transfer immunotherapy. *Clin. Cancer Res.* 17(13), 4550–4557 (2011).

67. Sarnaik A, Kushalani NI, Chesney JA *et al.* Safety and efficacy of cryopreserved autologous tumor infiltrating lymphocyte therapy (LN-144, lifileucel) in advanced metastatic melanoma patients who progressed on multiple prior therapies including anti-PD-1. *ASCO Annual Meeting* Chicago, IL, USA (2019).

68. Yee C. Adoptive T-cell therapy for cancer: boutique therapy or treatment modality? *Clin. Cancer Res.* 19(17), 4550–4552 (2013).

69. Teng MW, Ngiow SF, Ribas A, Smyth MJ. Classifying cancers based on T-cell Infiltration and PD-L1. *Cancer Res.* 75(11), 2139–2145 (2015).

70. Dudley ME, Gross CA, Somerville RP *et al.* Randomized selection design trial evaluating CD8+-enriched versus unselected tumor-infiltrating lymphocytes for adoptive cell therapy for patients with melanoma. *J. Clin. Oncol.* 31(17), 2152–2159 (2013).

71. Scheper W, Kelderman S, Fanchi LF *et al.* Low and variable tumor reactivity of the intratumoral TCR repertoire in human cancers. *Nat. Med.* doi:10.1038/s41591-018-0266-5 (2018).

- **Evidence pointing toward the difficulty of interpreting the presence of T cell infiltration as a suitable reservoir of tumor-reactive T cells, even from indications where T cell infiltration is found and also a favorable prognostic marker.**

72. Morgan RA, Dudley ME, Wunderlich JR *et al.* Cancer regression in patients after transfer of genetically engineered lymphocytes. *Science* 314, 126–129 (2006).

73. Clay TM, Custer MC, Sachs J, Hwu P, Rosenberg SA, Nishimura MI. Efficient transfer of a tumor antigen-reactive TCR to human peripheral blood lymphocytes confers anti-tumor reactivity. *J. Immunol.* 163, 507513 (1999).

74. Kawakami Y, Rosenberg SA. Human tumor antigens recognized by T-Cells. *Immunol. Res.* 16(4), 313–339 (1997).

75. Johnson LA, Morgan RA, Dudley ME *et al.* Gene therapy with human and mouse T-cell receptors mediates cancer regression and targets normal tissues expressing cognate antigen. *Blood* 114(3), 535–546 (2009).

76. Robbins PF, Morgan RA, Feldman SA *et al.* Tumor regression in patients with metastatic synovial cell sarcoma and melanoma using genetically engineered lymphocytes reactive with NY-ESO-1. *J. Clin. Oncol.* 29(7), 917–924 (2011).

77. Parkhurst MR, Yang JC, Langan RC *et al.* T cells targeting carcinoembryonic antigen can mediate regression of metastatic colorectal cancer but induce severe transient colitis. *Mol. Ther.* 19(3), 620–626 (2011).

78. Morgan RA, Chinnasamy N, Abate-Daga D *et al.* Cancer regression and neurological toxicity following anti-MAGE-A3 TCR gene therapy. *J. Immunother.* 36(2), 133–151 (2013).

79. Kageyama S, Ikeda H, Miyahara Y *et al.* Adoptive transfer of MAGE-A4 T-cell receptor gene-transduced lymphocytes in patients with recurrent esophageal cancer. *Clin. Cancer Res.* 21(10), 2268–2277 (2015).

80. Chapuis AG, Egan DN, Bar M *et al.* T cell receptor gene therapy targeting WT1 prevents acute myeloid leukemia relapse post-transplant. *Nat. Med.* 25, 1064–1072 (2019).

81. Rapoport AP, Stadtmauer EA, Binder-Scholl GK *et al.* NY-ESO-1-specific TCR-engineered T cells mediate sustained antigen-specific antitumor effects in myeloma. *Nat. Med.* 21(8), 914–921 (2015).

82. Robbins PF, Kassim SH, Tran TL *et al.* A pilot trial using lymphocytes genetically engineered with an NY-ESO-1-reactive T-cell receptor: long-term follow-up and correlates with response. *Clin. Cancer Res.* 21(5), 1019–1027 (2015).

83. Linette GP, Stadtmauer EA, Maus MV *et al.* Cardiovascular toxicity and titin cross-reactivity of affinity-enhanced T cells in myeloma and melanoma. *Blood* 122(6), 863–871 (2013).

- **Underscores the complexity of TCR engineering. An affinity-matured MAGE-A3 TCR resulted in cardiac toxicity due to cross-reactivity with a peptide derived from TITIN.**

84. Van Loenen MM, De Boer R, Amir AL *et al.* Mixed T cell receptor dimers harbor potentially harmful neoreactivity. *Proc. Natl Acad. Sci. USA* 107(24), 10972–10977 (2010).

85. Kuball J, Dossett ML, Wolfl M *et al.* Facilitating matched pairing and expressionof TCR hains introduced into human T cells. *Blood* 109, 2331–2338 (2007).

86. Bethune MT, Gee MH, Bunse M *et al.* Domain-swapped T cell receptors improve the safety of TCR gene therapy. *eLife* 5, pii: e19095 (2016).

87. Kunert A, Obenaus M, Lamers CHJ, Blankenstein T, Debets R. T-cell receptors for clinical therapy: *in vitro* assessment of toxicity risk. *Clin. Cancer Res.* 23(20), 6012–6020 (2017).

88. Gonzalez-Galarza FF, Takeshita LY, Santos EJ *et al.* Allele frequency net 2015 update: new features for HLA epitopes, KIR and disease and HLA adverse drug reaction associations. *Nucleic Acids Res.* 43(Database issue), D784–788 (2015).

89. Challa-Malladi M, Lieu YK, Califano O *et al.* Combined genetic inactivation of beta2-Microglobulin and CD58 reveals frequent escape from immune recognition in diffuse large B cell lymphoma. *Cancer Cell* 20(6), 728–740 (2011).

90. So T, Takenoyama M, Mizukami M *et al.* Haplotype loss of HLA Class I antigen as an escape mechanism from immune attack in lung cancer. *Cancer Res.* 65, 5945–5952 (2005).

91. Eshhar Z, Waks T, Gross G, Schindler DG. Specific activation and targeting of cytotoxic lymphocytes through chimeric single chains consisting of antibody-binding domains and the γ or ζ subunits of the immunoglobulin and T-cell receptors. *Proc. Natl. Acad. Sci. USA* 90, 720–724 (1993).

92. Gilham DE, O'neil A, Hughes C *et al.* Primary polyclonal human T lymphocytes targeted to carcino-embryonic antigens and neural cell adhesion molecule tumor antigens by CD3ζ-based chimeric immune receptors. *J. Immunother.* 25(2), 139–151 (2002).

93. Guest RD, Hawkins RE, Kirillova N *et al.* The role of extracellular spacer regions in the optimal design of chimeric immune receptors. *J. Immunother.* 28(3), 203–211 (2005).

94. Gong MC, Latouche JB, Krause A, Heston WDW, Bander NH, Sadelain M. Cancer patient T cells genetically targeted to prostate-specific membrane antigen specifically lyse prostate cancer cells and release cytokines in response to prostate-specific membrane antigen. *Neoplasia* 1, 123–127 (1999).

95. Ren-Heidenreich L, Mordini R, Hayman GT, Siebenlist R, Lefever A. Comparison of the TCR zeta-chain with the FcR gamma-chain in chimeric TCR constructs for T cell activation and apoptosis. *Cancer Immunol. Immunother.* 51(8), 417–423 (2002).

96. Stancovski I, Schindler DG, Waks T, Yarden Y, Sela M, Eshhar Z. Targeting of T lymphocytes to Neu/HER2-expressing cells using chimeric single chain Fv receptors. *J. Immunol.* 151, 6577–6582 (1993).

97. Kershaw MH, Westwood JA, Parker LL *et al.* A Phase I study on adoptive immunotherapy using gene-modified t cells for ovarian cancer. *Clin. Cancer Res.* 15, 6106–6115 (2006).

98. Pule MA, Savoldo B, Myers GD *et al.* Virus-specific T cells engineered to coexpress tumor-specific receptors: persistence and antitumor activity in individuals with neuroblastoma. *Nat. Med.* 14(11), 1264–1270 (2008).

99. Lamers CH, Langeveld SC, Groot-Van Ruijven CM, Debets R, Sleijfer S, Gratama JW. Gene-modified T cells for adoptive immunotherapy of renal cell cancer maintain transgene-specific immune functions in vivo. *Cancer Immunol. Immunother.* 56(12), 1875–1883 (2007).

100. Till BG, Jensen MC, Wang J *et al.* Adoptive immunotherapy for indolent non-Hodgkin lymphoma and mantle cell lymphoma using genetically modified autologous CD20-specific T cells. *Blood* 112, 2261–2271 (2008).

101. Park JR, Digiusto DL, Slovak M *et al.* Adoptive transfer of chimeric antigen receptor re-directed cytolytic T lymphocyte clones in patients with neuroblastoma. *Mol. Ther.* 15(4), 825–833 (2007).

102. Jensen MC, Popplewell L, Cooper LJ *et al.* Antitransgene rejection responses contribute to attenuated persistence of adoptively transferred CD20/CD19-specific chimeric antigen receptor redirected T cells in humans. *Biol. Blood Marrow Transplant.* 16(9), 1245–1256 (2010).

103. Zheng PP, Kros JM, Li J. Approved CAR T cell therapies: ice bucket challenges on glaring safety risks and long-term impacts. *Drug Discov. Today* 23(6), 1175–1182 (2018).

104. Carpenito C, Milone MC, Hassan R *et al.* Control of large, established tumor xenografts with genetically retargeted human T cells containing CD28 and CD137 domains. *Proc. Natl Acad. Sci. USA* 106(9), 3360–3365 (2009).

105. Imai C, Mihara K, Andreansky M *et al.* Chimeric receptors with 4–1BB signaling capacity provoke potent cytotoxicity against acute lymphoblastic leukemia. *Leukemia* 18(4), 676–684 (2004).

106. Hombach A, Wieczarkowiecz A, Marquardt T *et al.* Tumor-specific T cell activation by recombinant immunoreceptors: CD3 ζ signaling and CD28 costimulation are simultaneously required for efficient IL-2 secretion and can be integrated into one combined CD28/CD3ζ signaling receptor molecule. *J. Immunol.* 167, 6123–6131 (2001).

107. Krause A, Guo HF, Latouche JB, Tan C, Cheung NKV, Sadelain M. Antigen-dependent CD28 signaling selectively enhances survival and proliferation in genetically modified activated human Primary T lymphocytes. *J. Exp. Med.* 188, 619–625 (1998).

108. Maher J, Brentjens RJ, Gunset G, Rivière I, Sadelain M. Human T-lymphocyte cytotoxicity and proliferation directed by a single chimeric TCRζ/CD28 receptor. *Nat. Biotechnol.* 20, 70–74 (2002).

109. Finney HM, Lawson ADG, Bebbington CR, Weir ANC. Chimeric receptors providing both primary and costimulatory signaling in T cells from a single gene product. *J. Immunol.* 161, 2791–2797 (1998).

110. Alvarez-Vallina L, Hawkins RE. Antigen-specific targeting of CD28-mediated T cell co-stimulation using chimeric single-chain antibody variable fragment-CD28 receptors. *Eur. J. Immunol.* 26, 2304–2309 (1996).

111. Heuser C, Hombach A, Lösch C, Manista K, Abken H. T-cell activation by recombinant immunoreceptors: impact of the intracellular signalling domain on the stability of receptor expression and antigen-specific activation of grafted T cells. *Gene Ther.* 10, 1406–1419 (2003).

112. Emtage PC, Lo AS, Gomes EM, Liu DL, Gonzalo-Daganzo RM, Junghans RP. Second-generation anti-carcinoembryonic antigen designer T cells resist activation-induced cell death, proliferate on tumor contact, secrete cytokines, and exhibit superior antitumor activity *in vivo*: a preclinical evaluation. *Clin. Cancer Res.* 14(24), 8112–8122 (2008).

113. Kochenderfer JN, Dudley ME, Feldman SA *et al.* B-cell depletion and remissions of malignancy along with cytokine-assocaited toxicity in a clinical trial of anti-CD19 chimeric-antigen-receptor-transduced T cells. *Blood* 119, 2709–2720 (2012).

114. Kochenderfer JN, Dudley ME, Carpenter RO *et al.* Donor-derived CD19-targeted T cells cause regression of malignancy persisting after allogeneic hematopoietic stem cell transplantation. *Blood* 122, 4129–4139 (2013).

115. Lee DW, Kochenderfer JN, Stetler-Stevenson M *et al.* T cells expressing CD19 chimeric antigen receptors for acute lymphoblastic leukaemia in children and young adults: a phase 1 dose-escalation trial. *The Lancet* 385(9967), 517–528 (2015).

116. Porter DL, Hwang WT, Frey NV *et al.* Chimeric antigen receptor T cells persist and induce sustained remissions in relapsed refractory chronic lymphocytic leukemia. *Sci. Transl. Med.* 7, 1–12 (2015).

117. Maude SL, Frey N, Shaw PA *et al.* Chimeric antigen receptor T cells for sustained remissions in leukemia. *N. Engl. J. Med.* 371(16), 1507–1517 (2014).

118. Brentjens RJ, Riviere I, Park JH *et al.* Safety and persistence of adoptively transferred autologous CD19-targeted T cells in patients with relapsed or chemotherapy refractory B-cell leukemias. *Blood* 118(18), 4817–4828 (2011).

119. Davila ML, Riviere I, Wang X *et al.* Efficacy and toxicity management of 19–28z CAR T cell therapy in B cell acute lymphoblastic leukemia. *Sci. Transl. Med.* 6(224), 224ra225 (2014).

120. Grupp SA, Kalos M, Barrett D *et al.* Chimeric antigen receptor-modified T cells for acute lymphoid leukemia. *N. Engl. J. Med.* 368(16), 1509–1518 (2013).

121. Brentjens RJ, Davila ML, Riviere I *et al.* CD19-targeted T cells rapidly induce molecular remissions in adults with chemotherapy-refractory acute lymphoblastic leukemia. *Sci. Transl. Med.* 5(177), 177ra138 (2013).

122. Kochenderfer JN, Dudley ME, Kassim SH *et al.* Chemotherapy-refractory diffuse large B-cell lymphoma and indolent B-cell malignancies can be effectively treated with autologous T cells expressing an anti-CD19 chimeric antigen receptor. *J. Clin. Oncol.* 33(6), 540–549 (2015).

123. Schuster SJ, Svoboda J, Chong EA *et al.* Chimeric antigen receptor T cells in refractory B-cell lymphomas. *N. Engl. J. Med.* 377(26), 2545–2554 (2017).

124. Neelapu SS, Locke FL, Bartlett NL *et al.* Axicabtagene ciloleucel CAR T-cell therapy in refractory large B-cell lymphoma. *N. Engl. J. Med.* 377(26), 2531–2544 (2017).

• **A comprehensive review of the toxicities of CAR-T cells and methods that are currently being used to mitigate them.**

125. Sadelain M. CD19 CAR T Cells. *Cell* 171(7), 1471 (2017).

126. Teachey DT, Bishop MR, Maloney DG, Grupp SA. Toxicity management after chimeric antigen receptor T cell therapy: one size does not fit 'ALL'. *Nat. Rev. Clin. Oncol.* 15(4), 218 (2018).

127. Neelapu SS, Tummala S, Kebriaei P *et al.* Chimeric antigen receptor T-cell therapy – assessment and management of toxicities. *Nat. Rev. Clin. Oncol.* 15(1), 47–62 (2018).

128. Brudno JN, Kochenderfer JN. Toxicities of chimeric antigen receptor T cells: recognition and management. *Blood* 127(26), 3321–3330 (2016).

129. Park JH, Riviere I, Gonen M *et al.* Long-term follow-up of CD19 CAR therapy in acute lymphoblastic leukemia. *N. Engl. J. Med.* 378(5), 449–459 (2018).

130. Shah NN, Fry TJ. Mechanisms of resistance to CAR T cell therapy. *Nat. Rev. Clin. Oncol.* 16(6), 372–385 (2019).

131. Ahmed N, Brawley VS, Hegde M *et al.* Human epidermal growth factor receptor 2 (HER2) -specific chimeric antigen receptor-modified T cells for the immunotherapy of HER2-positive sarcoma. *J. Clin. Oncol.* 33(15), 1688–1696 (2015).

132. Katz SC, Burga RA, Mccormack E *et al.* Phase I hepatic immunotherapy for metastases study of intra-arterial chimeric antigen receptor-modified t-cell therapy for CEA+ liver metastases. *Clin. Cancer Res.* 21(14), 3149–3159 (2015).

133. O'rourke DM, Nasrallah MP, Desai A *et al.* A single dose of peripherally infused EGFRvIII-directed CAR T cells mediates antigen loss and induces adaptive resistance in patients with recurrent glioblastoma. *Sci. Transl. Med.* 9(399), (2017).

134. Brown CE, Alizadeh D, Starr R *et al.* Regression of glioblastoma after chimeric antigen receptor T-cell therapy. *N. Engl. J. Med.* 375(26), 2561–2569 (2016).

135. Adusumilli PS, Zauderer MG, Rusch VW *et al.* Regional delivery of mesothelin-targeted CAR T cells for pleural cancers: safety and preliminary efficacy in combination with anti-PD-1 agent. Presented at: *ASCO annual Meeting.* Chicago, USA (2019).

136. Salter AI, Ivey RG, Kennedy JJ *et al.* Phosphoproteomic analysis of chimeric antigen receptor signaling reveals kinetic and quantitative differences that affect cell function. *Science signaling* 11 (2018).

137. Turtle CJ, Hanafi LA, Berger C *et al.* CD19 CAR-T cells of defined CD4+:CD8+ composition in adult B cell ALL patients. *J. Clin. Invest.* 126(6), 2123–2138 (2016).

138. Maude SL, Laetsch TW, Buechner J *et al.* Tisagenlecleucel in children and young adults with B-cell lymphoblastic leukemia. *N. Engl. J. Med.* 378(5), 439–448 (2018).

139. Helsen CW, Hammill JA, Lau VWC *et al.* The chimeric TAC receptor co-opts the T cell receptor yielding robust anti-tumor activity without toxicity. *Nat. Commun.* 9(1), 3049 (2018).

•• **Development of the TAC platform, which utilizes a membrane-linked scFv to engage tumor antigens and separate scFv to engage the CD3 complex for T cell activation.**

140. Xu Y, Yang Z, Horan LH *et al.* A novel antibody-TCR (AbTCR) platform combines Fab-based antigen recognition with gamma/delta-TCR signaling to facilitate T-cell cytotoxicity with low cytokine release. *Cell Discov.* 4, 62 (2018).

•• **Development of the AbTCR platform in which a fusion protein comprising antibody fragments is tethered to either the TCRγ or TCRδ subunits.**

141. Antibody/T-cell receptor chimeric constructs and uses thereof. *WO 2017/070608 A1* (2017).

142. Baeuerle PA, Ding J, Patel E *et al.* Synthetic TRuC receptors engaging the complete T cell receptor for potent anti-tumor response. *Nat. Commun.* 10(1), 2087 (2019).

•• **Description of the TRuC™ T cell platform, which is based on the fusion of antibody fragments to TCR and CD3 subunits, which become an integral part of the TCR complex and can target one or multiple tumor antigens in a HLA-independent manner.**

143. Long AH, Haso WM, Shern JF *et al.* 4-1BB costimulation ameliorates T cell exhaustion induced by tonic signaling of chimeric antigen receptors. *Nat. Med.* 21(6), 581–590 (2015).

144. Mamonkin M, Da Silva DG, Mukherjee M *et al.* Tonic 4–1BB signaling from chimeric antigen receptors (CARs) impairs expansion of T cells due to Fas-mediated apoptosis. *J. Immunol.* 196, 143–147 (2016).

145. Watanabe N, Bajgain P, Sukumaran S *et al.* Fine-tuning the CAR spacer improves T-cell potency. *Oncoimmunology* 5(12), e1253656 (2016).

146. Frigault MJ, Lee J, Basil MC *et al.* Identification of chimeric antigen receptors that mediate constitutive or inducible proliferation of T cells. *Cancer Immunol. Res.* 3(4), 356–367 (2015).

147. Gomes-Silva D, Mukherjee M, Srinivasan M *et al.* Tonic 4–1BB costimulation in chimeric antigen receptors impedes T cell survival and is vector-dependent. *Cell Rep.* 21(1), 17–26 (2017).

148. Feucht J, Sun J, Eyquem J *et al.* Calibration of CAR activation potential directs alternative T cell fates and therapeutic potency. *Nat. Med.* 25(1), 82–88 (2019).

•• **Demonstrates that reducing the multiplicity of ITAMs of the CAR could reduce exhaustion of the CAR T cells.**

149. Kochenderfer JN, Yu Z, Frasheri D, Restifo NP, Rosenberg SA. Adoptive transfer of syngeneic T cells transduced with a chimeric antigen receptor that recognizes murine CD19 can eradicate lymphoma and normal B cells. *Blood* 116(19), 3875–3886 (2010).

150. Boucher JC, Li G, Shrestha B *et al.* Mutation of the CD28 costimulatory domain confers increased CAR T cell persistence and decreased exhaustion. *J. Immunol.* 200(1 Supplement)57, 28 (2018).

151. Eyquem J, Mansilla-Soto J, Giavridis T *et al.* Targeting a CAR to the *TRAC* locus with CRISPR/Cas9 enhances tumour rejection. *Nature* 543(7643), 113–117 (2017).

•• **Demonstrates that locating the CAR on the *TRAC* gene locus can reduce overall CAR surface expression, remove endogenous TCR-α and enable more natural TCR-like regulation of the CAR gene upon antigen engagement.**

152. Alcover A, Alarcón B, Di Bartolo V. Cell biology of the T cell receptor expression and regulation. *Annu. Rev. Immunol.* 36, 85–107 (2018).

153. Guy CS, Vignali KM, Temirov J *et al.* Distinct TCR signaling pathways drive proliferation and cytokine production in T cells. *Nat. Immunol.* 14(3), 262–270 (2013).

154. D'angelo SP, Melchiori L, Merchant MS *et al.* Antitumor activity associated with prolonged persistence of adoptively transferred NY-ESO-1 (c259)T cells in synovial sarcoma. *Cancer Discov.* 8(8), 944–957 (2018).

155. Prickett TD, Crystal JS, Cohen CJ *et al.* Durable complete response from metastatic melanoma after transfer of autologous T cells recognizing 10 mutated tumor antigens. *Cancer Immunol. Res.* 4(8), 669–678 (2016).

156. Townsend MH, Shrestha G, Robison RA, O'neill KL. The expansion of targetable biomarkers for CAR T cell therapy. *J. Exp. Clin. Cancer Res.* 37(1), 163 (2018).

157. Choi BK, Kim S-H, Kim YH, Byoung SK. Cancer immunotherapy using tumor antigen-reactive T cells. *Immunotherapy* 10, 235–245 (2018).

Empower Your Research With Incucyte® Live-Cell Analysis

Simplifying Progress

The Incucyte® Live-Cell Analysis System speeds scientific discovery by combining lab-tested protocols and reagents with powerful, automated image acquisition and analysis. Gain dynamic insights into the health, morphology, movement and function of cell models, all from the stable environment of a tissue culture incubator.

Select an Incucyte® for your research at **www.sartorius.com/incucyte**

SARTORIUS

Expert Opinion

BioTechniques

Empowering chimeric antigen receptor T-cell therapy with CRISPR

Xuanzhu Zhou*,[1]

Ever since the first chimeric antigen receptor T- (CAR-T) cell therapy, Kite Pharma's Yescarta® for treating non-Hodgkin lymphoma, was approved by the US FDA in October 2017, numerous CAR-T-cell therapies for a variety of cancer types have been granted Investigational New Drug clearance and entered clinical phases. CAR-T therapy researchers are now fueled with enthusiasm and optimism, aiming to declare cancer a curable disease.

WHAT IS CAR-T-CELL THERAPY?

CAR-T-cell therapy involves using engineered T cells expressing tumor antigen-specific CARs for targeting cancer cells. A basic CAR consists of three parts: one extracellular antigen recognition domain, one transmembrane domain and one intracellular signaling domain. The antigen recognition domain is typically a single-chain variable fragment derived from a monoclonal antibody against tumor-associated cell surface antigens. The transmembrane domain of a CAR is commonly from CD28, which provides stability to the CAR. The intracellular signaling domain is generally comprised of a CD3ζ structure, costimulatory molecules and/or cytokine expression cassettes, for enhanced downstream signaling and T-cell function [1].

> *"Exploration of other potential CRISPR/Cas9 gene targets for multiplex editing is of interest now for developing the optimal 'off-the'shelf' allogeneic CAR-T cells."*

KEYWORDS

CAR-T cell therapy • CRISPR • CRISPR HDR template

[1]GenScript USA Inc., Piscataway, 08854 NJ, USA; *Author for correspondence: claire.zhou@genscript.com

BioTechniques 68: 169-171 (April 2020) 10.2144/btn-2019-0107

AUTOLOGOUS VERSUS ALLOGENEIC CAR-T THERAPY

Depending on the source of the T cells, CAR-T therapy can be classified into two categories: autologous or allogeneic. In autologous CAR-T-cell therapy, T cells derived from a patient are engineered as 'living drugs' to recognize and attack the patient's own cancer cells. This patient-specific treatment involves the collection, preservation, shipment, genetic engineering and readministration of T cells from and into the same patient [2]. Currently, the two CAR-T-cell therapies approved by the FDA (Yescarta and Novartis' Kymriah®) are both autologous therapies. Despite the promising results shown in treating certain forms of hematopoietic malignancies, autologous therapy also has its limitations. Not only is it time consuming (which can be extremely critical for late-stage cancer patients), but it also comes with astonishing price tags (US$373,000 for Yescarta and US$475,000 for Kymriah) [3]. In addition, it is not always possible to collect and manufacture enough functional T cells from patients who may already be lymphopenic due to previous treatments or their disease status.

To overcome the limitations of autologous CAR-T-cell therapy, some researchers have moved on to developing allogeneic CAR-T cell therapy, which involves engineering T cells isolated from healthy donors to target patients' tumor-associated antigens in order to defeat cancer. This allogeneic approach is able to bypass the limitations of autologous cell therapy, as T cells from healthy donors are easier to collect and can be engineered with a more controlled and streamlined manufacturing process. However, it poses several other risks to the patients. Because the allogeneic T cells have been isolated from foreign donors, patients may face graft-versus-host disease resulting from human leukocyte antigen mismatch mediated by the donor's T-cell αβ receptor (TCR-αβ) and/or host-versus-graft treatment rejection due to the patient's T-cell human leukocyte antigen mismatch [4]. The most promising strategy to date to circumvent these issues is to couple the power of genome editing, especially the revolutionary CRISPR/Cas9 genome editing technology, with CAR-T engineering.

HOW IS CRISPR/CAS9 USED IN DEVELOPING ALLOGENEIC CAR-T THERAPY?

One essential decision to make in designing CAR-T cells is to choose the correct DNA template for CAR expression. An ideal DNA template has the following qualities: allows flexible insert sizes, inserts at target sites with high efficiency, is highly specific with no off-target insertion, has low cellular toxicity and can be obtained easily and rapidly. Traditionally, viral vectors are used for the delivery of CARs due to their high transduction efficiency. The most commonly used viral vector systems are γ-retroviruses, lentiviruses, adenoviruses and adeno-associated viruses [5]. However, when using viral vectors, there are always concerns regarding their integration into the wrong genome location, which may lead to the onset of other diseases [6]. With the maturation of CRISPR/Cas9 technology, it is now possible to insert large genes at specific genetic sites in T cells for CAR-T engineering without using

viral vectors, minimizing off-target integrations [7].

In 2013, CRISPR/Cas9 technology was first described as a powerful eukaryotic cell genome editing tool, which can create precise double-stranded breaks (DSBs) at a predefined target DNA site and lead to gene mutation. Now, it is widely used in both research and clinical studies. There are two essential components of CRISPR technology: a guide RNA (gRNA) designed for recognizing the protospacer adjacent motif sequence on target DNA, and a Cas9 protein that exerts endonuclease function for creating DSBs. The DSBs will trigger two distinct mechanisms for repair. One mechanism is through the nonhomologous end joining (NHEJ) repair pathway, which introduces mutations to the DSB sites, leading to gene knockout. The other DSB repair mechanism is homology-directed repair (HDR), which enables the donor DNA templates to be accurately inserted at the break sites for gene knock-in [8]. By employing CRISPR HDR pathway, researchers are able to precisely insert a CAR expression cassette into T cells without using viral vectors.

MULTIPLEX EDITING WITH CRISPR/CAS9 FOR PREVENTING ALLOGENEIC CAR-T SIDE EFFECTS

Taking advantage of the multiplex gene editing capability of CRISPR/Cas9, potential safety issues associated with allogeneic CAR-T therapy can be addressed simultaneously during CAR insertion. For example, to prevent graft-versus-host disease, the general approach is to knockout the expression of TCR-αβ of the donor T cells. TCR-αβ heterodimer function requires the expression of both α- and β-chains [9]. In order to disrupt TCR-αβ donor T-cell expression, the α-chain can be knocked out by using CRISPR gRNA specific to the gene encoding TCR-α, *TRAC*. Eyquem *et al.* showed that, by targeting CAR insertion to the *TRAC* exon, CAR expression can be placed under the control of endogenous transcriptional regulation, leading to sustained T-cell function and delayed cell exhaustion [10]. Host-versus-graft rejection can also be resolved by knocking out β_2-microglobulin, part of major histocompatibility complex class I molecules, using CRISPR to prevent surface alloantigen presentation [11]. Moreover, multiplexing additional gRNAs targeting immune inhibitory receptors, such as PD-1 or LAG-3, has shown potential benefits in enhancing the antitumor activity of CAR-T cells [12–14]. Exploration of other potential CRISPR/Cas9 gene targets for multiplex editing is of greatest interest now for developing the optimal 'off-the-shelf' allogeneic CAR-T cells.

KEY CONSIDERATIONS FOR EMPLOYING CRISPR/CAS9 HDR PATHWAY FOR T-CELL ENGINEERING

CRISPR/Cas9 delivery format: use ribonucleoprotein system for optimal delivery

To eliminate the chance of introducing any foreign DNA and inducing insertional mutagenesis, it is best practice to deliver the CRISPR/Cas9 system in the form of ribonucleoprotein, a complex formed by incubating Cas9 protein and gRNA together [15]. Purified Cas9 proteins, as well as other Cas proteins (e.g., Cpf1) are readily available from different vendors. Chemically synthesized full-length gRNA (about 100 nucleotides long) is preferred over *in vitro* transcribed gRNA, which has been shown to induce strong innate immune responses. Another important factor to consider when choosing a gRNA provider is its purification method. High-purity synthetic gRNA purified via HPLC is recommended, with a higher ratio of full-length gRNA products and homogeneity leading to a higher editing efficiency and consistency.

HDR DNA donor template format: ssDNA versus dsDNA

The major concern with regard to gene-edited CAR-T cells is off-target integration [16], which is predominantly influenced by the HDR donor template format. The HDR DNA donor template requires one homology arm (typically around 500 bp) on each side of the gene insert flanking the DNA cut site. Traditionally, dsDNA was widely used due to its ease of production via PCR amplification, whereas producing long ssDNA was almost impossible. However, dsDNA donors are associated with high off-target integration rates, as they can be inserted via not only the HDR pathway but also the error-prone NHEJ process. Incorporation through NHEJ could result in duplication of the homology arms at gRNA target sites, integration at off-target sites or even random insertion to endogenous DSBs that have occurred naturally [17–19]. When compared with dsDNA, ssDNA demonstrates significantly improved editing specificity and reduces off-target integration. A recent study published by Roth *et al.* in *Nature* demonstrated that ssDNA templates have similar gene knock-in efficiency but significantly reduced off-target integration (by over 20-fold) compared with dsDNAs in T cells [20]. These characteristics make ssDNA the ideal template for CRISPR-based gene insertion and replacement. Recent technology breakthroughs have made long ssDNA encoding large genes, up to 3 kb or longer, commercially available to expedite the development of safer CAR-T cells.

Other factors to consider may include the possibility of increasing HDR efficiency, as HDR predominantly occurs at the S/G2 phase of the cell cycle. Several methods have been developed to upregulate HDR, including suppressing NHEJ and activating HDR using chemical and genetic approaches, cell cycle manipulation to prolong the S/G2 phase and colocalization of CRIPSR ribonucleoprotein and ssDNA donor to targeted DSBs via covalent bonding.

FUTURE PERSPECTIVE

From autologous to allogeneic CAR-T cells, from treating liquid tumors to solid tumors, the development of CAR-T-cell therapy is marking a new era in immunotherapy. Using a CRISPR/Cas9-mediated, locus-specific HDR pathway for CAR insertion and ssDNA as an HDR template in T-cell engineering holds great promises in developing safer and more effective 'off-the-shelf' CAR-T-cell products as a universal treatment solution.

FINANCIAL & COMPETING INTERESTS DISCLOSURE

This article was funded in its entirety by GenScript USA global life science contract research organization. The author has no other relevant affiliations or financial involvement with any organization or entity

with a financial interest in or financial conflict with the subject matter for materials discussed in the manuscript apart from those disclosed.

No writing assistance was utilized in the production of this manuscript.

OPEN ACCESS

REFERENCES

1. Zhang C, Liu J, Zhong JF, Zhang X. Engineering CAR-T cells. *Biomark. Res.* 5, 22 (2017).
2. Frey NV, Porter DL. The promise of chimeric antigen receptor T-cell therapy. *Oncology (Williston Park)* 30(10), 880–888 890 (2016).
3. Hay AE, Cheung MC. CAR T-cells: costs, comparisons, and commentary. *J. Med. Econ.* 22(7), 613–615 (2019).
4. Yang Y, Jacoby E, Fry TJ. Challenges and opportunities of allogeneic donor-derived CAR T cells. *Curr. Opin. Hematol.* 22(6), 509–515 (2015).
5. Qin DY, Huang Y, Li D, Wang YS, Wang W, Wei YQ. Paralleled comparison of vectors for the generation of CAR-T cells. *Anticancer Drugs* 27(8), 711–722 (2016).
6. Jin C, Fotaki G, Ramachandran M, Nilsson B, Essand M, Yu D. Safe engineering of CAR T cells for adoptive cell therapy of cancer using long-term episomal gene transfer. *EMBO Mol. Med.* 8(7), 702–711 (2016).
7. Liu J, Zhou G, Zhang L, Zhao Q. Building potent chimeric antigen receptor T cells with CRISPR genome editing. *Front. Immunol.* 10, 456 (2019).
8. Kan Y, Ruis B, Takasugi T, Hendrickson EA. Mechanisms of precise genome editing using oligonucleotide donors. *Genome Res.* 27(7), 1099–1111 (2017).
9. Torikai H, Reik A, Liu PQ *et al.* A foundation for universal T-cell based immunotherapy: T cells engineered to express a CD19-specific chimeric-antigen-receptor and eliminate expression of endogenous TCR. *Blood* 119(24), 5697–5705 (2012).
10. Eyquem J, Mansilla-Soto J, Giavridis T *et al.* Targeting a CAR to the TRAC locus with CRISPR/Cas9 enhances tumour rejection. *Nature* 543(7643), 113–117 (2017).
11. Riolobos L, Hirata RK, Turtle CJ *et al.* HLA engineering of human pluripotent stem cells. *Mol. Ther.* 21(6), 1232–1241 (2013).
12. Ren J, Liu X, Fang C, Jiang S, June CH, Zhao Y. Multiplex genome editing to generate universal CAR T cells resistant to PD1 inhibition. *Clin. Cancer Res.* 23(9), 2255–2266 (2017).
13. Liu X, Zhang Y, Cheng C *et al.* CRISPR-Cas9-mediated multiplex gene editing in CAR-T cells. *Cell Res.* 27(1), 154–157 (2017).
14. Zhang Y, Zhang X, Cheng C *et al.* CRISPR-Cas9 mediated LAG-3 disruption in CAR-T cells. *Front. Med.* 11(4), 554–562 (2017).
15. Seki A, Rutz S. Optimized RNP transfection for highly efficient CRISPR/Cas9-mediated gene knockout in primary T cells. *J. Exp. Med.* 215(3), 985–997 (2018).
16. Peng R, Lin G, Li J. Potential pitfalls of CRISPR/Cas9-mediated genome editing. *FEBS J.* 283(7), 1218–1231 (2016).
17. Miura H, Quadros RM, Gurumurthy CB, Ohtsuka M. Easi-CRISPR for creating knock-in and conditional knockout mouse models using long ssDNA donors. *Nat. Protoc.* 13(1), 195–215 (2018).
18. Li H, Beckman KA, Pessino V, Huang B, Weissman JS, Leonetti MD. Design and specificity of long ssDNA donors for CRISPR-based knock-in. *bioRxiv* doi: 10.1101/178905 178905 (2017) (Epub ahead of print).
19. Quadros RM, Miura H, Harms DW *et al.* Easi-CRISPR: a robust method for one-step generation of mice carrying conditional and insertion alleles using long ssDNA donors and CRISPR ribonucleoproteins. *Genome Biol.* 18(1), 92 (2017).
20. Roth TL, Puig-Saus C, Yu R *et al.* Reprogramming human T cell function and specificity with non-viral genome targeting. *Nature* 559(7714), 405–409 (2018).

SARTORIUS

White Paper

September 12, 2019

Keywords or phrases:
Live-Cell Analysis, Cytotoxic T Cells, Natural Killer Cells, Immune Cell Killing, 3D Tumor Immune Cell Killing, Antibody Dependent Cytotoxicity

The Evolution of Immune Cell Killing Assays Using Live-Cell Analysis

How Enhanced Data Analytics and Translational Models Can Provide New Biological Insights

Introduction

In the ongoing battle to understand cancer and develop new therapeutic strategies, researchers are exploring the role of the patient's own immune system in defending the body against tumors. A critical component of this anti-cancer response is the ability of certain immune cells, such as cytotoxic T and natural killer cells, to induce malignant cell death through the process of immune cell killing (ICK). Modeling ICK *in vitro* is therefore of paramount importance.

There are multiple techniques traditionally used to assess ICK, such as flow cytometry and biochemical readouts. While these are valuable tools, they derive measurements from single time point analyses and do not characterize dynamic cellular interactions, limiting the biological insights that can be gained. Therefore, to develop a more comprehensive understanding of ICK, researchers are seeking new assays which can provide complementary information to supplement current workflows.

Scientists have a particular need for methods that can capture, visualize, and quantify the dynamic changes associated with ICK. Additionally, as increasingly translational models become more widely used, researchers require flexible ICK assays that can be applied to 3D tumor spheroids as well as adherent and non-adherent 2D co-cultures. This white paper demonstrates how the technique of real-time, live-cell analysis has evolved to meet these changing requirements of immuno-oncology research.

Assessing Immune Cell Killing in Cancer Research: The Key Challenges

Given the complexity of ICK, researchers often face numerous challenges when modeling this process *in vitro*. One key difficulty is the inability to determine cell-specific cytotoxic signals in co-culture models due to global well measurements. For example, with techniques that measure enzyme release (such as the LDH and GAPDH release assays), it is not possible to determine whether signals derive from the death of tumor or immune cells within the co-culture model. To address this challenge, the 51 Cr release assay can be employed to isolate cell-specific signals. However, background signals can still limit the conclusions drawn from this assay as many cancer cells do not effectively take up or retain the chromium label.[1,2]

Even with the most reliable analysis of tumor cell cytotoxicity, such aggregate measures of cell death cannot reflect the subtleties of the complex cellular interactions involved in ICK. Different T cell subsets, for instance, can have distinct functional roles when inducing tumor cell death.[3] Researchers exploring these differences in behavior will need to study the morphological characteristics of the activated immune cells and their spatial relationship with cancer cells. However, methods traditionally used to assess ICK are non-image based and often require cell lifting. Therefore, scientists looking to gather phenotypic and spatial insight into this dynamic process will need to employ complementary techniques.

Alongside the difficulties in obtaining reliable and comprehensive data, traditional assays also lack the temporal resolution required to fully characterize the process of ICK. Since most methods assess parameters at a single pre-determined endpoint, it is not possible to gain insights into dynamic changes in biology.[4] An additional concern is the variability in cell maturity and health at the point of data collection, which can limit the quality and reliability of results. Moreover, when a problem is identified, troubleshooting to determine the cause can involve repeated experimental runs that consume valuable material and can take significant time.

The Growing Need for Flexibility and Multiplexing

As cell culture models become more complex, the challenges associated with measuring ICK become significantly harder to overcome. This is a pressing issue in immuno-oncology research, as scientists are often moving away from simple 2D culture systems to embrace advanced 3D models with greater physiological relevance. For example, tumor spheroid models are increasingly employed to reveal how the tumor microenvironment (TME) affects the interaction between cancer and the immune response.[5,6] As a further strategy to gain more translational insights, many researchers are now incorporating patient-derived material such as biopsy tissue or chimeric antigen receptor (CAR) T cells into ICK models, which could help unlock the full potential of personalized medicines. In this expanding landscape of translational cellular research, scientists are increasingly seeking flexible ICK assays which can be adapted to a range of different culture models.

The complex cultures involved in these translational models tend to be more delicate. As such, they are more susceptible to perturbations in environmental conditions, making it technically challenging to obtain reliable results. However, since these fragile cultures are much more precious than cell lines, it is vital to gain the most value from each assay. Consequently, researchers are recognizing the need for new ICK methods that enable better monitoring of cells and have the multiplexing capacity to extract the most information from the smallest possible amount of material. For scientists looking to meet these requirements, a particularly promising approach is live-cell analysis.

Live-Cell Analysis: A Flexible Solution to Meet New Requirements

Live-cell analysis utilizes time-lapse imaging to capture the behavior of living cells in real-time. Cultures are maintained upon an imaging platform contained within the incubator, providing a dynamic view of biological events and behavioral changes throughout the experiment. Scientists can therefore continually assess the culture and schedule manipulations and measurements when most appropriate. Such flexibility is a key benefit for researchers contending with biological variability between cultures, particularly when there is the need to maximize the amount of data gained from precious material.

The technique of live-cell analysis can be applied to measure ICK across a variety of *in vitro* models, including both 2D and 3D cultures. In the simplest 2D application, tumor cells are maintained in a basic co-culture with selected immune cells such as T cells or human peripheral blood mononuclear cells (PBMCs) that are activated with soluble cytokines, antibodies, or beads. Most typically, tumor cells will be labeled with a nuclear-restricted fluorescent protein which can be quantified as a marker of proliferation, while apoptosis will be measured in a second fluorescence channel using reagents such as

Incucyte® Caspase 3/7 or Annexin V Dye. To mitigate the contribution of immune cell apoptosis, size-gating filter settings are employed to exclude the smaller effector cells, thus reducing contaminating signals.

Crucially, since the mix-and-read reagents are added at the beginning of the experiment and the imaging platform is contained within the incubator, cells are undisturbed throughout the duration of the assay. This is a major advantage for delicate cultures which require a stable environment.

To illustrate the value of live-cell analysis for measuring ICK, Incucyte® Nuclight Red A549 tumor cells (2,000 cells/well) were cultured in combination with PBMCs (20,000 cells/well, target:effector (T:E) ratio of 1:10). All wells contained Incucyte® Caspase 3/7 Green Dye to measure apoptosis. To activate the T cells in select wells, anti-CD3 in combination with IL-2 was added. Images were captured every two hours over a period of four days. These images were then analyzed to assess target cell proliferation using the count of red objects (nuclei), and to quantify target cell death using the count of green objects over time (Figure 1). Results revealed that wells containing activated T cells showed signs of target cell death and reduced proliferation.

A.

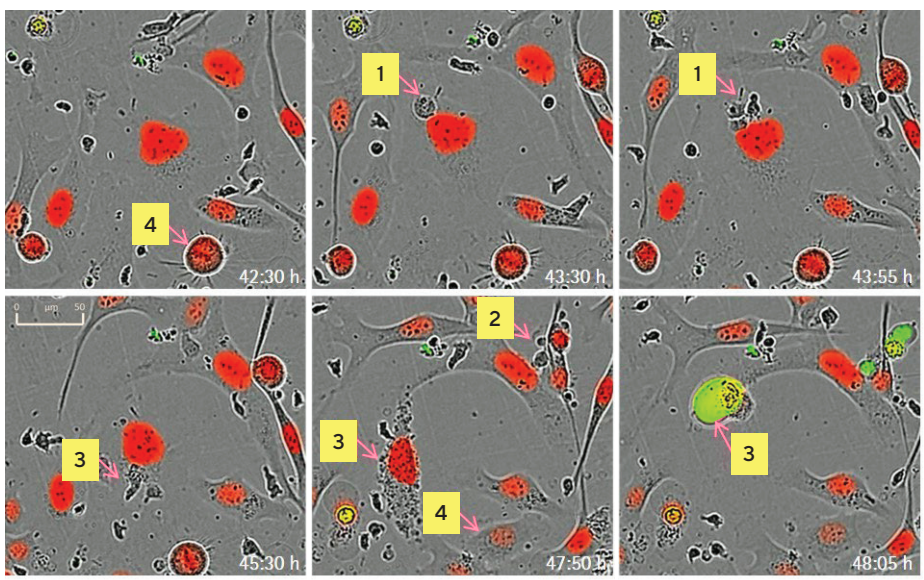

Real-Time Images Capture Morphological Changes and Cellular Interactions, While Tumor Cell Proliferation and Apoptosis Can Be Quantified Using Image Analysis.

1. Physical contact between a small cytotoxic T cell and a larger labeled tumor cell (red).
2. Tumor cells under attack from a cytotoxic T lymphocyte: The "kiss of death".
3. Tumor cell cytoplasmic granulation immediately followed by Incucyte® Caspase 3/7 labeling (green), nuclear condensation and cell death.
4. Tumor cell mitosis: One cell becomes two.

B.

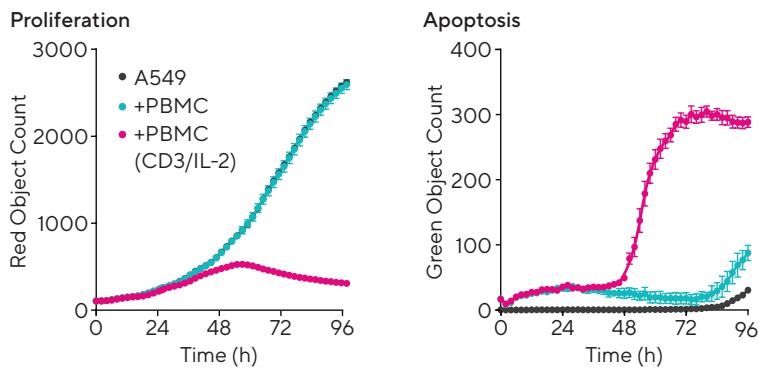

Figure 1: The use of live-cell analysis to assess immune cell killing in a simple 2D co-culture model. (A) Visualization of the interplay between immune cells and tumor cells. (B) Quantification of tumor cell proliferation and death in real-time. Images were analyzed for red object count to assess tumor cell proliferation and green object count to assess tumor cell death. Wells in which T cells were activated showed increased target cell death and reduced proliferation.

The images obtained from these wells clearly show the interactions between immune cells and T cells, illustrating the process of T cell attack followed by cytoplasmic granulation and Incucyte® Caspase 3/7 labeling. In addition to static images, it is possible to create videos to fully capture the process of ICK. This wealth of visual data allows researchers to gather rich biological information and can also prove invaluable for troubleshooting and quality control (QC).

The study presented above demonstrates the basic use of live-cell analysis—to obtain aggregate measures of tumor cell proliferation and apoptosis, and to provide valuable qualitative data showing the interplay between cell types.

Gaining Additional Insights With Enhanced Data Analytics

As the analytical capacity of live-cell analysis has evolved, scientists have gained new abilities to shed light on ICK. A key step forward has been the development of advanced image processing algorithms to define individual cells. Therefore, rather than simply using red object count to quantify tumor cells, scientists can now employ cell masking software (such as Incucyte® Cell-by-Cell Analysis) to recognize all cells within the image. Since tumor cells will be labeled with RFP, the cells can then be classified into effector and target populations based on the presence or absence of red fluorescence.

This ability to distinguish different cell types raises several advantages. Firstly, researchers can enumerate effector cells without the use of labels. Secondly, scientists can improve cell classification in studies involving non-adherent target cells. These tumor cells can look very similar to immune cells, making it challenging to isolate target apoptosis from contaminating effector cell signals using the size-gating method employed in standard analysis.

To illustrate the use of cell masking software in non-adherent cultures, Incucyte® Nuclight Red Ramos cells (10,000 cells/well) were mixed with an increasing ratio of pre-activated or non-activated PBMCs in the presence of Incucyte® Annexin V Green Dye as a marker of apoptosis (Figure 2). Advanced image processing algorithms within the Incucyte® Cell-by-Cell Analysis Software Module were used to mask individual cells, which could then be classified into target and effector cell populations based on the presence or absence of red fluorescence. The target cell population (red) displayed a decrease in proliferation and an increase in apoptosis in the presence of increasing numbers of effector cells. In contrast, the effector cell population (non-red) displayed proliferation over time, but only for activated cells.

Advances in image analysis software also enable scientists to visualize and quantify interactions between immune and tumor cells. For instance, quantifying the coincidence or overlay of two cell masks enables the assessment of immune and target cell interaction. To demonstrate this, Incucyte® Cytolight Red A549 tumor cells (5,000 cells/well) were cultured with either pre-activated or non-activated PBMCs (25,000 cells/well, T:E ratio of 1:5) in the presence of Incucyte® Fabfluor-488-α-CD45 and Incucyte® Opti-Green to label the total lymphocyte population (Figure 3). Two hours after PBMC addition, image processing software was used to mask the cells, enabling the spatial information of the target and effector cells to be quantified. Consistent with expectations, activated PBMCs showed a much greater interaction with target cells, aligning with increased ICK.

A.

Effector Cells (Yellow Mask)
Target Cells (Blue Mask)

Nuclight Red Ramos + act PBMC

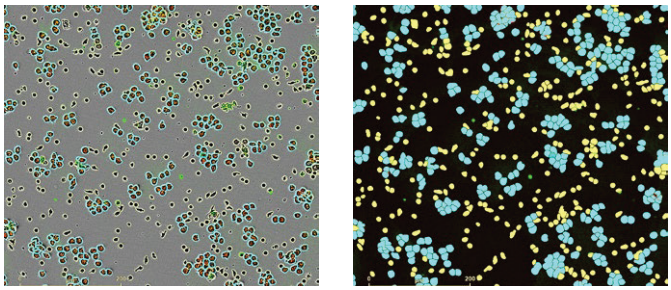

Nuclight Red Ramos + non-act PBMC

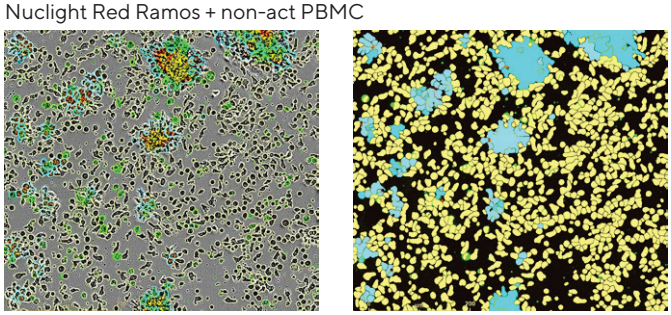

Non-Adherent Target Cells and Effector Cells Can Easily Be Classified Into Distinct Populations With the Latest Image Analysis Software.

B.

Classification of Populations

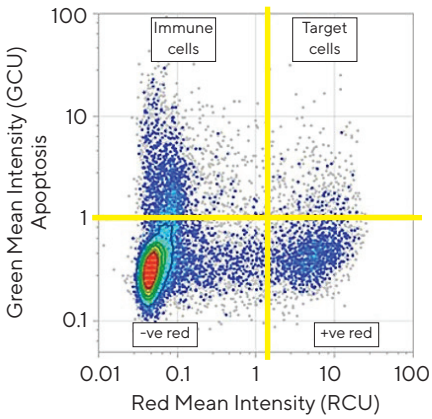

C.

Target Cell Proliferation
+ve Red Pop

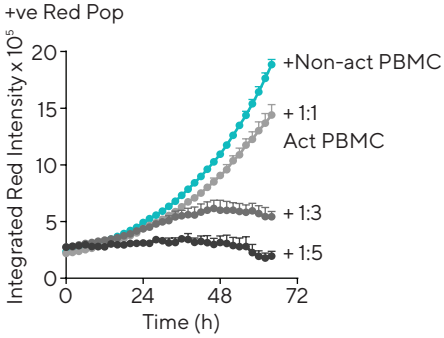

Target Cell Apoptosis
+ve Red Pop

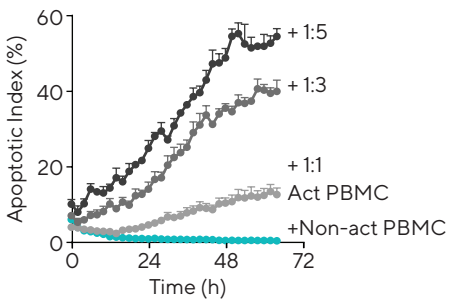

Effector Cell Proliferation
+ve Red Pop

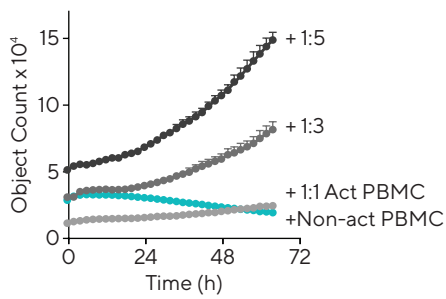

Figure 2: Enhanced image quantification using Incucyte® Cell-by-Cell Analysis Software Module. (A) Images show individual cell masking of the total population with the Cell-by-Cell Analysis Software. Target (blue) and effector (yellow) sub-populations were distinguished based on red fluorescence. (B) Sub-populations were classified based on red and green fluorescence. (C) Quantification of proliferation and apoptosis over time. The target cell population (positive red cells) show a decrease in proliferation and increase in apoptosis (% of red cells also green) in the presence of increasing numbers of effector cells. The effector cell population (non-red cells) show proliferation when activated. Data shown as mean +/- SEM, n = 4 wells.

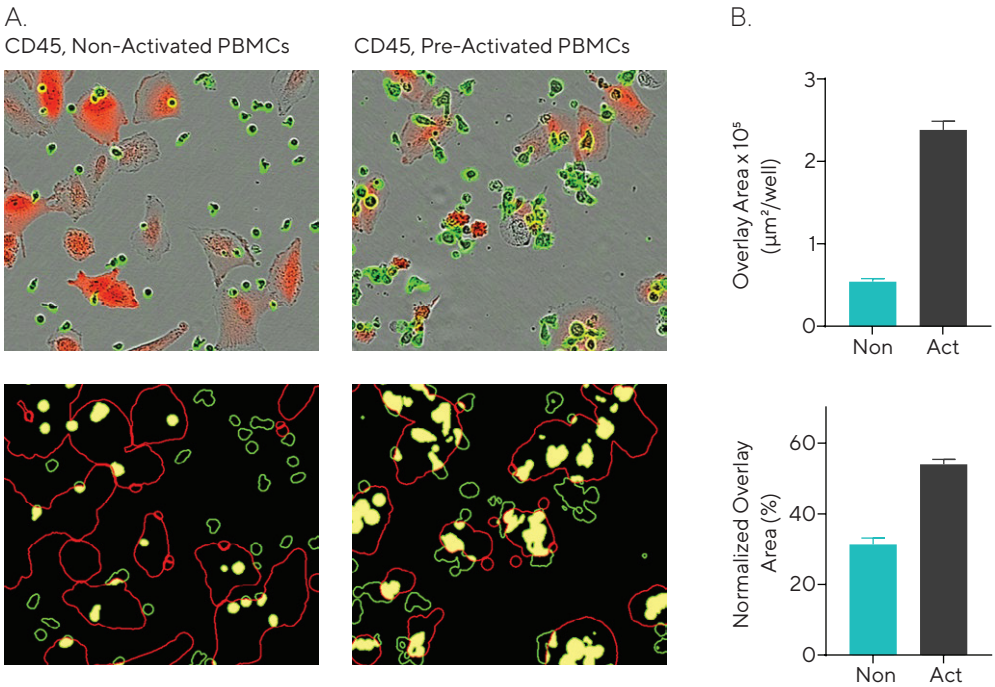

Cellular Interactions Can Be Quantified and Analyzed by Using Image Processing Algorithms to Define Cell Coincidence.

Figure 3: Visualization and quantification of immune and tumor cell interactions. (A) Images at two hours after PBMC addition show interactions between CD45+ cells (green) and A549 cells (red). The overlay between the two cell types is shown with the yellow mask. (B) Quantification of the overlay reveals a markedly higher interaction for activated compared to non-activated effector cells.

By measuring and quantifying cellular interactions, scientists can gain additional morphological and spatial insights to better characterize the process of ICK. Ultimately, this information could support the identification of novel therapeutic candidates. Assessing the duration of cellular interactions, for example, could prove very valuable for drug discovery programs, since a longer contact time between immune and cancer cells is potentially associated with increased ICK.

A further application of enhanced image processing is to use antibodies specific to surface markers to independently assess distinct effector cell subtypes. This type of subset analysis in conjunction with interaction assessment allows scientists to determine which immune cell populations are interacting with target cells. As a result, this approach could distinguish a greater therapeutic effect on a small subset of cells from a lesser therapeutic effect on all cells. Since heterogeneity between different effector cell types is a major complicating factor in immuno-oncology drug discovery, these new capabilities provide a significant advantage over assays that employ aggregate measures based on consolidating the information from all cells.

Applying Live-Cell Analysis to 3D Tumor Spheroid Models

A growing body of evidence highlights the importance of the tissue environment and architecture in modulating the complex relationship between immune and tumor cells. Consequently, many scientists are now employing 3D models to gain more physiologically relevant data when assessing cancer immunotherapy agents *in vitro*. Indeed, evidence shows that tumor cells cultured in 3D can exhibit heightened resistance to cytotoxicity, which is more reflective of the *in vivo* situation.[6]

Tumor spheroid models, which incorporate 3D cellular aggregates formed of cancer cells, provide a useful way of reflecting the 3D TME as they model important features such as cell-to-cell contact and oxygen gradients.[7,8] One type of spheroid model commonly used in ICK research uses single spheroids, aggregates which can be formed by seeding tumor cells in ultra-low attachment plates. These provide a useful tool for studying ICK in solid tumors which may have hypoxic cores.

To demonstrate the use of single spheroid models to assess ICK, Incucyte® Nuclight Red A549 tumor cells were seeded in a round-bottom 96-well plate (2,500 cells/well) and allowed to form spheroids over three days. Once formed, spheroids were co-cultured with PBMCs at a T:E ratio of 1:2.5 in the presence or absence of activating cytokines (anti-CD3 and IL-2). Incucyte® HD phase and fluorescence images were then used to monitor the spheroids over several days. Results show a marked loss of fluorescence intensity for spheroids in the presence of activated PBMCs, reflecting an increased death of tumor cells.

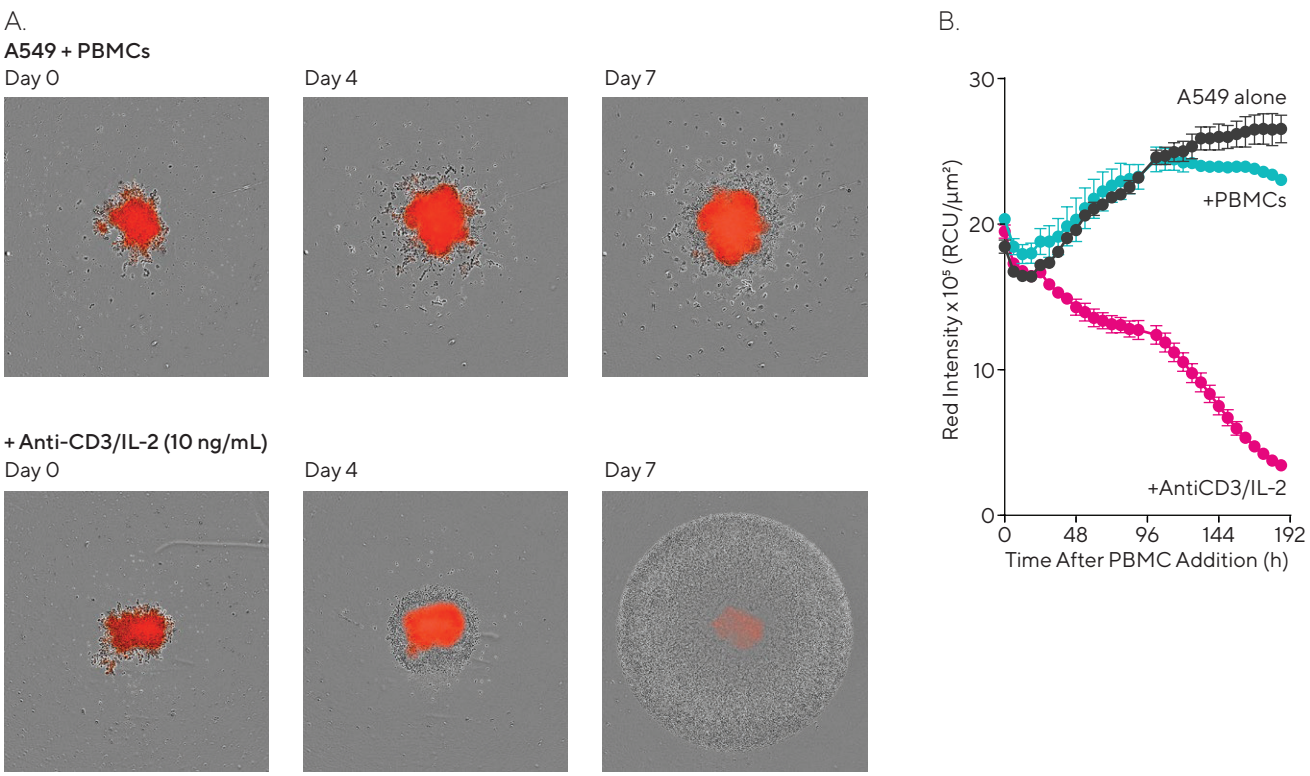

Figure 4: Impact of activated PBMCs on tumor spheroid proliferation. (A) High-definition phase and fluorescence images compare the effect of PBMCs on spheroid proliferation in the absence (top panel) and presence (bottom panel) of activating cytokines. A marked loss of fluorescence intensity can be seen in the presence of activated PBMCs. (B) Time-course plot shows spheroid cytotoxicity quantified as a loss of fluorescence intensity over time. Data was collected over seven days at six-hour intervals. Data shown as mean +/- SEM, n = 3 wells.

Multi-Spheroid Models

Multi-spheroid models, which incorporate components of the extracellular matrix (ECM), provide an alternative option for immuno-oncology researchers. The ECM plays an important role in ICK, as it can influence cellular interactions and affect the infiltration of immune cells into 3D structures. In multi-spheroid models, the biomatrix alters the formation process so that multiple heterogeneous spheroids are created in each well.

Live-cell analysis can easily be employed to measure ICK within these multi-spheroids. An example of one such study is shown in Figure 5. In this assay, the antibody dependent cytotoxicity (ADCC) of Herceptin on Her2 positive cells was assessed. Her2 negative MCF-7 cells expressing nuclear-restricted RFP (Incucyte® Nuclight Red MCF-7) or Her2 positive BT-474 cells expressing cytoplasmically-restricted green fluorescent protein (Incucyte® Cytolight Green BT-474) were seeded in flat-bottom 96-well plates (1,000 cells/well) on a bed of Matrigel®.

Multi-spheroids were allowed to form over three days before Herceptin was added in either the presence or absence of PBMCs (5,000 cells/well, T:E ratio of 1:5). Over the following seven days, brightfield and fluorescence images were used to monitor the spheroids. Results demonstrate a concentration-dependent loss of fluorescence in the presence of Herceptin in only the Her2 positive BT-474 cells and not the Her2 negative MCF-7 cells. A loss of fluorescence intensity was seen in both cell types with the addition of treatments activating the T cell populations (anti-CD3 and IL-2).

A.

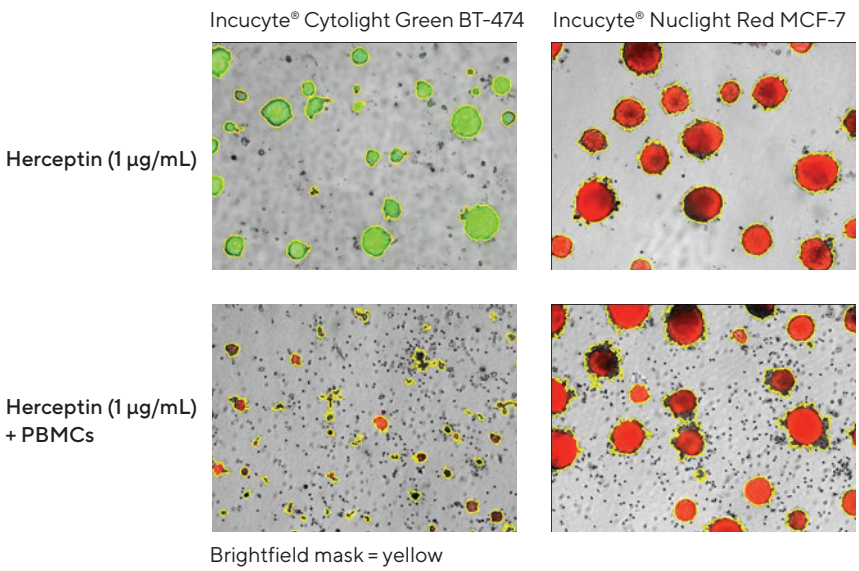

In Both Single and Multi-Spheroid Models, ICK Can Be Easily Quantified.

B.

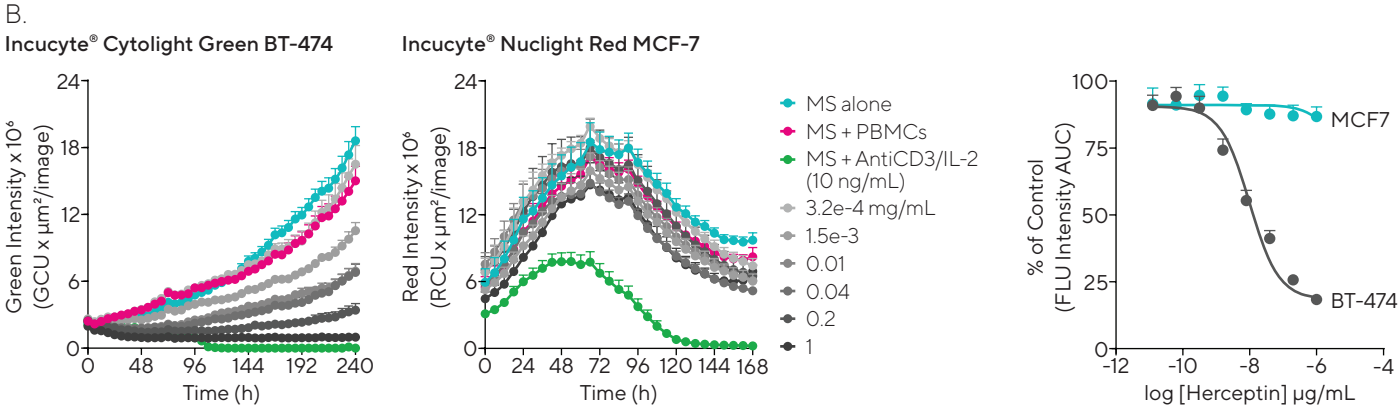

Figure 5: Impact of Herceptin-induced PBMCs on multi-spheroid proliferation. (A) Incucyte® brightfield and fluorescence images taken at seven days (Incucyte® Nuclight Red MCF-7) or ten days (Incucyte® Cytolight Green BT-474) show the effect of Herceptin on spheroid proliferation in the absence (top panel) and presence (bottom panel) of PBMCs. The brightfield outline mask is shown in yellow. (B) Time-courses show multi-spheroid death quantified as a loss of fluorescence intensity within the spheroid brightfield object. Increased cytotoxicity was seen with the addition of treatments activating T cell populations (anti-CD3 and IL-2). Data was collected over ten days at six-hour intervals. Data shown as mean +/- SEM, n = 4 wells.

Adapting to the Evolving Landscape of Immunology Research

In the quest to better understand the process of ICK, scientists are seeking deeper biological insights from more complex translational models. The evidence we have presented so far shows that live-cell analysis can easily be adapted to facilitate this research. It is also likely that this technique will be applied to newer models as the landscape of immunology research continues to evolve.

Multicultures: Live-cell analysis could be used in multicultures involving three or more cell types. Such models are likely to be increasingly used in immuno-oncology research, given the growing evidence for the important role of interactions with stromal cells in tumorigenesis.[9] For scientists assessing ICK in these complex models, live-cell analysis provides an ideal solution as the technique can flexibly accommodate complex culture models.

Another key translational approach is to incorporate patient-derived material, such as biopsy tissue or CAR-T cells, into ICK assays. Again, live-cell analysis can easily be adapted to such studies. Indeed, this method has already been successfully used to develop and test new CAR-T cell constructs and assess their *in vitro* activity[10,11], and it could also prove useful in the comparison of expansion and activity between batches for QC purposes. So far, the use of live-cell analysis for CAR-T cell therapies is limited to the preclinical stage, but clinical applications are likely to develop as technology and instrumentation advances.

Immune cell infiltration: A further use for these assays could be in assessing the invasion of immune cells into 3D structures. This is a focus of interest in immuno-oncology, as the infiltration of T lymphocytes into solid tumors is correlated with clinical outcomes.[12] However, tumors employ many defense mechanisms which can limit the migration of immune cells. Therefore, the process of immune invasion is a developing area of research for scientists investigating new therapeutic approaches. In fact, this field is expanding fast, with the recent development of novel 3D high-throughput assays to investigate immune cell homing.[6] Given the flexibility of live-cell analysis in adapting to 3D models, it is likely that this method will play a key role in this exciting avenue of research.

Conclusion

In this white paper, we have illustrated how live-cell analysis has evolved to address the growing challenges of immuno-oncology research. The introduction of enhanced data analytics, coupled with the validation of this approach in more translational 3D culture models, has enabled live-cell analysis to become a flexible solution to meet the current and future requirements of this field.

Essentially, the unique value of this method stems from its capacity to maximize the amount of data gained from each culture. There are two main reasons for this: firstly, signals of interest will never be missed with real-time monitoring so cultures will not be wasted; and secondly, scientists can now increase the depth of information gathered from each sample by using new metrics and analyses. In this way, researchers can achieve a richer understanding of ICK without additional expense in terms of time or material. This resource-efficiency is crucial for translational models, which often incorporate more precious and delicate cultures.

To gain even greater value from each experiment, it is possible to couple live-cell analysis with other techniques. Since cells are unperturbed throughout the course of the experiment, researchers can remove supernatant samples, or alternatively lift cells after the assay and analyze them with methods such as flow cytometry. As such, scientists can maximize the biological information gained from precious cultures.

Overall, the flexibility and multiplexing capacity of live-cell analysis make this method a valuable solution to supplement traditional ICK workflows, offering great potential to advance immuno-oncology research and therapy discovery.

References

1. Zaritskaya L, Shurin MR, Sayers TJ, and Malyguine AM. **New flow cytometric assays for monitoring cell-mediated cytotoxicity.** *Expert Rev Vaccines,* Jun;9(6);601–16 (2010)
2. Nelson DL, Kurman CC, and Serbousek DE. **51 Cr Release Assay of Antibody-Dependent Cell-Mediated Cytotoxicity (ADCC).** *Current Protocols in Immunology,* 8(1);7.27.1-7.27.8 (2001)
3. Golubovskaya V and Wu L. **Different Subsets of T Cells, Memory, Effector Functions, and CAR-T Immunotherapy.** *Cancers (Basel),* Mar 15;8(3);36 (2016)
4. Cerignoli F, *et al.* ***In vitro* immunotherapy potency assays using real-time cell analysis.** *PLoS One,* Mar;13(3);e0193498 (2018)
5. Verjans ET, Doijen J, Luyten W, Landuyt B, and Schoofs L. **Three-dimensional cell culture models for anticancer drug screening: Worth the effort?** *J Cell Physiol,* Apr;233(4);2993–3003 (2018)
6. Sherman H, Gitschier HJ, and Rossi AE, **A Novel Three-Dimensional Immune Oncology Model for High-Throughput Testing of Tumoricidal Activity.** *Front Immunol,* 9;857 (2018)
7. Däster S, *et al.* **Induction of hypoxia and necrosis in multicellular tumor spheroids is associated with resistance to chemotherapy treatment.** *Oncotarget,* Jan;8(1);1725–1736 (2017)
8. Riffle S and Hegde RS. **Modeling tumor cell adaptations to hypoxia in multicellular tumor spheroids.** *J. Exp. Clin Cancer Res,* Dec;36(1);102 (2017)
9. Radisky D, Hagios C, and Bissell MJ. **Tumors are unique organs defined by abnormal signaling and context.** *Semin Cancer Biol,* Apr;11(2);87–95 (2001)
10. Foster AE, *et al.* **Regulated Expansion and Survival of Chimeric Antigen Receptor-Modified T Cells Using Small Molecule-Dependent Inducible MyD88/CD40.** *Mol Ther,* Sept;25(9);2176–2188 (2017)
11. Li H, *et al.* **Antitumor activity of EGFR-specific CAR-T cells against non-small-cell lung cancer cells *in vitro* and in mice.** *Cell Death Dis,* Fed;9(2);177 (2018)
12. Fridman WH, Pagès F, Sautès-Fridman C, and Galon J. **The immune contexture in human tumours: impact on clinical outcome.** *Nat Rev Cancer,* Apr;12(4);298–306 (2012)

SARTORIUS

Application Note

June 19, 2020

Keywords or phrases:
Cell Cycle, FUCCI, Cell Cycle Modulation, Differentiation, Immune Cell Killing

Real-Time Quantification of Cell Cycle Phase in Live-Cell Models

Introduction

Cell cycle is critical in maintaining cellular homeostasis through tightly regulated signaling pathways which control the frequency of DNA duplication and eventually cellular division. Without this regulation, cells divide in an uncontrolled manner, propagating uncorrected mutations and evading programmed cell death. Therefore, the cell cycle and its checkpoints are an attractive target for cancer therapies, which aim to arrest unchecked cell division as well as promote apoptosis[1,2]. Following this series of coordinated events, however, requires optimized technology and cell cycle indicator reagents. Current end-point solutions fail to study cell cycle over multiple cell divisions and do not fully integrate data acquisition and analysis. Live-cell imaging and analysis is uniquely suited to providing temporal information on the cell cycle through real-time, automated quantification and visualization of the events leading up to cell arrest, senescence or death.

Assay Principle

The Incucyte® Cell Cycle Lentivirus reagents (Green | Red or Green | Orange) have been developed to distinguish between cells in the G1 and S | G2 | M cell cycle phase without altering cell function. As Geminin is highly expressed during S | G2 | M phase and Cdt1 during G1, fragments of these proteins are used to target fluorescent proteins for degradation during certain cell cycle phases. The Incucyte® Cell Cycle Lentivirus reagents incorporate a single cassette indicator expressing both the Geminin-TagGFP2 (green fluorescent protein) and either Cdt1-TagRFP (orange fluorescent protein) or Cdt1-mKate2 (red fluorescent protein). Therefore, cells fluoresce green during S | G2 | M and red or orange during G1; cells are colorless during the transition from M to G1 and yellow (expressing green and red, or green and orange, simultaneously) in transition from G1 to S phase. Images of cells expressing Incucyte® Cell Cycle can be acquired and analyzed automatically in the Incucyte® Live-Cell Analysis System to identify phases of cell cycle in individual cells for real-time measurements of cell cycle dynamics. The schematic in Figure 1 shows the expression of green and red, or green and orange, fluorophores across the cell cycle, and the time course of images demonstrate the change in fluorescence as the cell divides. The indicated cell with red fluorescence is in G1 phase at 0 h. By 4 h the cell is transitioning from G1 to S, and at 7 h the cell is green indicating S | G2 | M phase. At 9 h the cell is mitotic, and by 11 h daughter cells in G1 are observed.

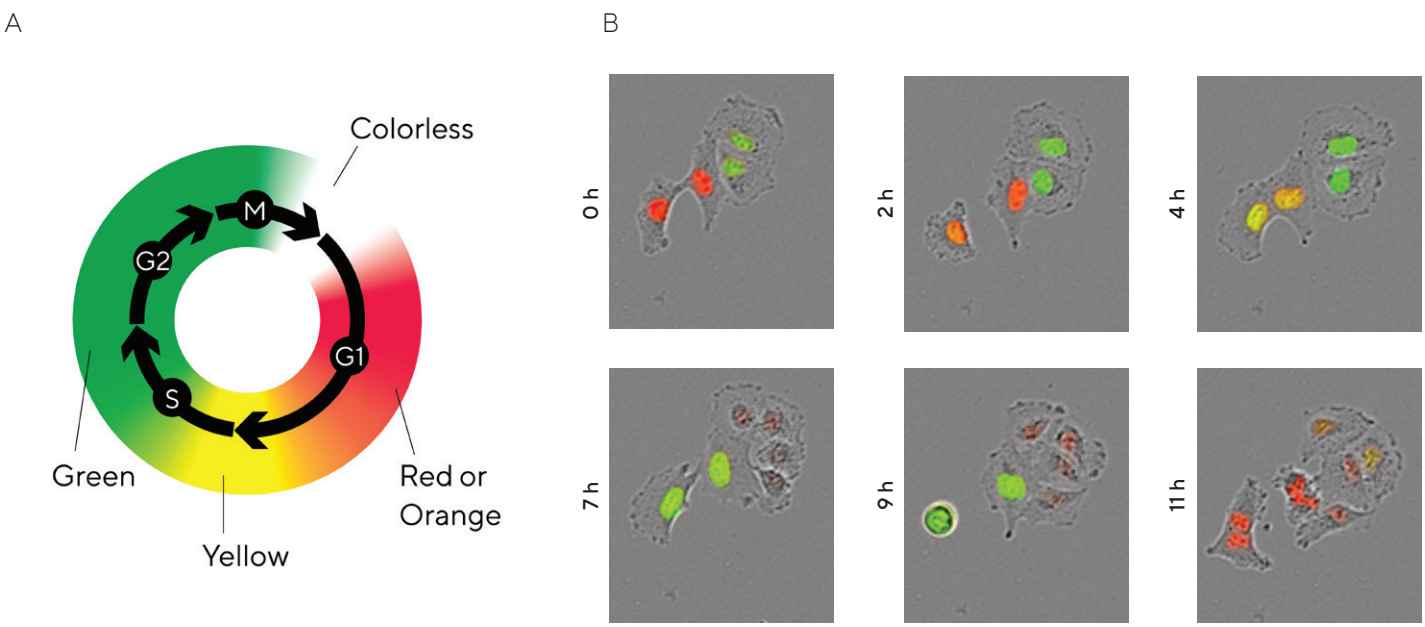

Figure 1: Incucyte® Cell Cycle Lentivirus. Schematic displays the fluorescence expressed at each stage of the cell cycle (A). Cells expressing Incucyte® Cell Cycle will exhibit green fluorescence during S | G2 | M and red or orange fluorescence during G1. Transition from M–G1 is non-fluorescent, and transition from G1–S displays yellow fluorescence, i.e., both green and red, or green and orange. Images of HeLa cells were acquired on the Incucyte® Live-Cell Analysis System (B). Sequential images show a cycling cell over time starting in G1 at 0 h with red fluorescence.

Materials and Methods

To generate a cell line with stable Incucyte® Cell Cycle expression, the lentivirus was used to transduce the cell line of choice[3]. Using the Incucyte® Live-Cell Analysis System to monitor fluorescent marker expression and cell health, appropriate reagent multiplicity of infection (MOI) was chosen. When cells were observed to express the Cell Cycle reagent, puromycin selection was applied to remove non-expressing cells from the culture. By thorough examination of cell morphology and proliferation, a number of infected and parental cell lines were compared, demonstrating that the Incucyte® Cell Cycle Lentivirus generates cell lines that have comparable morphology and growth profiles to the parental phenotype.

Quick Guide

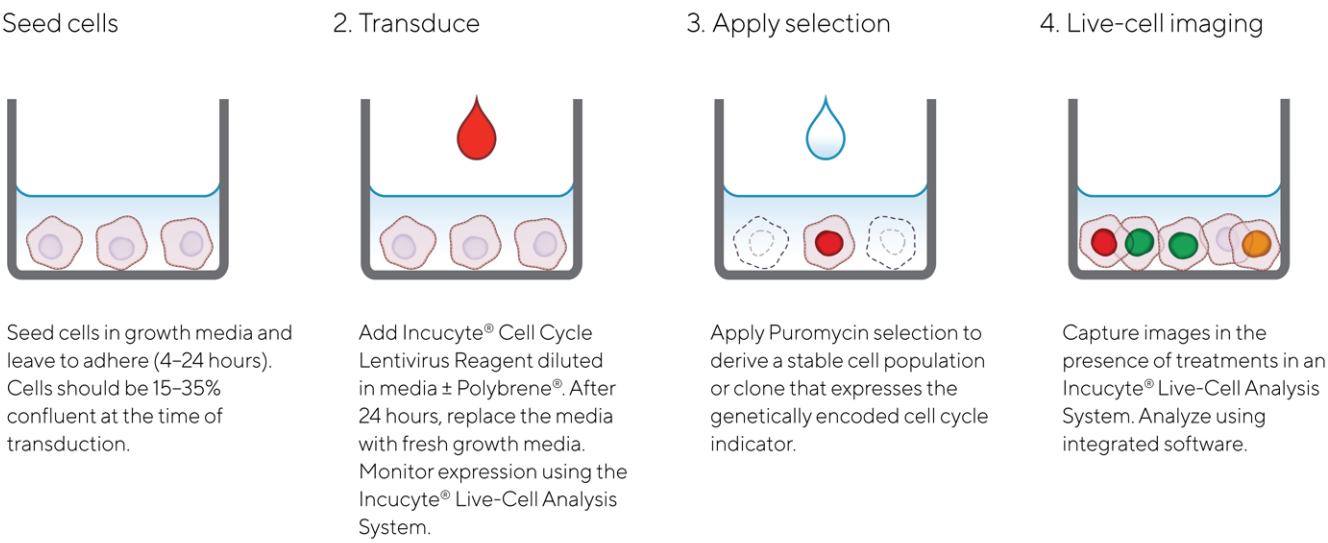

Figure 2: Quick guide to generation of a cell line stably expressing Incucyte® Cell Cycle. Using a simple protocol, cells can be treated with Incucyte® Cell Cycle Lentivirus reagent and begin expressing the fluorescent ubiquitination-based cell cycle indicator (FUCCI).

Quantification of Cell Cycle Phase

The Incucyte® Cell-by-Cell analysis module enables individual cells in the field of view to be segmented in the phase contrast image, and metrics can be extracted per cell relating to fluorescence within the segmented boundary. Using the integrated analysis software, cell populations can be classified based on fluorescence characteristics. In combination with the Incucyte® Cell Cycle Lentivirus, this enables the percent cells in each phase to be rapidly quantified, as demonstrated in Figure 3. Cells expressing high green fluorescence (S | G2 | M) can be separated from those expressing high red fluorescence (G1), and transition phases can also be identified with high red and green (G1–S) or low red and green (M–G1). Both adherent and non-adherent cells can be quantified with this method.

Cells expressing Incucyte® Cell Cycle can also be monitored by counting the number of green and red objects (or green and orange objects, depending upon the lentivirus used) using basic fluorescence segmentation. Cells transitioning from G1–S appear yellow and can also be quantified by measuring objects with overlapping green and red fluorescence; yellow objects should be subtracted from the green object and red object counts to avoid over-estimation of these objects. This method enables evaluation of alterations in cell cycle progression in co-culture models, however information on the M–G1 phase is not available as these cells will be non-fluorescent and cannot be distinguished from a secondary non-labelled cell type.

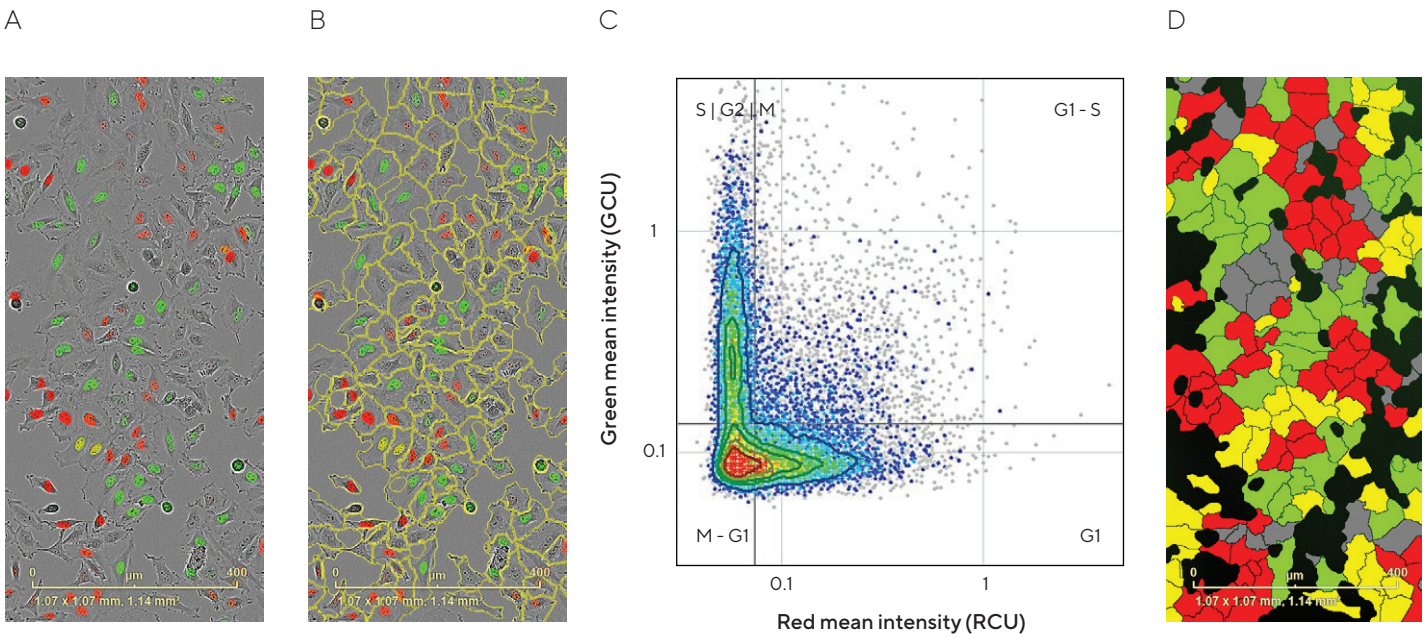

Figure 3: Cell cycle quantification. Images acquired in Incucyte® Cell-by-Cell Software Analysis Module allow individual cells to be segmented (A, B). Cells can be classified according to red and green fluorescence intensity (C). Classification mask shows cells identified as red, green, yellow or non-fluorescent (D).

Cell Cycle Synchronization

In order to study cell cycle specific mechanisms and regulation, cells are often synchronized[4]. This process results in an enriched population of cells in the same phase which can be examined and quantified using Incucyte® Cell-by-Cell Analysis module. Temporary arrest is induced by serum starvation or compound treatment until all cells have reached the same phase. The block is then removed by replenishing culture media and nutrients, and synchronized cells re-enter the cell cycle at the same phase.

Thymidine, a DNA synthesis inhibitor, is a commonly used method of synchronizing cells by blocking progression beyond the S phase[5], and Figure 4 demonstrates this process. When HeLa cells expressing Incucyte® Cell Cycle were treated with Thymidine (2.5 mM, 24 h), DNA synthesis was inhibited and cells arrested in S phase. The block was removed and cells were allowed to progress through the cell cycle. Quantification of the percent cells in each phase of the cell cycle was achieved by acquiring images in the Incucyte® Cell-by-Cell Software Analysis Module, with individual cell segmentation and subsequent classification based on red and green fluorescence intensity.

An increase in cells expressing green fluorescence was observed, with a maximum of 75% green cells reached at 24 h. Around 6 h after removal of Thymidine, the percent green cells (S | G2 | M) decreased, and was followed by sequential peaks in non-fluorescent cells (M–G1 transition), red cells (G1), yellow cells (green and red, G1–S transition). Finally, another peak in green expressing cells was observed around 17 h after the previous peak in green as the cycle resumed. The temporal profiles of these peaks can yield insight into cell proliferation. For example, the time between peaks of the same color can be considered one full cell cycle. Additional cell lines synchronized with Thymidine displayed variation in peak-to-peak time, where that of MDA-MB-231 cells was 16 h, while that of SKOV3 was 24 h.

Comparison of the HeLa non-fluorescent population time course and that of label-free cell count demonstrated that the transition between M and G1 is associated with a sharp rise in cell number as cells divide (Figure 4C). This validates that mitosis is occurring during the non-fluorescent M–G1 phase.

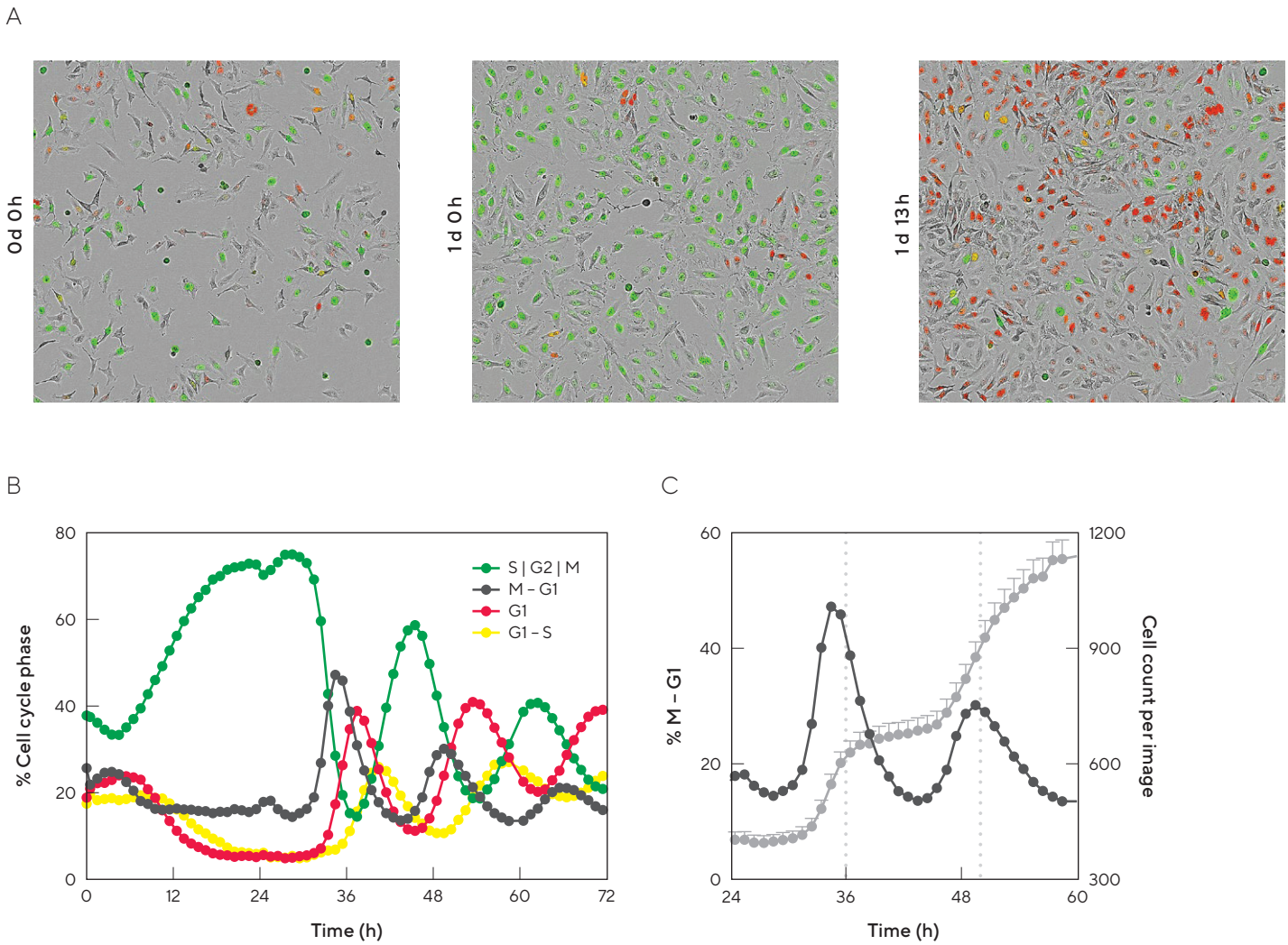

Figure 4: Synchronization of cell cycle phase. Image at 0 h shows unsynchronized cells expressing a mix of red and/or green fluorescence (A). After 1 day treatment with arresting agent, Thymidine cells have arrested in S | G2 | M and are prominently green. Thymidine block was released at 1 d and 13 h later, a peak in red fluorescence is observed as synchronized cells reach G1. Quantification was achieved using Incucyte® Cell-by-Cell Analysis. Time course of cell cycle phase shows cells accumulating in S | G2 | M during the first 24 h of Thymidine treatment (B). When the block is removed, consecutive peaks in M–G1, G1, and G1–S are observed. Overlay of cells in M–G1 (dark gray) with cell count (light gray) show increase in cell number during this transition period consistent with cell division (C).

Cell Cycle Modulation

Cell cycle arrest can be induced by treatment with chemicals or via serum starvation, and is a target for novel anti-cancer therapeutic agents, such as 5-fluorouracil (5-FU)[6]. Using Incucyte® Live-Cell Analysis, the effect of these treatments can be visualized and quantified in 96- or 384-well throughput, to accurately track and quantify cell cycle arrest in a specific phase. Here, we highlight the ability to accurately study targeted cell cycle therapies using 5-FU and cisplatin. 5-FU depletes available nucleotides which are required for DNA synthesis, rendering cells unable to enter S phase, whereas cisplatin is a chemotherapeutic DNA intercalator which damages DNA and causes checkpoint activation and cell cycle arrest in the S | G2 | M phase[7].

Treatment of HT1080 fibrosarcoma cells expressing Incucyte® Cell Cycle with 5-FU (0—50 µM) caused an increase in the percent of cells in G1 over 24 h, indicating that the cell cycle was arrested. In contrast, cisplatin treatment reduced the percent cells in G1 as cells arrested in S | G2 | M. Quantification of these effects demonstrated a time- and concentration-dependent cell cycle arrest. Figure 5 shows a 96-well plate view of percent cells in G1 phase over time, which provided an overview of compound effects, as well as an indication of assay robustness and well-to-well reproducibility. EC_{50} values were rapidly calculated within Incucyte® software to provide a measure of compound potency.

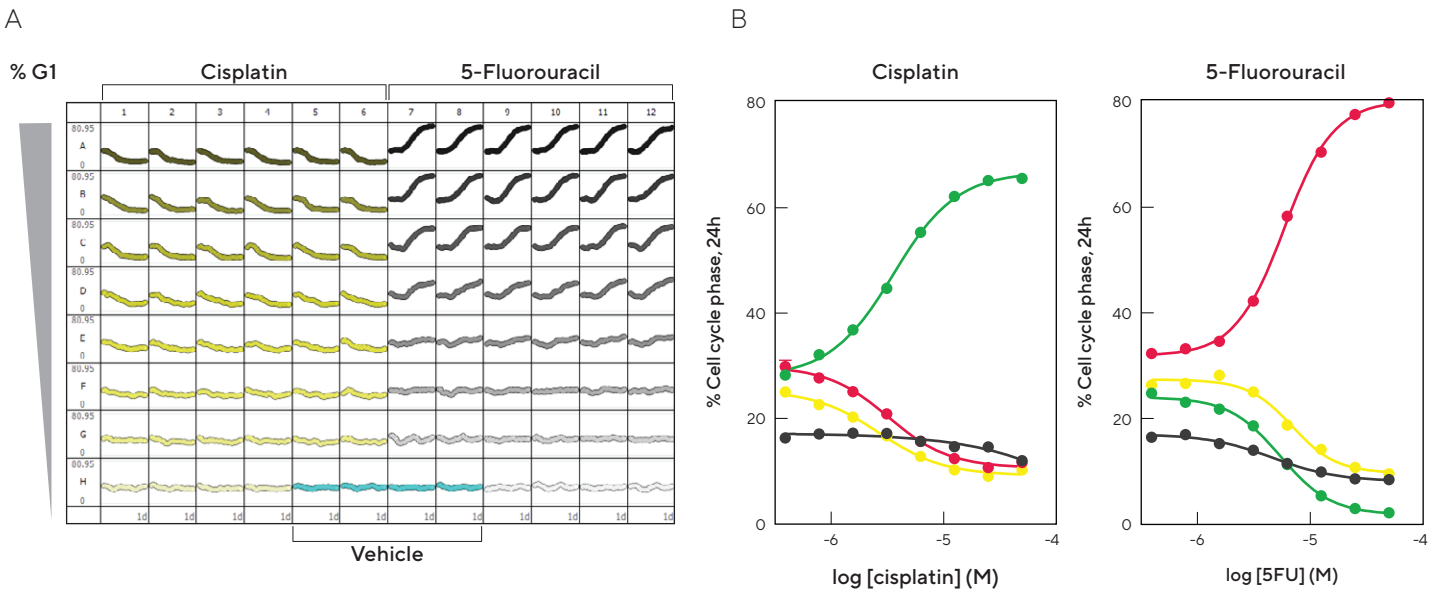

Figure 5: Concentration dependence of cell cycle modulators. HT1080 cells expressing Incucyte® Cell Cycle were treated with cisplatin (0—50 µM) or 5-fluorouracil (5-FU, 0—50 µM). Plate view shows the time course of percentage of cells in G1 phase in each well of a 96-well plate, over 1 day treatment with cisplatin or 5-FU. A) Concentration response curves indicate the efficacy of cisplatin and 5-FU at 1 d and percent change in each population over the concentration ranges tested (B).

Cell Cycle Arrest Can Be Distinguished From Apoptosis

The Incucyte® SX5 Live-Cell Analysis System incorporates three fluorescence channels (green, orange, and Near IR). By multiplexing the compatible Cell Cycle Green | Orange Lentivirus with Annexin V NIR, the effect of experimental treatments on cell cycle arrest and cell viability can be determined. Figure 6 demonstrates that differential compound effects can be explored, as well as the temporal relationship between cell cycle arrest and apoptosis. Phase and fluorescence images acquired at 3 days post-treatment show the change in cell number and fluorescence induced by each compound.

In the absence of compound treatment (vehicle), AU565 and MDA-MB-231 cells showed a mixture of green and orange fluorescence, where a small peak in green fluorescence corresponded to a small dip in orange fluorescence and vice versa. As these cells were healthy and proliferating, there was a very low number of cells which were apoptotic (Annexin V NIR positive).

Carboplatin, a non-selective DNA intercalator with a similar mechanism to cisplatin[8], induced rapid arrest in S | G2 | M. In both cell types the percentage of green cells rapidly increased within 48 h, remaining stable until approximately 72 h, when the number of apoptotic cells began to increase as cells started to undergo apoptosis. Phase image shows that carboplatin has a strong morphological effect on MDA-MB-231.

Lapatinib is a dual HER2 | EGFR inhibitor, targeting receptors expressed by the AU565 cells[9]. Treatment of AU565 with lapatinib caused arrest in G1, and the percentage of orange cells increased over time while other populations decreased. This effect was not observed in MDA-MB-231 cells which lack the appropriate cell surface receptors, and as the image shows, continued to proliferate in the presence of lapatinib.

Camptothecin, a cytotoxic DNA synthesis inhibitor, induced a transient increase of G1 cells in AU565 cells, which reached a peak at 48 h and then diminished. The percent S | G2 | M cells reduced over time while the apoptotic cells increased over the 96 h time course. In MDA-MB-231 cells the G1 cells plateaued 8 h after treatment, while the percentage of S | G2 | M cells dropped and the percent apoptotic increased. These data demonstrated that camptothecin has a cell cycle-dependent toxicity, and is more potent on cells in S | G2 | M than those in G1, correlating with camptothecin mechanism of action which inhibits cells in the S (DNA synthesis) phase. It is also consistent with reports that the apoptotic population of camptothecin-treated cells is derived from cells in S phase[10].

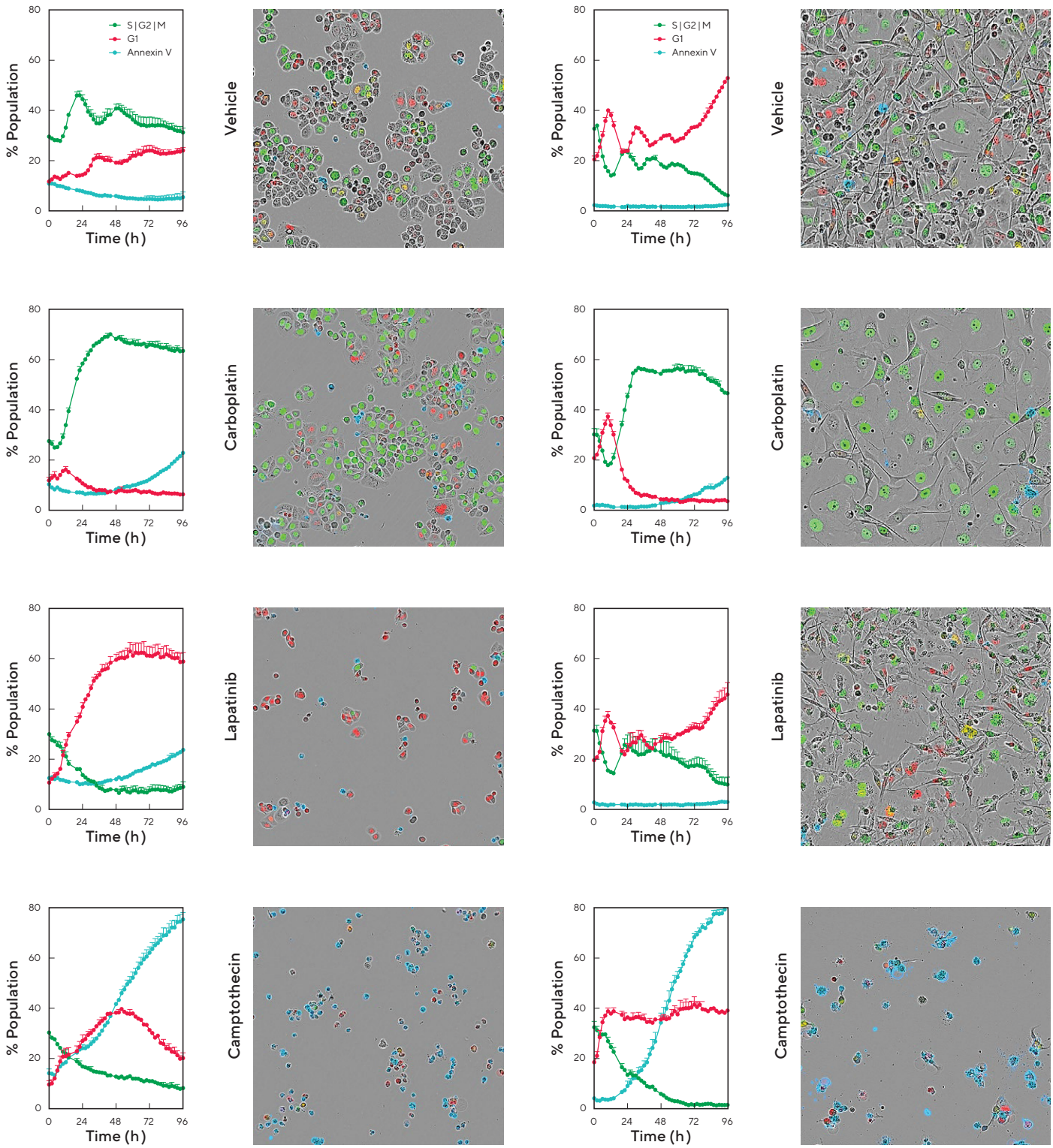

Figure 6: Combining Cell Cycle and Annexin V Reagents enables added insight into compound mechanism. AU565 and MDA-MB-231 cells expressing Incucyte® Cell Cycle Green | Orange were treated with carboplatin (100 µM), lapatinib (0.1 µM) and camptothecin (10 µM) in the presence of Annexin V NIR (1:200). Scans were acquired and analyzed in Incucyte® SX5 using the Incucyte® Cell-by-Cell Software Analysis Module. Time courses show the populations of cells in S | G2 | M (green) or G1 (red) overlaid with the population of Annexin V positive objects (teal). Carboplatin arrests cells in S | G2 | M. Lapatinib targets specific cell receptors and is, therefore, effective on AU565 but not MDA-MB-231. Camptothecin induces apoptosis in both cell lines. Phase and fluorescence (green, orange NIR) blended images show AU565 or MDA-MB-231 cells at 3 d post treatment.

Effect of Differentiation on Cell Cycle and Function

Incucyte® Cell Cycle Lentivirus reagents enable quantification of cell cycle phase by determination of percentage of cells in each phase of the cell cycle. Non-fluorescent metrics can also be derived from the Phase HD channel relating to cell count, area, and eccentricity. Combining these data with the reagent provides additional insight into morphological changes and cell behavior.

The THP-1 cell line is commonly used as a model of human monocyte function and for differentiation into macrophages[11, 12]. In order to determine the relationship between cell differentiation and cell cycle, THP-1 cells expressing Incucyte® Cell Cycle were stimulated using two common treatments: PMA (100 nM) or LPS with IFNγ (both 100 ng/mL). Studies of the cell cycle phase (Figure 7) indicated that both stimulants caused cells to arrest in G1, with an increase in cells expressing red fluorescence. Morphological differences between cells activated with PMA vs. LPS | IFNγ were noted, with cells treated with PMA changing from non-adherent to adherent morphology, with an increase in cell area and eccentricity, whereas LPS | IFNγ-treated cells displayed a mixed phenotype containing small, rounded, star-like shapes. Although the cell cycle was arrested, cell functionality was retained and stimulated cells (PMA and LPS | IFNγ) demonstrated the ability to phagocytose bioparticles. To assess phagocytosis, the total phase channel confluence of zymosan bioparticles was compared in the presence and absence of PMA or LPS | IFNγ treated cells. In the absence of cells, bioparticles settled to the bottom of the well within 12 h and the confluence remained constant after this time. In the presence of functionally active cells, bioparticles were engulfed and the confluence decreased over time. Cells differentiated with PMA were highly phagocytic, achieving 30% clearance of bioparticles, while those treated with LPS | IFNγ achieved approximately 15% clearance of bioparticles. LPS | IFNγ stimulation is known to increase the phagocytic capacity of THP-1 cells[12], however PMA treatment produces a macrophage-like phenotype which has a higher phagocytic potential[11].

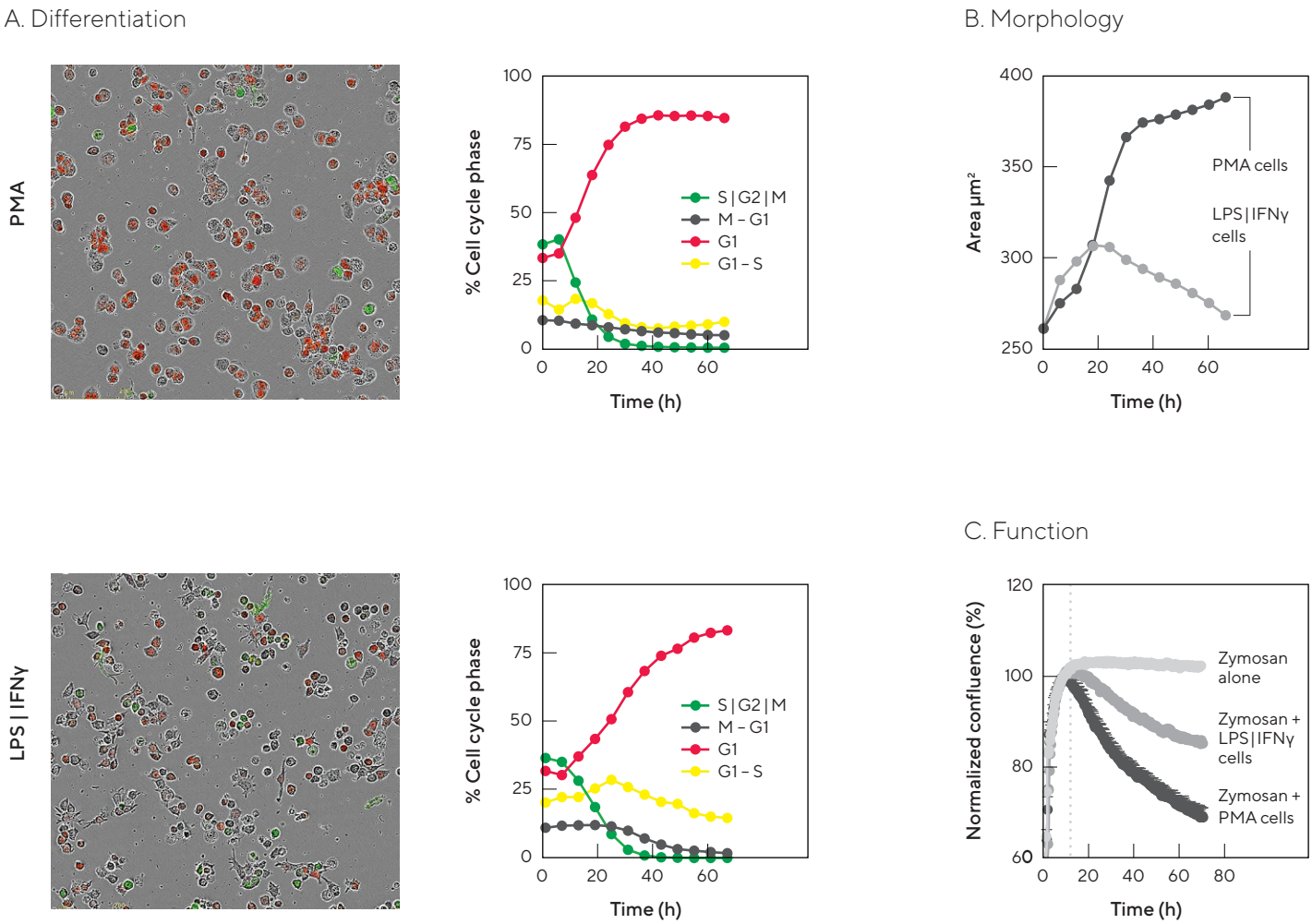

Figure 7: Differentiation of THP-1 arrests cell cycle, alters morphology, and results in phagocytic cells. THP-1 cells expressing Incucyte® Cell Cycle Lentivirus were differentiated by treatment with PMA (100 nM) or LPS | IFNγ (100 ng/mL each) for 62 h (A). Blended phase and fluorescence images show cells with altered morphology and a high proportion of red cells. Time courses of cell cycle phase indicate that both treatments induce arrest in G1, with PMA acting more rapidly than LPS | IFNγ. Average cell area shows a rapid increase in the size of PMA treated cells while LPS | IFNγ-treated cells become slightly enlarged before returning to approximately 260 µm². To assess functional capacity, stimulated cells were washed with media to remove non-adherent and dead cells, and Zymosan bioparticles (1.5 µg per well) were added (B). Total confluence was measured using basic phase segmentation, and once the bioparticles had settled (confluence of bioparticles alone reaching a maximum value at 12 h), confluence was normalized to 100%.

Immune Cell Killing and Cell Cycle Arrest

While simplistic 2D monocultures can be quantified using Incucyte® Cell Cycle Assay, more complex co-culture models can be evaluated for deeper insight into cellular interactions and functional changes. For example, the interplay between tumor and immune cells is critical in understanding the ability of immune cells to induce cell death or suppress growth of tumor cells.

To evaluate if tumor cell death by activated immune cells is cell cycle dependent, peripheral blood mononuclear cells (PBMCs) were co-cultured with target tumor cells expressing Incucyte® Cell Cycle. Using basic fluorescence masking and analysis of green and red objects, tumor cell cycle status was continuously monitored throughout the assay as activated immune cells induced apoptotic death (Figure 8).

T47D cells expressing Incucyte® Cell Cycle sensor were exposed to increasing densities of activated, freshly isolated PBMCs. The time courses of green and red objects indicate that the cells in S | G2 | M were preferentially targeted as the green object count drops rapidly, while the cells in G1 were less affected by the PBMCs. Red object count only decreased at the two highest PBMC densities, at a slower rate than the green objects. At lower PBMC densities the red object count continues to increase, suggesting that cells are arresting.

MDA-MB-231 cells exhibited different behavior in the presence of PBMCs to T47D cells. The green object count plateaued but did not decrease, and red object count was entirely unaffected by the presence of immune cells. Together, these data suggest a cytostatic mechanism consistent with reports that T cells can suppress tumor cell growth via IFNγ-mediated cell cycle arrest[13].

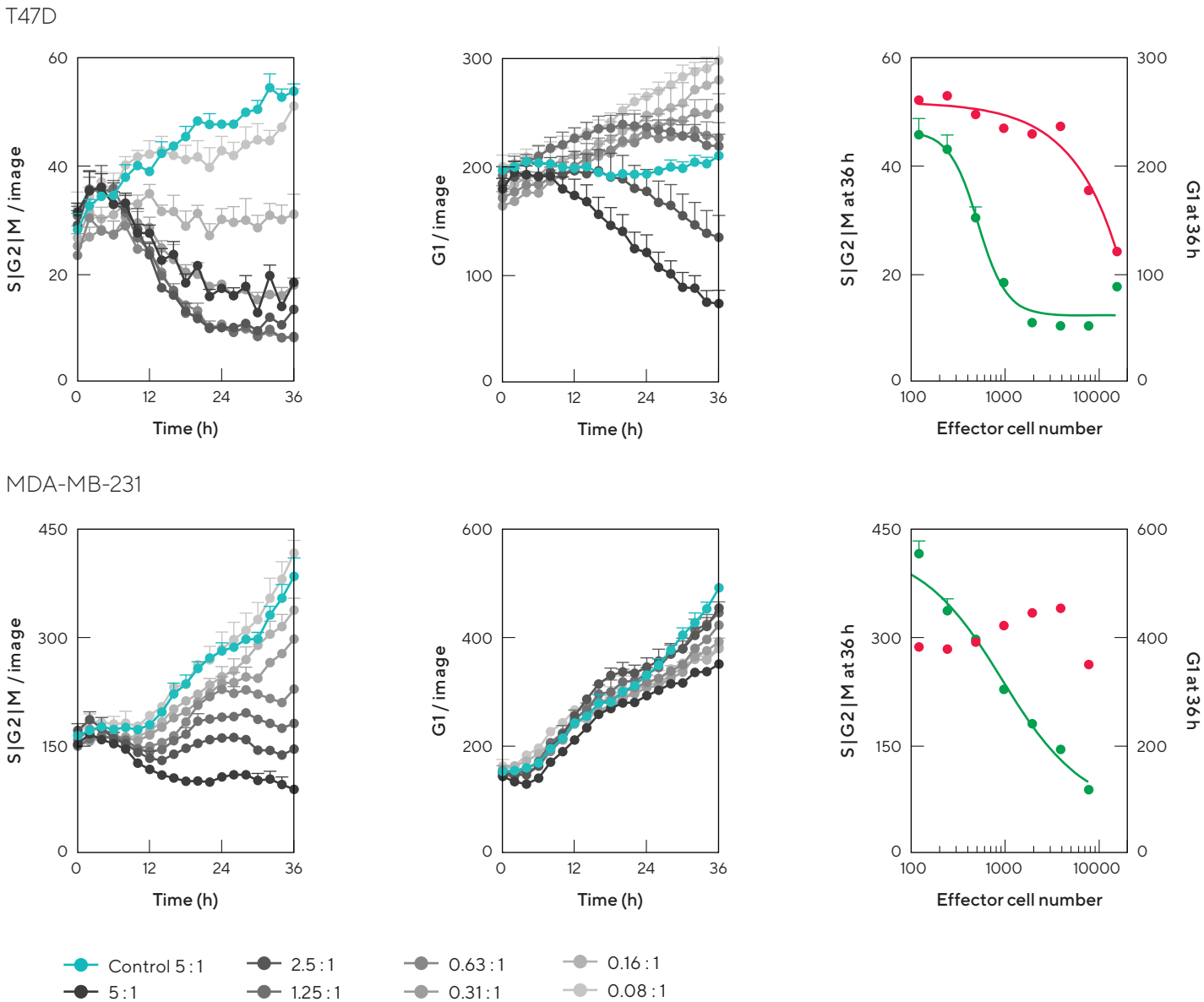

Figure 8: Incucyte® Cell Cycle Lentivirus reagent elucidates mechanism of T cell interactions with tumor cells. T47D and MDA-MB-231 breast cancer cells expressing Incucyte® Cell Cycle were incubated with increasing ratio of pre-activated PBMCs (anti-CD3, 72 h). Phase and fluorescence images were acquired over 3 days and green and red fluorescent objects were counted using basic fluorescence segmentation. S | G2 | M cells were quantified by subtracting overlap (yellow) object count from green object count. G1 cells were similarly quantified. Time courses for T47D cells (top row) show a density-dependent decrease in S | G2 | M and G1 cells, with cells in S | G2 | M (green objects) being affected more rapidly and at lower PBMC density than cells in G1 (red objects). This is highlighted by the data showing cell populations at 36 h, which show a reduction of cells in S | G2 | M at low PBMC densities, while loss of cells in G1 is only observed at the two highest PBMC densities. Time courses for MDA-MB-231 show that only cells in S | G2 | M are affected by the presence of activated PBMCs while the number of cells in G1 is unaffected. This is confirmed by data showing populations at 36 h.

Summary and Outlook

Cell cycle is a dynamic process, and following this transition is critical in many therapeutic areas, such as oncology and immuno-oncology. Using Incucyte® Cell Cycle Lentivirus reagents with real-time image acquisition and analysis, a quantitative picture of this changing landscape can be achieved. Combining the cell cycle data with cell morphology, function and cell health readouts enable multiple aspects of a treatment or culture conditions to be considered in a single well. More advanced cell models, such as co-cultures with immune cells, can also benefit from the information yielded by the Incucyte® Cell Cycle Lentivirus reagents, under physiologically relevant conditions, to deepen our understanding of temporal patterns of cell cycle progression.

References

1. Otto T and Sicinski P. **Cell cycle proteins as promising targets in cancer therapy.** *Nature Reviews Cancer,* 17;93–115 (2017)
2. Mills C, Kolb EA, and Sampson V. **Development of Chemotherapy with Cell-Cycle.** *Cancer Research,* 78(2);320–325 (2018)
3. Essen Bioscience. **Incucyte® Cell Cycle Assay.** https://www.essenbioscience.com/media/uploads/files/Cell_Cycle_Red-Green_Lentivirus_Reagent_Protocol-8000-0701-A00.pdf_.pdf (Apr 24, 2020)
4. Banflavi G. **Overview of cell synchronization.** *Methods in Molecular Biology,* 761;1–23 (2011)
5. Chen G. **Cell Synchronization by Double Thymidine Block.** *Bio-protocol,* 8(15);e2994 (2018)
6. Yoshikawa R, *et al.* **Dual antitumor effects of 5-fluorouracil on the cell cycle in colorectal carcinoma cells: a novel target mechanism concept for pharmacokinetic modulating chemotherapy.** *Cancer Research,* 61(3);1029–1037 (2001)
7. Basu A and Krishnamurthy, S. **Cellular Responses to Cisplatin-Induced DNA Damage.** *Journal of Nucleic Acids,* 1–16 (2010)
8. Dasari S, and Tchounwou P. **Cisplatin in cancer therapy: molecular mechanisms of action.** *European Journal of Pharmacology,* 364–378 (2014)
9. Tang L, *et al.* **Lapatinib induces p27Kip1-dependent G1 arrest through both transcriptional and post-translational mechanisms.** *Cell Cycle,* 12(16);2665–2674 (2013)
10. Johnson N, Tony TC, and Parkin JM. **Camptothecin causes cell cycle perturbations within T-lymphoblastoid cells followed by dose dependent induction of apoptosis.** *Leukemia Research,* 21(10);961–972 (1997)
11. Park EK, *et al.* **Optimized THP-1 differentiation is required for the detection of responses to weak stimuli.** *Inflammation Research,* 56;45–50 (2007)
12. Widdrington JD, *et al.* **Exposure of Monocytic Cells to Lipopolysaccharide Induces Coordinated Endotoxin Tolerance, Mitochondrial Biogenesis, Mitophagy, and Antioxidant Defenses.** *Frontiers in Immunology,* 9 (2018)
13. Kakimi K, *et al.* **CTLs regulate tumor growth via cytostatic effects rather than cytotoxicity: a few T cells can influence the growth of many times more tumor cells.** *OncoImmunology,* 4(3);e970464 (2015)

Sales and Service Contacts

For further contacts, visit www.sartorius.com

Essen BioScience, A Sartorius Company
www.sartorius.com/incucyte
E-Mail: AskAScientist@sartorius.com

North America
Essen BioScience Inc.
300 West Morgan Road
Ann Arbor, Michigan, 48108
USA
Telephone +1 734 769 1600
E-Mail:
orders.US07@sartorius.com

Europe
Essen BioScience Ltd.
Units 2 & 3 The Quadrant
Newark Close
Royston HertfordshireSG8 5HL
United Kingdom
Telephone +44 1763 227400
E-Mail:
euorders.UK03@sartorius.com

APAC
Essen BioScience K.K.
4th Floor Daiwa Shinagawa North Bldg.
1-8-11 Kita-Shinagawa
Shinagawa-ku, Tokyo
140-0001
Japan
Telephone: +81 3 6478 5202
E-Mail:
orders.US07@sartorius.com

Document version 2020 | 08